The Dissertation Committee for Youngok Kim
certifies that this is the approved version of the following dissertation:

Ultra-Wideband Systems Exploiting Orthonormal Waveforms

Committee:

Baxter F. Womack, Supervisor

Michael F. Becker

Brian L. Evans

Gary A. Hallock

Earl E. Swartzlander, Jr.

Preston S. Wilson

Ultra-Wideband Systems Exploiting Orthonormal Waveforms

by

Youngok Kim, B.S., M.S.

DISSERTATION

Presented to the Faculty of the Graduate School of

The University of Texas at Austin

in Partial Fulfillment

of the Requirements

for the Degree of

DOCTOR OF PHILOSOPHY

THE UNIVERSITY OF TEXAS AT AUSTIN

May 2006

Dedicated to my wife Hyesun Hong

and all of family members.

Acknowledgments

I thank God for letting me finish the dissertation. Until now, I am sure God has led me to here and I believe Jesus Christ will lead my family to where to be. God teaches me how to think and what to do through my life. I was nobody before I know Him but I am somebody in Him now. Jesus said "I am the vine; you are the branches. If a man remains in me and I in him, he will bear much fruit; apart from me you can do nothing (John 15:5)."

I thank Dr. Baxter F. Womack for his guidance as my academic supervisor. He always encouraged me to challenge against unknown world and supported me with invaluable advices and warm consolation when I was frustrated. I thank Dr. Becker for guiding me to do deeper research on ultra-wideband technology. I thank all of my other committee members, a good instructor and kind reminder Dr. Evans, generous and positive reviewers Dr. Hallock and Dr. Swartzlander. I thank Dr. Wilson for being my committee member and his interest on ultra-wideband technology. I thank my laboratory mates, Jihoon, Sanghyun, Eunho, Haewoon, Yeoujun for their friendship and valuable discussion.

I thank my parents, parents-in-law, brothers and sister and all of my other family members for their constant support and love. Specially, I thank to my wife Haesun Hong for her unwavering love and prayers.

Ultra-Wideband Systems Exploiting Orthonormal Waveforms

Youngok Kim, Ph.D.
The University of Texas at Austin, 2006

Supervisor: Baxter F. Womack

Ultra-wideband impulse radio (UWB-IR) is a promising short range radio technique for low-power applications in wireless communications, networking, radar, imaging, and position ranging systems. The UWB-IR radiates a train of extremely short baseband pulses on the order of nanoseconds or subnanoseconds. Thus, the energy of the radio signal occupies from near DC to several GHz. Since the frequency spectrum of the UWB signals is extremely broad, the UWB radio must operate under Federal Communications Commission (FCC) regulations to avoid interference with other existing systems such as Global System for Mobile Telecommunication (GSM), Wireless Local Area Networks (WLAN), Global Positioning System (GPS), Universal Mobile Telecommunications System (UMTS), Wideband Code Division Multiple Access (WCDMA). In addition, UWB radios must contend with various

interfering signals to preserve reliable communications.

In general, the power spectral density of the radiated signal is predominantly controlled by the pulse shape. Moreover, the choice of pulse shape strongly affects the bit error rate performance and the performance degradation in multipath propagations as well as multiuser interference environments. Thus, the challenge has been to design new pulses that exploit the available bandwidth to support practical applications while satisfying a spectral mask. However, most pulses require additional frequency shifting or bandpass filters to comply with the spectral mask. On the other hand, algorithms have been developed for designing multiple orthogonal pulses, such as the modified Hermite polynomial function and a pulse design algorithm utilizing ideas of the prolate spheroidal wave function. The purpose of the algorithms is to achieve high data-rate transmissions.

In this dissertation, the limitations of previous pulse shapes, including the multiple orthogonal pulse shapes, are reviewed, and then I propose the principle of generating new orthonormal pulse shapes that comply with the spectral mask without additional frequency shifting or bandpass filters. Under various conditions, such as multipath fading, timing mismatch, and multiuser interference, the performance of the systems using the proposed waveforms is analyzed and compared with the systems using different waveforms. I also propose several schemes using the multiple orthogonal pulses to achieve higher data rates or enhanced transmission reliability in UWB systems.

Table of Contents

List of Tables

List of Figures

xiii

Chapter 1

Introduction

Telecommunication can be defined as any transmission or reception-between or among points specified by the user-of voice, data, or other information of any nature by wire, radio, or other electromagnetic systems. In modern times, information is generated by many individuals, and the amount of information is growing remarkably. Much of the generated information tends to be communicated by personal devices such as mobile cell phones, personal computers, PDAs, MP3 players, digital cameras, and digital camcorders.

A simplified block diagram for a digital communication system is shown in Fig. 1.1. One message of desired information to be sent is selected from a finite message set, and the transmitter sends a corresponding signal or a waveform to the receiver. The transmitted signal or waveform travels through the channel and is then detected by the receiver. The receiver decides which message was sent by comparing the estimated message with the finite message set. Thus, the desired information is reconstructed from the estimated message at the receiver. The information, however, is naturally distorted during transmission because of the effects of the channel, noise, and interference. Moreover, today's consumer electronics are exposed to harsh channel conditions, including numerous types of interference while at the same time they are required to

Information source		Transmitter		Channel		Receiver		Sink

i(t)

x(t)

y(t)

î(t)

Messages

Estimated messages
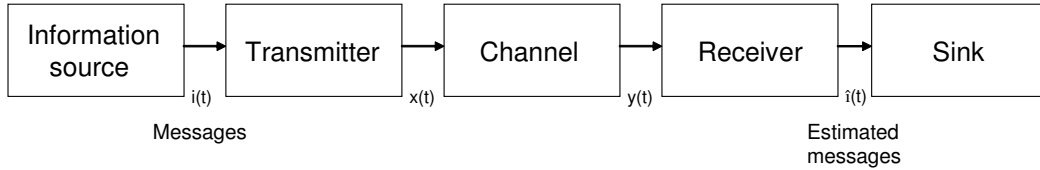
Figure 1.1: Simplified block diagram for a digital communication system

support higher data rates than before. Therefore, today's consumer electronics are required to be equipped with enhanced transmission techniques that improve transmission rates and transmission reliability and reduce cost and power consumption.

Recently, wireless connectivity has become the preferred communication method for many users because it is easy to install and provides greater mobility compared to what wired-line connectivity offers. For example, the entire home networking could easily be established by adopting currently developed wireless technologies, such as IEEE 802.11a, IEEE 802.11b, and IEEE 802.11g, whereas wired-line technologies, such as cable and digital subscriber lines, need to install cables in the home. Furthermore, wired-line technologies do not provide mobility. However, even though wireless technologies have matured since they emerged in the market, they demand high power consumption, which is a disadvantage for the applications requiring long battery life, and the technologies are too expensive to be implemented in low-power, low-cost applications.

In this dissertation, ultra-wideband impulse radio (UWB-IR) systems are addressed as potential candidates for low-power, low-cost applications.

UWB-IR is a promising short range radio technique for low-power applications in wireless communications, networking, radar, imaging, and position raging systems [2]. The UWB-IR radiates a train of extremely short baseband pulses on the order of nanoseconds or subnanoseconds. Since these short pulses occupy extremely broad bandwidth and can be transmitted directly, information can be transmitted without being modulated onto carriers in short ranges. Thus, the intermediate frequency processing, which is necessary for carrier-based communication systems, can be eliminated for low complexity implementation of the UWB-IR systems.

Additional advantages of UWB radios are summarized as follows [3]:

1. Enhanced capability of penetrating walls.

2. High accuracy in ranging.

3. Potential for very high data rates.

4. Robust against multipath interference.

5. Low power consumption.

6. Low cost, low complexity implementation and applicability to a small-size product.

Although the UWB has many attractive features, UWB technology was mainly considered for radar applications until the FCC released an enormous bandwidth as an unlicensed band, where the main frequency band resides between 3.1 GHz and 10.6 GHz. After the emission masks of UWB devices were released by FCC in February 2002, the commercial potential of UWB

technology has been recognized, and many research institutions, industry, and government agencies have assessed and exploited the potential of UWB radios in various areas, such as short-range, high-speed access to the Internet, accurate personnel and asset tracking for increased safety and security, precision navigation, surveillance, health monitoring, industrial inventory control, home sensing, logistics, and industrial process control and maintenance [3] [4]. The UWB market is at an early stage, but estimates predict that the UWB market will be worth $630 million by 2007 [5].

Global interest in the UWB technology is growing dramatically. The deregulation of UWB technology is currently underway in Korea, Singapore, Japan, and China, while Europe has undertaken substantive work to produce a coordinated approach across Europe [6] [7]. In addition to the European Telecommunications Standards Institute (ETSI) developing regulations, the European Union (EU) has funded a number of projects in the application and implementation of UWB technology [6].

Although interest in its commercial potential has been rapidly increasing recently, UWB has a long history dating back to the first UWB transmission during Heinrich Hertz's spark discharge experiment in 1893. The radio communication device invented by Guglielmo Marconi also used a spark-gap transmitters, and radio signals occupying enormous bandwidth were successfully transmitted. In the 1960s, with the development of techniques for sub-nanosecond (baseband) pulse generation, UWB technology again received notice when the U.S. military considered impulse radio transmissions for imaging,

radar, and covert communications [6] [8] [9] [10]. In the 1980s, UWB technology was alternately referred to as baseband or carrier-free until the U.S. Department of Defense (DoD) applied the term *ultra wideband* for devices occupying at least 1.5 GHz, or a -20 dB fractional bandwidth exceeding 25% [11]. In the early 1990s, much of the work in the UWB field was performed under classified U.S. government programs, but key technologies and concepts were brought into the public domain and the development of UWB technology has greatly accelerated since the late 1990s [12]. In 1998, the FCC opened rule making of UWB and issued the rules, referred to as the First Report and Order (R&O), in February 2002 [1].

The remainder of this chapter is organized as follows. Issues regarding regulations and standards are described in Section 1.1, and potential applications of UWB are summarized in Section 1.2. In Section 1.3, the thesis statement is presented. In Section 1.4, the contributions of this dissertation to research and organization of the dissertation are described. Section 1.5 defines the notation and the nomenclature that are used in the dissertation.

1.1 Regulations and Standards Issues

The International Telecommunication Union Radiocommunication Sector (ITU-R) plays a vital role in worldwide regulatory activity in UWB technology. The Task Group 1/8 (TG 1/8) of ITU-R has carried out studies concerning the compatibility between UWB and radiocommunication services. In Europe, the ETSI has been working to establish a legal framework for the deploy-

ment of license-free UWB devices and has proposed a UWB spectrum mask with the European Conference of Postal and Telecommunications Administrations (CEPT). In Asia, many countries, such as Korea (at the Electronics and Telecommunications Research Institute), Japan (at the the Ministry of Internal Affairs and Communications), and Singapore (at the Infocomm Development Authority) are making preparations for the UWB regulations [13].

In the USA, the FCC has defined UWB as any wireless transmission scheme for which the fractional bandwidth is more than 20%, or more than 500MHz of an absolute bandwidth [1]. The fractional bandwidth is defined as $2(f_H - f_L)/(f_H + f_L)$, where f_H is the upper frequency and f_L is the lower frequency at the -10 dB emission point. The center frequency of the signal spectrum emitted by such a system is defined as $f_C = (f_H + f_L)/2$ at the -10 dB emission point. Since the frequency spectrum of the UWB systems is extremely broad, it can cause interference with other systems, such as GPS, unmanned air vehicles (UAVs), aircraft radar, GSM, UMTS, and WLANs [3] [14] [15] [16] [17] [18] [19]. Thus, the FCC has regulated the main frequency band of UWB systems to be between 3.1 GHz and 10.6 GHz [1], as shown in Fig. 1.2. Moreover, the total allowable average effective isotropic radiated power (EIRP) from a UWB device is limited to 0.56 mW, and the power spectral mask for UWB applications is restricted as shown in Fig. 1.3.

Significantly, UWB technology has been considered for alternative air interfaces in IEEE standards, such as wireless personal area networks (WPANs) and wireless body area networks (WBANs). Since the UWB sig-

6
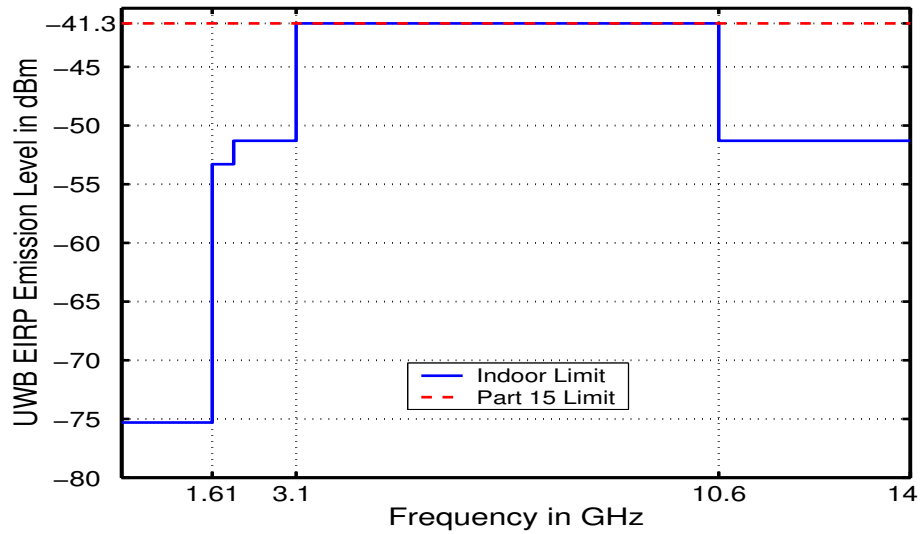
Figure 1.2: FCC Part 15 limit and power spectral mask for indoor UWB systems [1]

Frequency	Equivalent Isotropically Radiated Power (EIRP) [dBm]					
[MHz]	Indoor Comm.	Hand Held Comm.	Low Freq. Imaging	High Freq. Imaging	Med. Freq. Imaging	Vehicular Radar
<960	15.209 limits	15.209 limits	15.209 limits	15.209 limits	15.209 limits	15.209 limits
960–1610	–75.3	–75.3	–65.3	–65.3	–53.3	–75.3
1610–1900	–53.3	–63.3	–53.3	–53.3	–51.3	
1900–1990		–61.3				
1990–3100	–51.3			–51.3	–41.3	–61.3
3100–10,600	–41.3	–41.3		–41.3		
10,600–22,000			–51.3			
22,000–29,000	–51.3	–61.3		–51.3	–51.3	–41.3
20,000–31,000						–51.3
>31,000						–61.3

Figure 1.3: FCC power spectral mask for UWB applications

7

naling provides a new way to utilize the spectrum, many efforts are currently underway for developing a wide variety of applications of this technology. The UWB technology can be used for both high data-rate applications at short range and low data-rate, low-power applications with very fine range resolution, precision distance, and/or positioning measurement capabilities at longer ranges.

Recently, communication techniques for personal area networks have been improved to provide a high rate of data transmission as the demand of multimedia consumer electronics grows. Thus, high data-rate applications of the UWB wireless technology have initially drawn much attention, and the IEEE 802.15.3a study group has been established to investigate the UWB as a potential solution for short-range, high data-rate applications [20]. This study group has worked to develop a standard for applications such as video, multimedia links, or cable replacement with a minimum data rate of 110 Mbps at 10m. There are two UWB standards camps, UWB Forum and WiMedia Alliance, and those opposing camps has insisted their own approaches, direct-sequence-UWB and MultiBand Orthogonal Frequency Division Multiplexing UWB, to be the IEEE 802.15.3a UWB standards. After nearly three years of dispute, however, the IEEE committee 802.15.3a, which was tasked with developing a standard, voted unanimously to disband at a meeting in Hawaii on January 19, 2006, and the dispute has been passed to the marketplace. Now, two opposing camps continue to develop their own approaches and let the marketplace decide which one is the most convenient and useful technol-

ogy.

The IEEE 802.15.4a has been established for long-range, low-power, low data-rate applications with high precision capability [21]. The task group of IEEE 802.15.4a has been developing next generation of wireless technology, which can be applied to asset tagging, asset tracking, industrial inventory control, home sensing, and logistics. Recently, the task group, after reviewing 26 physical layer proposals, set a baseline standard, where the primary candidate is UWB-IR technology and the other is a chirp spread spectrum operating at 2.4 GHz [4]. The primary advantages of the UWB-IR technology considered are low cost, long battery life, multipath immunity, and communication ability with precision ranging capabilities on the order of 30 cm accuracy. The draft standard is likely to emerge in mid-2006 [21].

1.2 Potential Applications

While the efforts of regulations and standardization are underway across the world, the commercialization of UWB technology has been undertaken for developing a wide variety of applications in both short-range communication systems supporting high data-rate applications and low data-rate intelligent devices, including accurate location-tracking capabilities. Since UWB radios can increase link range at the cost of the reduced information rate, the two complementary usage regions can be implemented based on very similar architectures for scalable data rates/ranges [13]. A number of practical applications of UWB technology can be identified, but some of the major potential appli-

9

cations are summarized here.

1.2.1 Wireless Personal Area Networks

Digital communication techniques for personal area networks have been developed to provide high data-rate transmissions as the demand increases for multimedia consumer electronics, which require high-speed signal processing computation and data throughput, grows. The demand has been satisfied by interconnecting devices through wires such as Universal Serial Bus (USB) and IEEE 1394. Compared to wireless-based applications, however, conventional wire-based applications have an inherent handicap in the arrangement of the devices because wiring between the devices presents problems. Therefore, wireless-connectivity technology for high data-rate transmissions addressed to market and its demands has been on the increase.

Meanwhile, UWB technology has revolutionized home media and office networking by taking over the tasks of wired devices, such as distributing HDTV signals. In this case, the bit rate needed is in excess of 30 Mbps over a distance of at least a few meters, from a receiver to multiple TV sets around the home, for transmitting large picture files between digital cameras and computers, connecting monitors and printers to computers, connecting laptops and PDAs, and interconnecting any potential electronic medical devices with remote monitoring systems [22] [23]. Although systems for relatively longer-range wireless networks, such as IEEE 802.11b, 802.11a, or 802.11g, are considered as candidates for WPANs, they are not attractive solutions for

very high-bit-rate, low-cost, low-power wireless networks because of their high power consumption and cost [24] [25].

1.2.2   Wireless Sensor Networks

Wireless sensor networks can be characterized as a large number of densely deployed nodes, where each node transmits information by a low-power, low-cost device. For industrial or outdoor applications of wireless sensor networks, the potential sensing devices must have several features, such as low cost, long battery life, low-complexity, high link reliability, and communication ability with precision ranging capabilities [13] [26]. As stated in the previous section, UWB technology has all the above features as well as a number of additional properties, including multipath immunity, precise localization, tracking, and distance measuring capabilities. Thus, UWB technology is considered as a candidate for wireless sensor networks, as well as for asset tagging/tracking [21]. Meanwhile, Bluetooth is considered a less suitable technology for wireless sensor networks because its energy requirements and cost are higher than those for the UWB technology, while the precise localization capability of UWB outperforms that of Bluetooth technology [3] [27] [28].

1.2.3   Wireless Body Area Networks

WBANs consist of several autonomous wireless sensors that are spread over the human body by integrating them into the clothing or even implanting them inside the human body. The most promising application of WBANs

is healthcare applications such as remote sensing, health monitoring, locating assets/staff, and workplace safety. Thus, sensing devices must be suitable for providing scalable data rates over a short range at ultra-low power [29]. Therefore, UWB technology also is considered as the prime candidate for the air interfaces of WBANs. Furthermore, UWB signals are robust against interference and provide a high degree of reliability, which will be a key feature for accurate patient health information [6]. UWB radios also have an enhanced capability to penetrate materials, a property that could be applied to imaging or medical diagnostics in various medical applications.

1.3   Thesis Statement

This dissertation defends the following idea:

A UWB impulse radio system exploiting the proposed multiple orthonormal waveforms can provide a better data rate and/or transmission reliability than a system using any single type of waveform or previously developed multiple orthonormal waveforms.

1.4   Contributions and Organization of the Dissertation

As mentioned in the previous sections, since the frequency spectrum of the baseband pulses is extremely broad, the FCC has regulated the power spectrum to avoid interference with other systems. Unfortunately, the zeroth- and first-order Gaussian monocycle pulses that are commonly used in UWB

impulse radio do not meet the FCC indoor spectral constraints and should be filtered to contain its power distribution within a frequency band from 3.1 GHz to 10.6 GHz [30] [31] [32]. Note that the additional filtering can lengthen the pulse duration, and the lengthened pulse duration can reduce system capacity and increase cost.

Because of the FCC spectral regulations, therefore, the use of baseband pulses becomes difficult without the additional filtering or frequency shifting. As can be expected, the challenges lies in designing new pulses exploiting the available bandwidth to support practical applications while also satisfying the FCC spectral mask [32] [33] [34] [35] [36] [37] [38]. Table 1.1 briefly describes the pros and cons of the different approaches and more detailed discussion will be presented in Chapter 2.

The main contributions of this dissertation are described below:

I propose the principle of generating orthonormal pulse shapes that comply with the FCC mask without additional frequency shifting or band-pass filters for the high data-rate transmissions and/or the enhancement of transmission reliability in UWB systems (Chapter 3). Generally, the pulse shapes strongly affect the bit error rate (BER) performance and the performance degradation in multipath propagation environments. In asynchronous multiuser environments, moreover, the auto- and cross-correlations property of the pulse becomes an important factor in determining the effects of multiuser interference. Thus, I analyze the impact of properties of the proposed pulses, such as their auto- and cross-correlations, on the correlation receiver of the

Table 1.1: Pros and cons of different approaches for pulse design

Pulse shape	Pros	Cons
Luo's pulse	·Applicable for narrowband interference suppression	·Sensitive to pulse width constraint ·Single type of waveform
Wu's pulse	·Applicable for an arbitrary spectrum mask	·High complexity in pulse design ·Single type of waveform
Modified Hermite Polynomial pulses	·Multiple waveforms · Pulse width and bandwidth are almost same with respect to the order	· Need frequency shifting or bandpass filters to comply with spectral mask ·Complexity for generation is significantly increased as the order increases
Prolate spheroidal pulses	·Multiple waveforms ·Satisfy the spectral mask without frequency shifting or bandpass filters	·Sensitive to pulse width constraint ·Strong adjacent channel interference can be caused

UWB system based on the pulse position modulation (PPM). Furthermore, I compare the performance of the proposed pulses with different waveforms under various conditions, such as multipath fading, timing mismatch, and multiuser interference (Chapter 4). Then, I discuss modulation schemes using the multiple orthogonal pulses to achieve the enhancement of data rate in transmissions (Chapter 5). I also propose a novel space-shape (SS) coding scheme with multiple antennas and multiple orthonormal waveforms to enhance the transmission reliability of the UWB systems (Chapter 6).

The dissertation is organized as follows:

Chapter 2 discusses the effects of the modulation scheme and the pulse shape on the power spectral density (PSD) of the radiated signal, and then reviews the previous pulse shapes. In particular, recently developed multiple orthogonal pulses for achieving high data rate and/or enhanced transmission reliability are reviewed. Channel models for indoor UWB systems are also introduced.

Chapter 3 presents the limitations of two previous multiple orthogonal pulse shapes, which motivates the need of new pulse shapes for UWB-IR systems. Then, I propose novel orthonormal pulses that not only meet the power spectral mask of the FCC for indoor UWB systems, but also preserve orthogonality at the correlation receiver. The proposed pulses are derived from a parametric closed-form solution. Thus, multiple orthonormal pulses that comply with the FCC mask without additional frequency shifting or bandpass filters can be generated for high data-rate wireless connectivity and/or the enhancement of transmission reliability.

Chapter 4 analyzes the impact of the correlation characteristics of the proposed waveforms on the performance of a correlation receiver and provides a performance comparison with different waveforms under various conditions, such as multipath fading, timing mismatch, and multiuser interference. Through the results of a theoretical analysis and simulations, I show that the proposed orthonormal pulses provide enhanced BER performance of the correlation receiver compared to that of the well-known orthonormal modified Hermite polynomial function (MHP) pulses and even a Gaussian monocycle.

15

Chapter 5 discusses modulation schemes that use the proposed multiple orthogonal pulses to achieve the enhancement of data rate in transmissions. The results of simulations comparing different waveforms demonstrate the effectiveness of the proposed orthonormal pulses in various conditions.

Chapter 6 proposes a novel space-shape coding scheme with multiple antennas and multiple orthonormal waveforms for the UWB-IR systems. Since the proposed coding scheme can be applied for every frame, spatial diversity can be achieved even without the invariant channel condition over frames. Furthermore, the proposed scheme can provide an additional power gain to enhance the BER performance while the FCC spectral regulation is satisfied. The validation of the proposed scheme is demonstrated with simulations.

Chapter 7 presents the conclusions of the dissertation and proposes future research topics.

1.5   Notation and Nomenclature

In general, a letter in bold face stands for a matrix or a vector , as should be clear from context. The operation $*$ denotes a convolution operation; $(\cdot)^T$ stands for the matrix or the vector transpose; $(\cdot)^*$ represents complex conjugate; $(\cdot)_N$ denotes the modulo operation; $|\cdot|$ denotes absolute value; $\|\cdot\|^2$ denotes the squared Euclidean norm; $\delta(\cdot)$ is the Dirac delta functional; $(\cdot)_k$ denotes the kth element of the argument vector; $(\cdot)_{k,m}$ denotes the (k,m)th entry of the argument matrix; $\{\cdot\}$ is a finite set of integers; $<a,b>$ indicates the inner product between a and b; $R(\cdot)$ represents the auto-correlation; and

$\tilde{R}(x) = R(x) - R(x - \delta)$ denotes the correlation difference; $\hat{d}$ is the estimate of d; and $p(t; i, j)$ denotes the waveform $p(t)$ at the jth frame for i^{th} bit.

Table 1.2 describes the nomenclature used in the dissertation.

Table 1.2: Nomenclature

AWGN	:	Additive White Gaussian Noise
DFT	:	Discrete Fourier Transform
DoD	:	U.S. Department of Defense
FCC	:	Federal Communications Commission
EIRP	:	Effective Isotropic Radiated Power
IFT	:	Inverse Fourier Transform
GPS	:	Global Positioning System
GSM	:	Global System for Mobile Telecommunication
ISI	:	Intersymbol Interference
LCR	:	Large Current Radiator
LOS	:	Line-of Sight
MHP	:	Modified Hermite Polynomial Function
MRC	:	Maximal Ration Combining
MUI	:	Multiuser Interference
PPM	:	Pulse Position Modulation
PS	:	Prolate Spheroidal
PSD	:	Power Spectral Density
PSM	:	Pulse Shape Modulation
SEN	:	Squared Euclidean Norm
SLC	:	Square-Law Combining
SNR	:	Signal-to-Noise Ratio
SS	:	Space Shape
STC	:	Space-Time Coding
SUE	:	Spectrum Utilization Efficiency
TD-SCDMA	:	Time Division-Synchronous Code Division Multiple Access
TH	:	Time-Hopping
UAVs	:	Unmanned Air Vehicles
UMTS	:	Universal Mobile Telecommunications System
USB	:	Universal Serial Bus
UWB-IR	:	Ultra-Wideband Impulse Radio
WBANs	:	Wireless Body Area Networks
WCDMA	:	Wideband Code Division Multiple Access
WPANs	:	Wireless Personal Area Networks
WLAN	:	Wireless Local Area Network

Chapter 2

Pulse Shapes for UWB Systems

This chapter describes the effects of the modulation scheme and the pulse shape on the PSD of the radiated signal and then reviews the previous pulse shapes. The antenna and channel models for indoor UWB systems are also introduced.

The rest of the chapter is organized as follows. Issues for the PSD of UWB signal and interference with different systems are introduced in Section 2.1. In Section 2.2, the PSDs of PPM modulated UWB signals with both finite deterministic TH and infinite random TH are discussed. Previous waveforms for indoor UWB system are briefly reviewed in Section 2.3. In Section 2.4, antenna model is described and channel models for indoor UWB systems are discussed in Section 2.5. The summary is given in Section 2.6.

2.1 Introduction

As mentioned in Chapter 1, UWB radio communicates with ultra-short pulses. Thus, the energy of the radio signal occupies from near DC to several GHz. Since the frequency spectrum of UWB signals is extremely broad, the UWB radio must operate under Part 15 FCC regulations to avoid interfer-

ing with other existing systems, such as GSM and GPS. In addition, UWB radios must contend with various interfering signals to preserve reliable communications. For military applications, the major objective is to minimize the probability of detection and interception by malicious users. This objective requires that UWB signals be transmitted with extremely low spectral content while the average power level must be maintained enough for reliable communications. All of these requirements imply that the spectral occupancy and composition of a chosen time-hopping (TH) technique are important considerations in the design of a TH UWB multiple access communication system.

In general, the PSD of the radiated signal is shaped by the pulse shape as well as by the modulation scheme. The PSD of the UWB signal has been studied, and analytical expressions for various situations have been introduced in the literature [39] [40] [41] [42] [43] [44] [45]. In [39], the PSD of UWB signal based on analog pulse position modulation (PPM) is introduced and the analytical expressions of the PSD for variously modulated UWB signals, such as TH-PPM, binary antipodal modulation (BAM), and Direct-Sequence (DS) UWB signals, also are derived. The PSD of UWB signals with deterministic TH codes is derived in [40] and the effect of timing jitter on the PSDs of UWB signals with finite and infinite TH sequences is investigated in [42]. The effect of arbitrary timing jitter on the PSD of UWB signals is further examined in [41] [44] and the generalized expression with timing jitter is presented in [44] and [41] shows that the PSD of zero-mean and uncorrelated data stream is not affected by timing jitter. The PSD of nth-order Gaussian pulse is derived

in [43] and different version of the PSD of Gaussian pulse is derived under realistic multipath channel in [45].

Interference with other existing systems, such as GSM, WLAN, GPS, UMTS, SCDMA, have been studied in [14] [15] [16] [17] [18] [19] [46]. The co-existence with IEEE 802.11b and Bluetooth networks are studied in [14]. The study is based on experimental test measurements and the results show that both IEEE 802.11b system and Bluetooth networks are slightly suffer from the interference of UWB signal. Since fixed wireless access can be impaired by the interference of UWB signal, the coexistence issue has been analyzed and the result of non-practical risk is presented in [15]. When the distance between the devices is close, the throughput of the IEEE 802.11a system can be severely degraded by the UWB interference [16], but the interference of UWB signal to IEEE 802.11a system can be significantly mitigated in line-of sight (LOS) scenarios, even at close range [17]. Mutual interferences between UWB signals and other various systems, such as GSM900, UMTS/WCDMA, and GPS, are studied in terms of a UWB pulse width in [18] and, through the simulations, they concluded that the proper selection of UWB pulse shapes and pulse width can effectively avoid/mitigate the interferences between the devices. Through theoretical analysis and simulations, [19] shows that the interference of UWB signals to CDMA system is insignificant and the results of [46] indicate that asynchronous transmission of UWB signals can efficiently mitigate the interference to Time Division-Synchronous Code Division Multiple Access (TD-SCDMA).
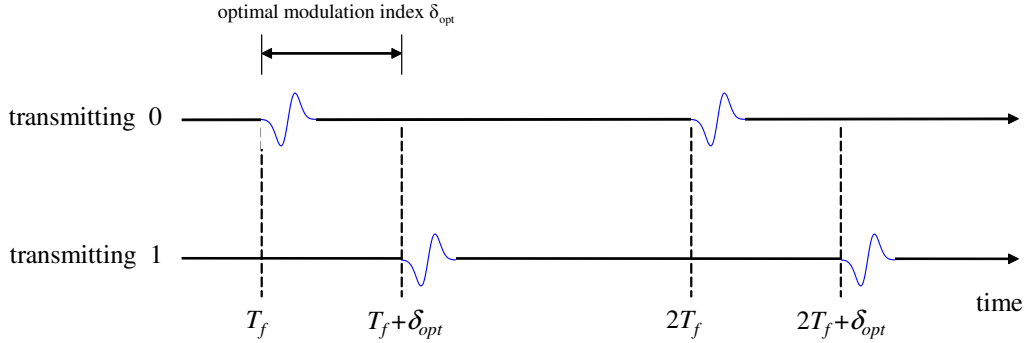
Figure 2.1: Pulse Position Modulation

In this chapter, the effect of the modulation scheme on the PSD of the radiated signal will be discussed first, followed by a discussion on the effect of the pulse shape on the PSD. In addition, various pulse shapes and the channel model for indoor UWB systems will be introduced.

2.2 Power Spectral Density (PSD) of Time-Hopping Pulse Position Modulation (TH-PPM) UWB Signals

For wireless communications, the data stream can be encoded into a train of baseband pulses by varying the position of a pulse within a repetition period [30], [31], [47]. Fig. 2.1 shows the pulse position modulation (PPM). As shown in the figure, δ_{opt} is the optimal time offset, which will be discussed more detail in Chapter 4, of binary PPM, and δ_{opt} is considered as a time shift to represent the data bit of value 0 or 1.

In binary PPM UWB systems, the TH sequence provides an additional time shift at every frame in the pulse train. The TH sequence is adopted for avoiding catastrophic collisions among users in multiple access systems [30]

22

[31]. In addition, the additional advantages of adopting TH sequence are summarized as follows [42] [48]:

1. The time shifted pulses are more difficult to detect and to intercept.

2. Without an additional time shift, the pulses tend to be peaky due to the overlap of multiple pulses. The TH sequence can reduce the PSD of the uniformly spaced pulse train.

3. Careful design of the TH codes minimizes the effects of multipath and multiuser interference (MUI).

4. Careful design of the TH codes controls the power spectrum for coexistence with other technologies.

5. Synchronization between the transmitter and the receiver can be improved.

In the following subsections, I will discuss the PSD of PPM modulated UWB signals with both finite deterministic TH and infinite random TH.

2.2.1 PSD of PPM UWB Signals with Finite TH Sequence

In the UWB systems adopting binary PPM and finite TH, the transmitted signal $s(t)$ is expressed as

$$s(t) = \sum_{i=-\infty}^{\infty} \frac{1}{\sqrt{N_s}} \sum_{j=0}^{N_s-1} p(t - iT_s - jT_f - c_{(iN_s+j)_{N_c}} T_c - \epsilon d_i), \qquad (2.1)$$

where N_s is the number of pulses to transmit a bit, $p(t)$ represents a pulse shape, $T_s(=N_s \cdot T_f)$ is the symbol duration, and T_f is the frame period,

which may be ten to a thousand times that of a single waveform's width, T_p. The expression $\{c_{(iN_s+j)_{N_c}} \in [0, N_c)\}$ is an integer TH sequence, where $c_{(iN_s+j)_{N_c}} \equiv c_{(iN_s+j)} \mod N_c$, and the TH sequence is repeated during transmission. T_c is the time period of a TH chip. ϵ is the time offset of binary PPM, and $d_i \in \{0, 1\}$ is the ith bit data transmitted during the symbol time T_s. Since the TH is a finite sequence, the periodically repeated sequence can be represented by the N_1 subsequences, where N_1 and N_2 are the smallest pair of integers satisfying the equation $(N_1 \cdot N_s = N_2 \cdot N_c)$. Thus, the N_1 subsequences can be considered as a deterministic sequence and the TH sequence can be expressed as a filter with a discrete impulse response, $c_i(t)$. When the modulation scheme, including the TH sequence, is represented as $m(t)$, the radiated signal $s(t)$ can be expressed as [42]

$$s(t) = m(t) * p(t), \tag{2.2}$$

where

$$m(t) = \sum_{r=-\infty}^{\infty} \sum_{i=0}^{N_1-1} \delta(t - iT_s - rN_1T_s - \epsilon d_i) * c_i(t), \tag{2.3}$$

$$c_i(t) = \frac{1}{\sqrt{N_s}} \sum_{j=0}^{N_s-1} \delta(t - c_{(iN_s+j)_{N_c}} T_c), \tag{2.4}$$

and $*$ represents convolution.

Meanwhile, the PSD of the radiated pulse is derived from (2.2) as

$$S_s(f) = |P(f)|^2 S_M(f), \tag{2.5}$$

where $P(f)$ is the Fourier transform of the transmitted waveform and $S_M(f)$ is the PSD of the modulation scheme. The time-average autocorrelation of the

24

modulation scheme is derived as

$$R_M(\tau) = \frac{1}{N_1 T_s} \int_0^{N_1 T_s} \mathbb{E}[m(t)m(t+\tau)]dt. \tag{2.6}$$

The PSD of the modulation scheme, $S_M(f)$, is derived by using the Wiener-Kinchine theorem [42] [49] as

$$S_M(f) = \frac{1}{N_1 T_s} \Bigg[\sum_{i=0}^{N_1-1} C_i^*(f)C_i(f) + \mathbb{E}_{i \neq i'}[e^{-j2\pi f\epsilon(d_{i'}-d_i)}].$$
$$\Big(\frac{1}{N_1 T_s} \sum_{r=-\infty}^{\infty} \sum_{i=0}^{N_1-1} \sum_{i'=0}^{N_1-1} \big(C_i^*(f)C_i(f)e^{-j2\pi fT_s(i'-i)}\delta(f - \frac{r}{N_1 T_s}) \big)$$
$$- \sum_{i=0}^{N_1-1} C_i^*(f)C_i(f) \Big) \Bigg], \tag{2.7}$$

where $C_i(f)$ is the Fourier transform of ith TH filter $c_i(t)$. In particular, when the equiprobable binary symbols are assumed for d_i, the PSD of the modulation scheme of (2.7) can be expressed as

$$S_M(f) = \frac{1}{2N_1 T_s} \big(1 - \cos(2\pi f\epsilon) \big) \sum_{i=0}^{N_1-1} |C_i(f)|^2 + \frac{1}{2(N_1 T_s)^2} \big(1 + \cos(2\pi f\epsilon) \big) \cdot$$
$$\sum_{r=-\infty}^{\infty} \sum_{i=0}^{N_1-1} \sum_{i'=0}^{N_1-1} \big(C_i^*(f)C_i(f)e^{-j2\pi fT_s(i'-i)}\delta(f - \frac{r}{N_1 T_s}) \big). \tag{2.8}$$

By inspecting (2.8), it can be observed that the PSD of the modulation scheme consists of a continuous component and a discrete component. Note that the spectral lines of the discrete component appears at multiples of $\frac{1}{N_1 T_s}$.

2.2.2 PSD of PPM UWB Signals with Infinite TH Sequence

To investigate the effect of the length of TH sequence on the PSD of modulation scheme, the TH sequence with an infinite length is considered. With an infinite TH sequence, the modulation scheme $m(t)$ can be expressed as

$$m(t) = \sum_{i=-\infty}^{\infty} \frac{1}{\sqrt{N_s}} \sum_{j=0}^{N_s-1} \delta(t - iT_s - jT_f - c_{iN_s+j}T_c - \epsilon d_i), \qquad (2.9)$$

and the PSD of the modulation scheme of (2.9) is derived in a similar way for the finite TH case and is expressed as

$$\begin{aligned}
S_M(f) = \frac{1}{T_s}\Bigg[&1 + \sum_{i=-\infty}^{\infty} \text{sinc}^2\big(\text{N}_\text{c}\pi\text{T}_\text{c}(\text{f} - \frac{\text{i}}{\text{T}_\text{c}})\big) \cdot \\
&\Big(\frac{1}{2}\big(1 - \cos(2\pi f\epsilon)\big)N_s \sum_{j=-\infty}^{\infty} \text{sinc}^2\big(\text{N}_\text{s}\pi\text{T}_\text{f}(\text{f} - \frac{\text{j}}{\text{T}_\text{f}})\big) - 1\Big) \\
&+ \frac{1}{2}\big(1 + \cos(2\pi f\epsilon)\big)\frac{N_s}{T_s} \sum_{r=-\infty}^{\infty} \delta(f - \frac{r}{T_s}) \cdot \\
&\sum_{i=-\infty}^{\infty} \text{sinc}^2\big(\text{N}_\text{c}\pi\text{T}_\text{c}(\text{f} - \frac{\text{i}}{\text{T}_\text{c}})\big) \cdot \sum_{j=-\infty}^{\infty} \text{sinc}^2\big(\text{N}_\text{s}\pi\text{T}_\text{f}(\text{f} - \frac{\text{j}}{\text{T}_\text{f}})\big)\Bigg],
\end{aligned} \qquad (2.10)$$

where $\text{sinc}(\text{x}) = \frac{\sin(\text{x})}{\text{x}}$. The PSD of the modulation scheme with the infinite TH sequence also consists of a continuous component and a discrete component, observed as with the modulation scheme with the finite TH sequence. However, it is observed that the spectral lines of the discrete component appear at multiples of $\frac{1}{T_s}$. Thus, the effect of the discrete component on the PSD can be mitigated by increasing the length of TH sequence, although the discrete component cannot be eliminated.
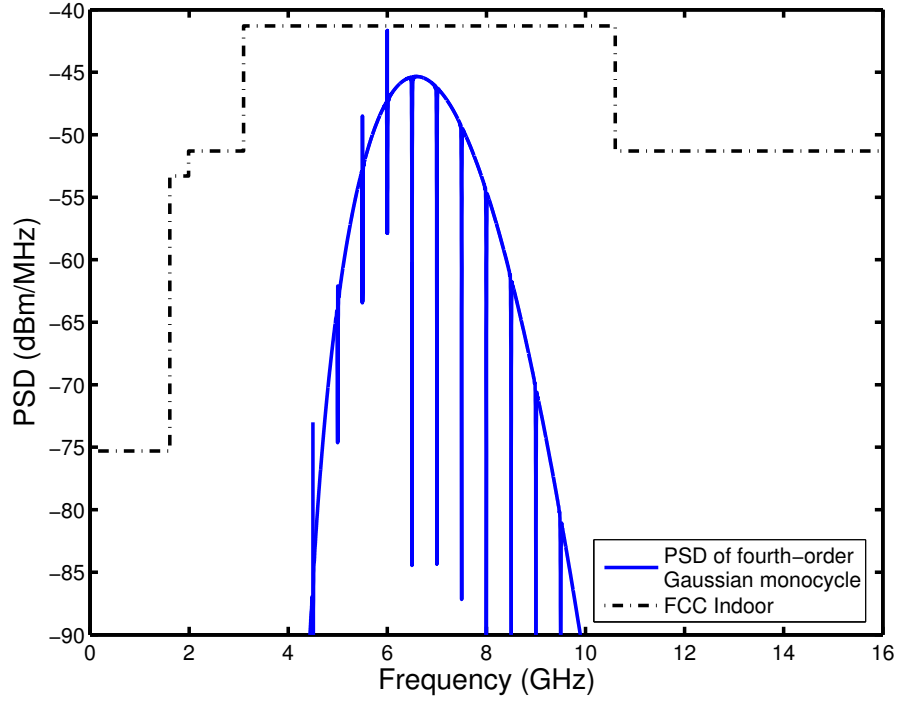
Figure 2.2: PSD of fourth-order Gaussian monocycle with an infinite TH sequence

Fig. 2.2 shows the PSD of fourth-order Gaussian monocycle with an infinite TH sequence. As shown in the figure, the spectral shape of the radiated signals is dominated by the pulse shape. In addition, the spectral lines of the discrete component is obvious in the figure, and it is confirmed that the modulation scheme also has an important influence on the spectral shape of the radiated signals in the TH-PPM UWB systems. The parameters used for the simulation are presented in Table 2.1.

Table 2.1: Simulation parameters for PSD of radiated fourth-order Gaussian monocycle with an infinite TH sequence

Parameter	Value
Time offset ϵ	0.2ns
TH chip T_c	2ns
Frame period T_f	50ns
Symbol duration T_s	200ns
N_s	4
N_c	8
τ_p for Gaussian monocycle	35ps

2.3 Previous Pulse Shapes

As shown in the previous section, the pulse shape is crucial because it plays an important role in shaping the PSD of the radiated signals. Thus, the challenge is to shape the spectrum by changing the pulse shape. In this section, the previous single type of waveforms are introduced, and then multiple orthogonal waveforms are reviewed.

2.3.1 Single Type of Waveform

The most commonly referred Gaussian monopulses were generated by using a rectangular beam waveguide resonator antenna [50]. The antenna was made by drilling circular holes on a rectangular beam waveguide resonator. Since it was easy to fabricate the antenna at low cost, the Gaussian monopulses became attractive waveforms for monopulse radar and tracking

[50]. After UWB large current radiator (LCR) antennas introduced [51], extremely short pulses, typically in the range of nanoseconds, could be generated by an inexpensive technology (CMOS chips) [39]. With LCR antennas, the short pulse can be generated by providing a step-function current. The short shape is called as a Gaussian pulse because its shape resembles a bell curve and different versions of the Gaussian pulses may be generated by applying derivatives to the zeroth-order Gaussian monocycle.

In addition to the fractional bandwidth requirement of UWB pulses, another fundamental characteristic of the UWB pulses is to have a zero DC offset for power-efficient radiation. Besides the most commonly adopted Gaussian pulses, satisfying these two conditions, several single type of waveforms (such as the Manchester monocycle, the Return-to-Zero Manchester monocycle as well as the Laplacian, Rayleigh, and cubic monocycle) have been proposed for UWB impulse radio systems [39] [52] [53] [54]. The Gaussian pulse, which is of the zeroth-order, can be represented as

$$p_{G0}(t) = A \cdot \exp\left[-2\pi\left(\frac{t}{\tau_p}\right)^2\right], \tag{2.11}$$

where A and τ_p are the amplitude and the bandwidth scaling factor, respectively. The most widely reported second-order Gaussian monocycle is given by

$$p_{G2}(t) = \left[1 - 4\pi\left(\frac{t}{\tau_p}\right)^2\right]\exp\left[-2\pi\left(\frac{t}{\tau_p}\right)^2\right]. \tag{2.12}$$

The Laplacian pulse is represented by

$$p_L(t) = \frac{1}{2\tau_p}\left[1 - \left(\frac{t}{\tau_p}\right)^2\right]\exp\left[-\frac{t}{\tau_p}\right], \tag{2.13}$$

and the Rayleigh pulse is given by

$$p_R(t) = \frac{t}{\tau_p^2} \exp\left[-\frac{t^2}{2\tau_p^2} \right], \tag{2.14}$$

and the cubic monocycle is represented by

$$p_C(t) = \frac{t^3}{\tau_p^4} \exp\left[-\frac{t^2}{2\tau_p^2} \right]. \tag{2.15}$$

All the above waveforms and their spectra are shown in Fig. 2.3. As shown in the figure, however, the waveforms violate FCC spectral constraints. Thus, there have been challenges of designing new pulses, satisfying with desirable spectral properties [32] [35] [36] [43] [55] [56] [57] [58] [59]. Moreover, it is known that the PSDs of the Gaussian pulses with orders higher than three can meet the FCC spectral constraints for indoor UWB communications when suitable values of τ_p are selected. The nth-order Gaussian monocycle is given by

$$p_{Gn}(t) = A_n \frac{d^n}{dt^n} \exp\left[-2\pi \left(\frac{t}{\tau_p} \right)^2 \right], \tag{2.16}$$

where A_n is a factor for normalization, and the PSDs of fourth- and fifth-order Gaussian monocycles and their PSDs are shown in Fig 2.4.

2.3.2 Multiple Orthogonal Waveforms

When UWB systems using orthogonal pulses were introduced [60], [61], the orthogonal pulses were based on coded monocycles or coded baseband waveforms. For the UWB pulse design, however, it may not be difficult to find orthogonal waveform sets mathematically; it is difficult, however, to find an

30
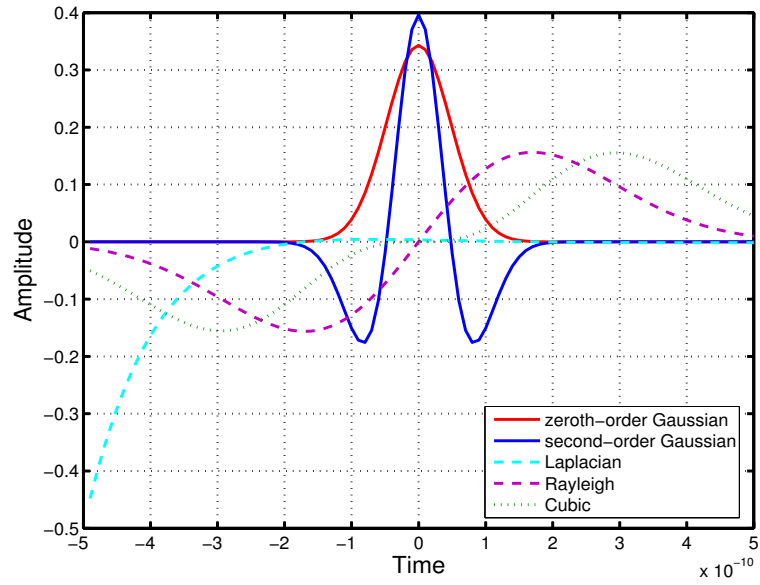
(a)
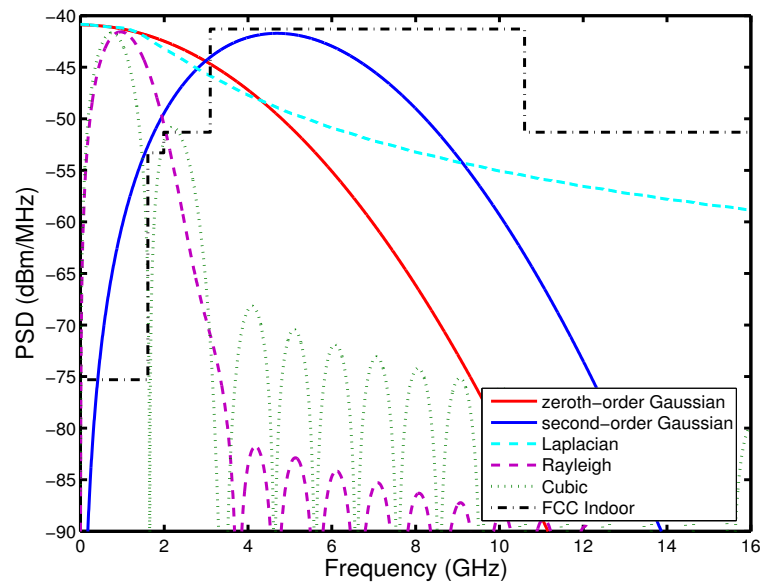
(b)

Figure 2.3: Various pulse shapes and their PSDs when $\tau_p = 0.17$ns (a) Pulse shapes and (b) PSDs

31
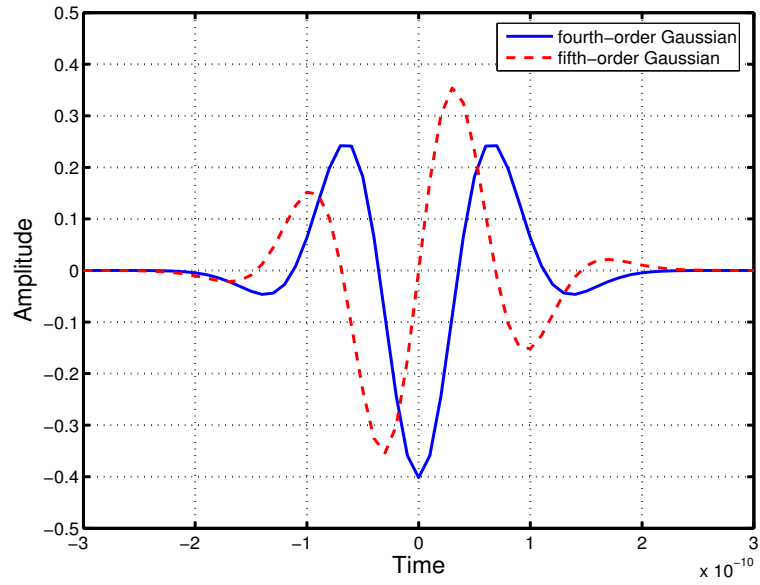
(a)
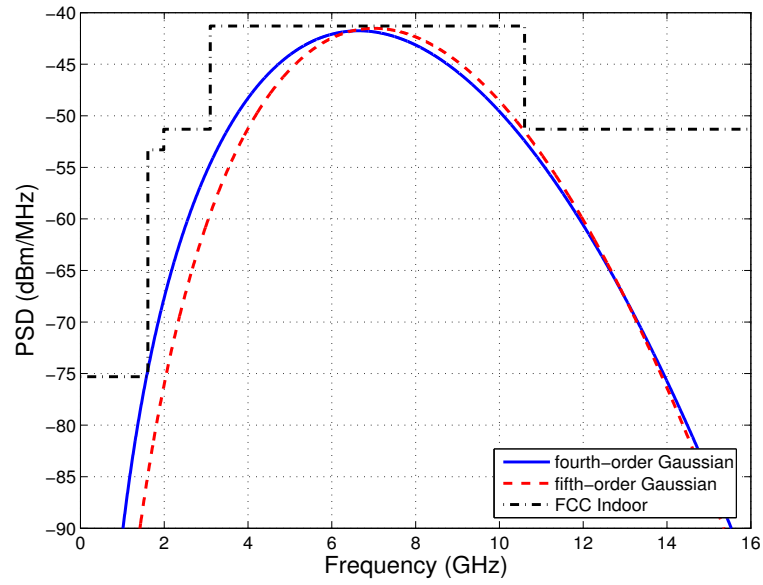
(b)

Figure 2.4: Fourth- and fifth-order Gaussian monocycles and their PSDs when $\tau_p = 0.17$ns and $\tau_p = 0.18$ns are selected for fourth- and fifth-order Gaussian monocycles, respectively (a) Pulse shapes and (b) PSDs

32

orthogonal set within which all the waveforms fit the FCC spectral mask well. Recently, the algorithms for designing multiple orthogonal pulses that satisfy the FCC constraints have been developed to achieve high data-rate transmissions and/or an enhancement of communication reliability. Such algorithms are the modified Hermite polynomial function (MHP) and a pulse design algorithm utilizing ideas of the prolate spheroidal wave function [32] [33] [36] [37] [38] [62] [63] [64].

Hermite pulses or Hermite functions were introduced in [65], and the Hermite transform was used in [66] to exploit spatio-temporal relationships in image processing. In addition, modified Hermite polynomials have been used to create orthogonal wavelets for multicarrier data transmission over high-rate digital subscriber loops [67] and UWB communications [62] [68]. In [68], a set of modulated orthogonal Hermite pulses were used for an M-ary biorthogonal communication UWB system. Given $M/2$ orthogonal Hermite pulses, $M/2$ waveforms were additionally generated by applying minus signs to the orthogonal pulses. Thus, the data rate can be enhanced by transmitting different waveforms. However, the proposed M-ary biorthogonal modulation scheme is based only on the different pulse shapes, which is called *pulse shape modulation* (PSM). Since PSM can be combined with conventional PPM, a higher data rate can be achieved with orthogonal waveforms. The combined PPM-PSM scheme will be discussed in the following Chapter 5.

The modified Hermite function is defined as

$$h_n(t) = (-1)^n \exp\left[\frac{t^2}{4}\right] \frac{d^n}{dt^n}\left(\exp\left[\frac{-t^2}{2}\right]\right), \qquad (2.17)$$

where $n=$ 0, 1, 2,... and $-\infty < t < \infty$. Examples of pulses from zeroth- to ninth-order polynomials are presented as follows:

$$h_0 = \frac{1}{\sqrt{1 \cdot \sqrt{0.5\pi}}} \cdot e^{\frac{-t^2}{4}} \tag{2.18}$$

$$h_1 = \frac{1}{\sqrt{1 \cdot \sqrt{0.5\pi}}} \cdot t \cdot e^{\frac{-t^2}{4}} \tag{2.19}$$

$$h_2 = \frac{1}{\sqrt{2 \cdot \sqrt{0.5\pi}}} \cdot (t^2 - 1) \cdot e^{\frac{-t^2}{4}} \tag{2.20}$$

$$h_3 = \frac{1}{\sqrt{6 \cdot \sqrt{0.5\pi}}} \cdot (t^3 - 3t) \cdot e^{\frac{-t^2}{4}} \tag{2.21}$$

$$h_4 = \frac{1}{\sqrt{24 \cdot \sqrt{0.5\pi}}} \cdot (t^4 - 6t^2 + 3) \cdot e^{\frac{-t^2}{4}} \tag{2.22}$$

$$h_5 = \frac{1}{\sqrt{120 \cdot \sqrt{0.5\pi}}} \cdot (t^5 - 10t^3 + 15t) \cdot e^{\frac{-t^2}{4}} \tag{2.23}$$

$$h_6 = \frac{1}{\sqrt{720 \cdot \sqrt{0.5\pi}}} \cdot (t^6 - 15t^4 + 45t^2 - 15) \cdot e^{\frac{-t^2}{4}} \tag{2.24}$$

$$h_7 = \frac{1}{\sqrt{5040 \cdot \sqrt{0.5\pi}}} \cdot (t^7 - 21t^5 + 105t^3 - 105t) \cdot e^{\frac{-t^2}{4}} \tag{2.25}$$

$$h_8 = \frac{1}{\sqrt{40320 \cdot \sqrt{0.5\pi}}} \cdot (t^8 - 28t^6 + 210t^4 - 420t^2 + 105) \cdot e^{\frac{-t^2}{4}} \tag{2.26}$$

$$h_9 = \frac{1}{\sqrt{362880 \cdot \sqrt{0.5\pi}}} \cdot (t^9 - 36t^7 + 378t^5 - 1260t^3 + 945t) \cdot e^{\frac{-t^2}{4}}, \tag{2.27}$$

and their time domain representations and PSDs are shown in Fig 2.5 and 2.6.

All the MHP pulses have zero DC components, and all the pulses are mutually orthogonal when all the width parameter are the same. Other favorable properties of the MHP pulses are that the time duration and the frequency bandwidth of the pulses do not change significantly with respect to the order, while the orthogonality of the pulses is preserved even with the differentiating effects of the transmit/receive antenna [37] [38]. Based on these properties,

34
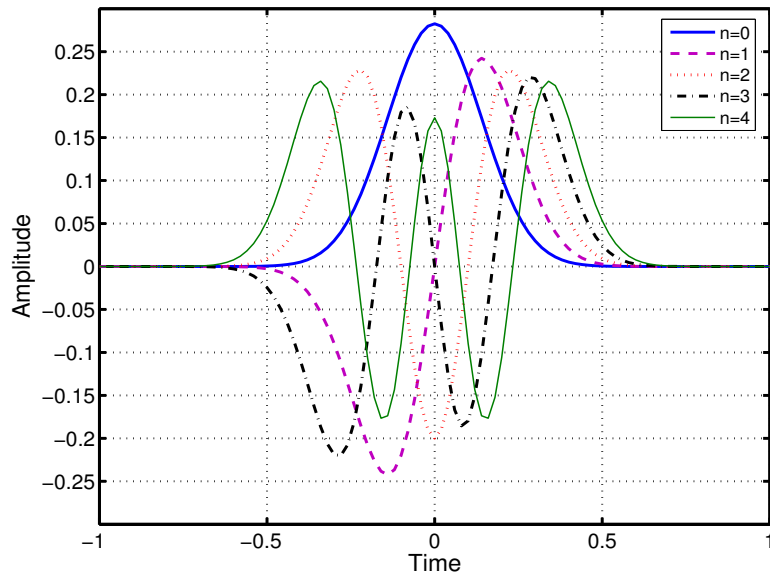
(a)
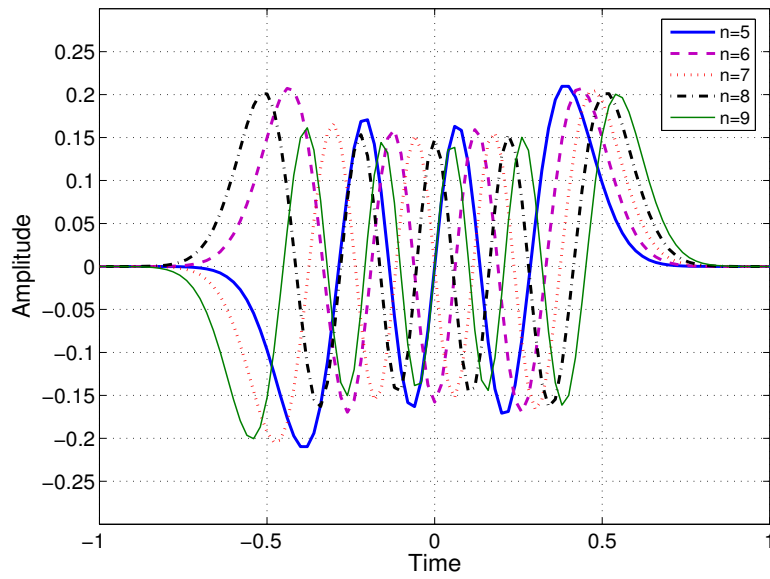
(b)

Figure 2.5: Normalized MHP pulses of orders (a) $n=$ 0, 1, 2, 3, 4 and (b) $n=$ 5, 6, 7, 8, 9.
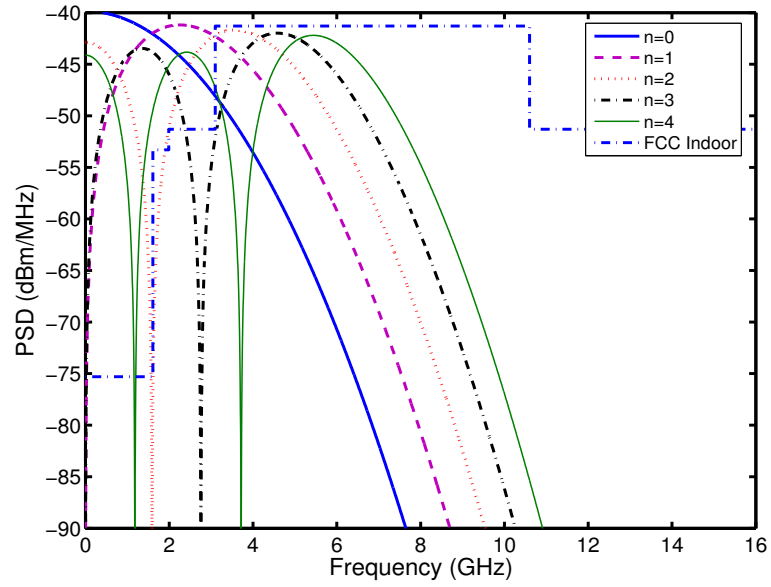
(a)
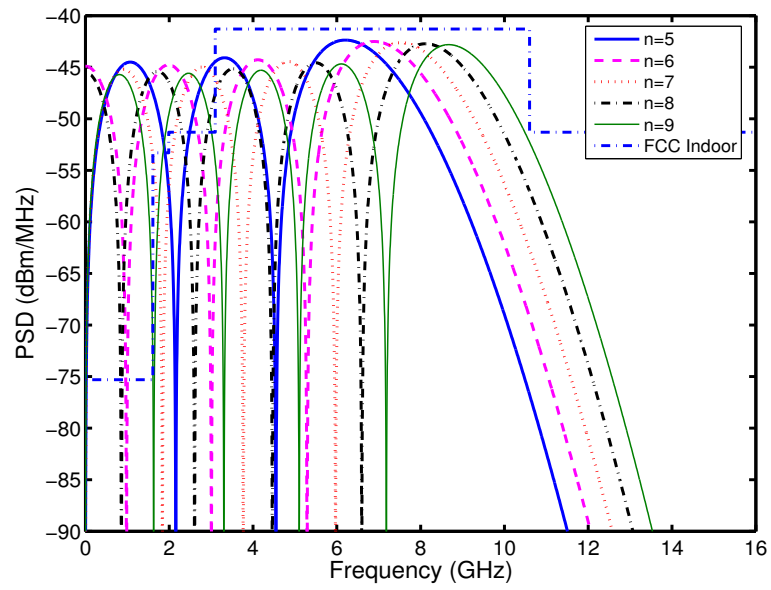
(b)

Figure 2.6: PSDs of the normalized MHP pulses of orders (a) n= 0, 1, 2, 3, 4 and (b) n= 5, 6, 7, 8, 9.

data rates higher than those of the conventional single pulse systems can be achieved by transmitting multiple orthogonal pulses simultaneously. Although the multiple orthogonal pulses can be generated by increasing the order of the MHP, the downside of increasing the order of the MHP has also been reported. Since the higher-order MHP pulses are generated by differentiation, the complexity of the higher-order pulses increases, and the autocorrelation of the waveforms becomes narrower. With the commonly employed correlation receiver, therefore, the probability of error increases as the higher-order pulses are used because the autocorrelation peak becomes narrower. Moreover, the orthogonality of the waveforms is lost when the pulse width parameters are not the same [69]. Particularly, when the received waveform consists of a number of multipath components that experienced different dispersive effects from the channel, the orthogonality of the waveforms will be destroyed. Therefore, additional techniques are required, such as the application of multiplicative delay operators to the multipath components and the exploitation of the correlation functions of the Hermite functions against the same order Hermite function with a different width parameter.

After the prolate spheroidal (PS) functions were introduced in [70] [71], a novel pulse design algorithm based on PS functions was proposed for UWB communications [32] [33], and a performance analysis of the system utilizing the proposed PS pulses was conducted in [63] [64]. The PS functions are considered very useful in UWB communications because both the time duration and the frequency band, which are expensive resources, can be limited simul-

37

taneously. Based on the PS functions, a novel pulse, $\psi(t)$, can be obtained by solving

$$\lambda\psi(t) = \int_{-T_p/2}^{T_p/2} \psi(\tau)h(t-\tau)d\tau, \qquad (2.28)$$

where T_p is the pulse width, and $h(t)$ is the impulse response of the bandpass filter, which operates between 3.1 GHz and 10.6 GHz. In [32] [33], (2.28) was solved by discretization, and the PS pulses whose power spectra fit the desired frequency mask were numerically generated. For reference, two examples of pulses, which were generated with $N = 64$ and $T_p = 1$ns, and their PSDs are plotted in Fig. 2.7. As shown in the figure, the PSDs of two PS pulses not only meet the FCC spectral mask for indoor UWB systems, but they are also concentrated mostly in the 3.1-10.6 GHz frequency band.

PS pulses have many advantages when they are compared with MHP pulses [32]. One important advantage is that the PS pulses do not need either frequency shifting or bandpass filters. Meanwhile, the lower-order MHP pulses require frequency shifting, as shown in Fig. 2.6 (a), and the higher-order MHP pulses need bandpass filters because multiple lobes of approximately equal amplitude exist over broad bandwidths, as shown in Fig. 2.6 (b).

The pulse design algorithm based on PS functions is very sensitive to the pulse width, T_p [32]. Thus, the PSDs of the pulses with smaller T_p have large sidelobes that can cause strong adjacent channel interference. In addition, it has been shown that the cross-correlation between two PS pulses is zero only at the sampling instants, and the values of the cross-correlation at other times are very large [32]. Therefore, the two PS pulses are considered

38
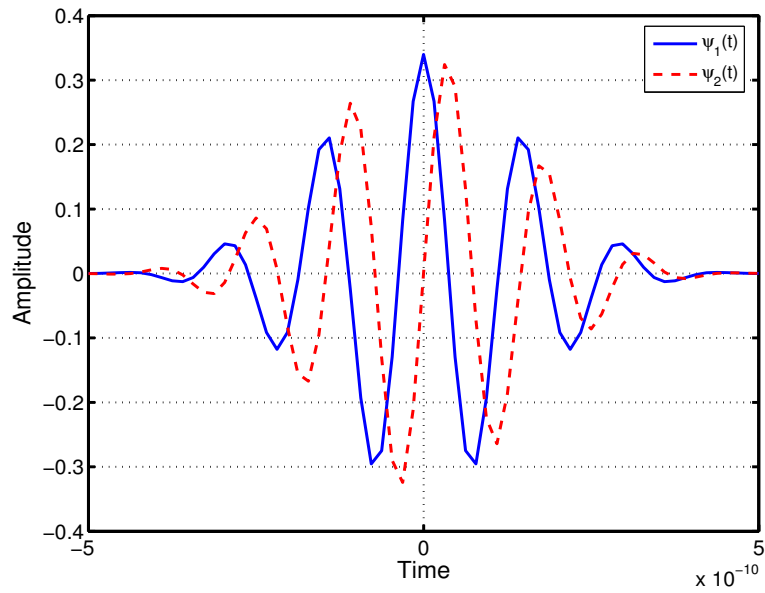
(a)
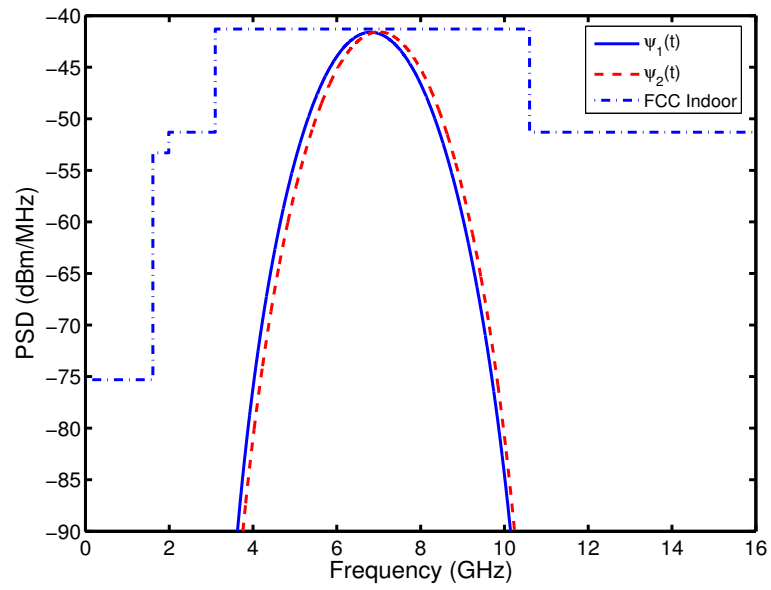
(b)

Figure 2.7: Normalized prolate spheroidal pulses and their PSDs (a) $\psi_1(t)$ and $\psi_2(t)$ and (b) PSDs

39

as inappropriate waveforms for asynchronous multiuser UWB systems [72]. Moreover, the mutual orthogonality of the PS pulses is not preserved with the distortion from the channel and the characteristics of the antennas. Thus, the received PS pulses do not preserve the orthogonality, which has a notable impact on the performance of the correlation receiver [73].

2.4 Antenna Modeling

As for an antenna model, the transmitted pulse $p_{txed}(t)$ can be expressed as

$$p_{txed}(t) = m(t) * p_{tx}(t) * a_1(t) * a_2(t) \qquad (2.29)$$

where $*$ is convolution, $m(t)$ represents a modulation scheme, $p_{tx}(t)$ is the pulse shape before the antenna, $a_1(t)$ is the impulse response of antenna, and $a_2(t)$ is the simplified differentiator model derived by Maxwell's equation for radiated/received waveform.

The effect of the antenna has been commonly modeled as differentiation in the previous studies of Dr. M. Z. Win, Dr. R. A. Scholtz, Dr. R. Kohno, and Dr. F. Ramirez-Mireles [36] [52] [74] [75], because they have focused on the pulse shapes and the performance analysis with the simplified received waveforms. They assumed ideal antennas with unity gain over the whole occupied bandwidth; that is, the frequency response of $a_1(t)$ is unity.

In this dissertation, I also focus on the design of new pulse shapes and the performance analysis of the system using the proposed multiple orthonormal pulses. Therefore, I adopted the same ideal antenna model in my

dissertation to ensure a fair comparison with other waveforms. Thus, examples of the proposed pulses are produced with the ideal antenna model, which has unity gain over the whole occupied bandwidth. There is a debate whether the antenna pair relationship is a first or second derivative. However, the proposed algorithm for pulse shape design in my dissertation is still valid with either of antenna models because the impulse response of antenna pair is used in formulation of the pulse shape design as will be shown in Chapter 3.

On the other hand, when the impulse response of a fielded antenna is measured and adopted for the systems considered, the transmitted and the received pulse shapes will be distorted by the antenna characteristics. Thus, there have been studies in which characterizations of UWB antennas have been investigated, and antenna models have been developed [76] [77]. The developed antenna models can be adopted for system-level simulations. Moreover, it has been shown that the frequency-domain patterns obtained from a time-domain antenna model of a Vivaldi antenna match well with the measured frequency-domain patterns [76].

Thus, in future work the pulse shape design can be investigated with more realistic antenna models. With the characteristics of the fielded antennas, furthermore, an optimum system design can be developed by simultaneously considering pulse shape design and modulation schemes.

2.5 Channel Modeling

The UWB indoor environment is characterized by a dense array of multipaths. An early channel model, which is called the Saleh-Valenzuela indoor channel model, was developed by two engineers, A.A.M. Saleh and R.A. Valenzuela, in 1987 [78]. The Saleh-Valenzuela model is based on measurements utilizing low-power 10ns, 1.5 GHz, radarlike pulses in a medium-size building (AT&T Bell Laboratories, Crawford Hill location in Holmdel, NJ). The results of measurements revealed that the observed channel was slowly time varying, with the delay spread extending over a range up to about 200ns and RMS values of up to about 50ns. Thus, based on the results of the multipath propagation measurements, a simple statistical multipath model of the indoor radio channel, which fit the measurements well and was extensible to other buildings, was developed.

In the Saleh-Valenzuela channel model, the multipath components arrive at the receiver in clusters, which have a Poisson distribution with rate Λ, and the rays within a cluster also form a Poisson arrival process with different rate λ, where $\lambda > \Lambda$. Thus, the complex, low-pass channel impulse response is given by

$$h(t) = \sum_{p=0}^{\infty} \sum_{q=0}^{\infty} \alpha_{p,q} e^{j\theta_{p,q}} \delta(t - \xi_p - \tau_{p,q}), \tag{2.30}$$

where $\delta(t)$ is the Dirac delta functional; $\alpha_{p,q}$ is the gain of the qth ray of the pth cluster, which is an independent Rayleigh random variable with an exponentially decaying power delay profile; $\theta_{p,q}$ is the phase of each multipath component, which is an independent uniform random variable over $[0, 2\pi)$; ξ_p

represents the delay of the pth cluster; and $\tau_{p,q}$ represents the delay of the qth ray of the pth cluster.

Recently, Intel Labs performed experiments to measure the indoor UWB channel in the 2-8 GHz band and developed a modified version of the Saleh-Valenzuela channel model [79]. Then, in November 2002 the IEEE 802.15.3a Task Group recommended a channel model based on the modified Saleh-Valenzuela channel model because the clustering phenomenon had been experimentally confirmed. In the modified Saleh-Valenzuela channel model, the Rayleigh distribution for the gain of each multipath component is replaced by the log-normal distribution, and the uniform distribution for the phase is replaced by random polarity, where $\theta_{p,q} = 0$ or π, to represent a real-valued channel model. Furthermore, based on the minimum multipath resolution, the impulse response of the channel can be expressed as

$$h(t) = \sum_{l=0}^{L-1} \alpha(l)\delta(t - lT_r), \qquad (2.31)$$

where L is the number of resolvable multipath components; $\delta(t)$ is the Dirac delta functional; $\alpha(l)$ is the fading coefficient, which is log-normal-distributed with random polarity, of the lth resolvable path; and T_r represents the minimum multipath resolution. Fig. 2.8 shows a typical realization of the channel impulse response generated by using the modified Saleh-Valenzuela channel model. The same parameters, which are given by Table 11 of [79], are chosen for a none-line-of-sight channel model.

According to the multipath characteristics of an indoor UWB channel,

43
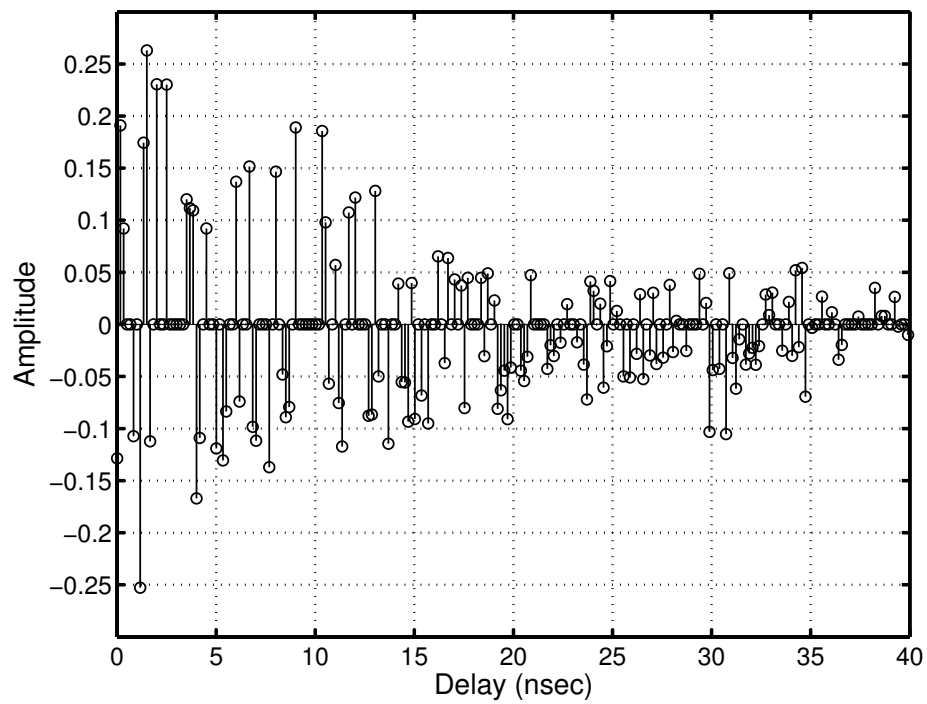
Figure 2.8: A typical realization of the channel impulse response generated using the modified Saleh-Valenzuela channel model

the received signal may contain a significant number of resolvable multipath components even when a single pulse is transmitted. Therefore, a RAKE receiver can be considered for collecting the resolvable multipath components to exploit the multipath diversity. However, a simple RAKE receiver with a single finger is assumed because in this dissertation I am focusing on the design of orthonormal waveforms and UWB systems exploiting orthonormal waveforms. Moreover, the dissertation provides an analysis of the impact of the properties associated with the proposed pulses, such as their auto- and cross-correlations, on the correlation receiver of the UWB system based on pulse position modulation, as well as a comparison of the proposed pulses with other well-known multiple orthogonal pulses. In addition, the BER performance of the system can be enhanced by exploiting multipath diversity. Thus, systems collecting more energy by using a RAKE receiver with multiple fingers and optimal schemes for combining fingers will be considered as a future work.

2.6   Summary

In this dissertation, a method is proposed for designing waveforms that comply with the FCC spectral mask and preserve the orthogonality at the receiver under arbitrary channel conditions. However, although the proposed method can design orthogonal waveforms for a multipath fading channel, for a fair comparison with different waveforms, example waveforms are produced as received waveforms at the correlation receiver under an AWGN channel condition.

For example, when the MHP pulses are transmitted through the frequency-selective fading channel, the orthogonality among the MHP pulses may not be preserved at the correlation receiver. Alternatively, MHP pulses can be used as the received waveforms to preserve the orthogonality at the correlation receiver. In that case, however, the different pulse shapes should be transmitted at the transmitter and the PSDs of the radiated pulses should be carefully checked for whether the FCC spectral mask is satisfied or not. Therefore, MHP pulses may not satisfy both the FCC mask and the orthogonality at the correlation receiver.

Then, by using the computer simulations based on the modified Saleh-Valenzuela channel, the performance of the proposed schemes using the proposed waveforms are compared with that of the systems using different waveforms. Furthermore, performance comparisons with different waveforms are performed under various conditions, such as non-resolvable multipath fading, timing mismatch, and multiuser interference.

Chapter 3

New Orthonormal Pulses for Indoor UWB Systems

Ultra-wideband (UWB) is a promising short-range radio technique for high data rates in indoor wireless personal area networks (WPANs) and base-band multiple access schemes [52]. As discussed in the preceding chapters, UWB radio is based on the radiation of a train of extremely short pulses, typically in the range of subnanoseconds, that results in low power spectral density (PSD) over extremely broad bandwidth.

Since the frequency spectrum of the UWB systems is extremely broad, it can cause interference with other systems. Thus, the FCC has regulated the main frequency band of the UWB systems to be between 3.1 GHz and 10.6 GHz [1]. However, the zeroth- and first-order Gaussian monocycle pulse that is commonly used in UWB impulse radio does not meet the FCC indoor spectral constraints and should be filtered to contain its power distribution within a frequency band from 3.1 GHz to 10.6 GHz [1] [31] [32]. Because of the limitations of the zeroth- and first-order Gaussian monocycle pulse, the design of new pulses, such as the MHP pulses and the PS pulses [32] [36], has been challenging. However, frequency shifting and bandpass filters are required for the MHP pulses of order 0 or 1 and higher-order MHP pulses,

respectively, to satisfy the FCC spectral mask. The mutual orthogonality of the pulses, which are generated using the prolate spheroidal function, is not preserved, because of the distortion of the channel and the characteristics of the antennas. Thus, the pulse design algorithm does not provide the orthogonality for received pulses, which has a notable impact on the performance of the correlation receiver [32] [36].

In this chapter, novel pulses are proposed that not only meet the FCC power spectral mask for indoor UWB systems but also preserve orthogonality at the correlation receiver. The proposed pulses are derived from a parametric closed-form solution. Thus, multiple orthonormal pulses that comply with the FCC mask without additional frequency shifting or bandpass filters can be generated for high-data-rate communications and/or the enhancement of transmission reliability.

The chapter is organized as follows. In Section 3.1, a system model for impulse radio systems is introduced in terms of the waveforms at both the transmitter and receiver sides. New orthonormal waveforms for indoor UWB system are proposed in Section 3.2. In Section 3.3, two examples of the waveforms are presented, and the power spectral densities of these pulse shapes are examined for compliance with the FCC frequency emission regulations. In Section 3.4, a modulation scheme using two orthonormal pulses is discussed, and its effectiveness is demonstrated by computer simulations. The summary is given in Section 3.5.

3.1 System Model

When the modulation scheme is represented as $m(t)$ in the UWB systems, the radiated pulse $p_{txed}(t)$ can be expressed as

$$p_{txed}(t) = m(t) * p_{tx}(t) * a_{tx}(t) \tag{3.1}$$

where $p_{tx}(t)$ is the pulse shape before the antenna and $a_{tx}(t)$ is the impulse response of the transmit antenna. In terms of pulse shape, however, it can simply be considered that the single pulse is transmitted and received via the antennas and channel. Thus, the received pulse $p_{rx}(t)$ can be expressed as

$$p_{rx}(t) = p_{tx}(t) * a_{tx}(t) * h_{ch}(t) * a_{rx}(t) \tag{3.2}$$

where $h_{ch}(t)$ and $a_{rx}(t)$ are the impulse responses of the channel and a receiving antenna, respectively. By arranging the Fourier transform of (3.2) for $P_{tx}(f)$, the frequency response of the pulse shape before radiation is derived as

$$P_{tx}(f) = \frac{P_{rx}(f)}{A_{tx}(f)H_{ch}(f)A_{rx}(f)} \tag{3.3}$$

The PSD of the radiated signal is related to the pulse shape and the modulation scheme. Thus, the PSD of the radiated pulse is derived from (3.1) as $S_{txed}(f) = |P_{tx}(f)A_{tx}(f)|^2 S_M(f)$ and can be rewritten with (3.3) as

$$S_{txed}(f) = \left| \frac{P_{rx}(f)}{H_{ch}(f)A_{rx}(f)} \right|^2 S_M(f) \tag{3.4}$$

where $S_M(f)$ is the PSD of a known modulation scheme [42]. When the frequency responses of the channel and antennas are also known, I can design

the received pulse to meet the FCC indoor mask with (3.4). The pulse shape at the transmitter is derived as the inverse Fourier transform (IFT) of (3.3) with the designed pulse.

3.2 Orthonormal Waveforms

In this section, I propose novel orthonormal waveforms as the received pulses. The basic waveform for the proposed waveforms is obtained from the Battle-Lemarie wavelet and expressed as

$$\psi(t) = \sqrt{2} \sum_l \sum_m g_l c_m \beta_n(2t - l - m) \tag{3.5}$$

where g_l and c_m are coefficients, and $\beta_n(t)$ is a B-spline function of order n [80]. With dilation and translation, a set of basic waveforms, $\{\psi_{j,k}(t)\}$, is defined as

$$\psi_{j,k}(t) = 2^{\frac{j}{2}} \psi(2^j t - k) \tag{3.6}$$

where $-\infty < j, k < \infty$ are integers, and the set forms an orthonormal basis of $L^2(R)$ [80]. The dilation parameter j doubles the center frequency of the waveform as it increases by 1, and the translation parameter k changes the phase of the waveforms. Thus, when n=3, I obtain the waveform whose center frequency is around 4 GHz with j=3 or 8 GHz with j=4, and those pulses satisfy the FCC indoor requirements. A different set of orthonormal waveforms also can be generated by changing the order of the B-spline function, although the orthonormality is preserved only within the set with a fixed n.

Since any two waveforms from the set $\{\psi_{j,k}(t)\}$ are orthonormal to each other, I can extend (3.6) with linear combinations. The extended set, $\{\gamma_{J,K}(t)\}$, is derived as

$$\gamma_{J,K}(t) = \frac{\sum_j \sum_k a_{j,k}\psi_{j,k}(t)}{\sqrt{\sum_j \sum_k |a_{j,k}|^2}} \tag{3.7}$$

where $J = \{j\}$ and $K = \{k\}$ are finite sets of integer j and k, respectively, and $\{a_{j,k}\}$ are coefficients. When the dilation parameter j is different from each other, any pair of waveforms in the extended set are orthonormal. Moreover, even if j is the same between the extended waveforms, the orthonormality can also be preserved by the exclusive combination of translation parameter, k. For example, $\gamma_{\{1\},\{1\}}$ is orthonormal with $\gamma_{\{1\},\{2\}}$, $\gamma_{\{1\},\{4\}}$, and $\gamma_{\{1\},\{6\}}$. In addition, $\gamma_{\{1\},\{3\}}$ and $\gamma_{\{1\},\{5\}}$ are also orthonormal with $\gamma_{\{1\},\{2\}}$, $\gamma_{\{1\},\{4\}}$, and $\gamma_{\{1\},\{6\}}$. Thus, the following extended waveforms are orthonormal to each other:

$$< \gamma_{\{1\},\{1,3,5\}}, \gamma_{\{1\},\{2,4,6\}} >= 0, \tag{3.8}$$

where $< a, b >$ indicates the inner product of a and b. From the extended set, (3.7), therefore, a subset of mutually orthonormal waveforms can be constructed if the basic waveform, $\psi_{j,k}(t)$, is used exclusively for all orthonormal waveforms within the subset.

The Fourier transform of the basic waveform, $\psi(t)$, is expressed as

$$\Psi(\omega) = -e^{-i\frac{\omega}{2}}H^*(\frac{\omega}{2} + \pi)\hat{\phi}(\frac{\omega}{2}) \tag{3.9}$$

where H^* represents complex conjugate of quadrature filter H, and $\hat{\phi}$ represents the Fourier transform of the scaling function $\phi(t)$ [80]. The Fourier

51

transform of the proposed waveforms, (3.7), is derived as

$$\Gamma_{J,K}(\omega) = \frac{\sum_j \sum_k a_{j,k} \Psi_{j,k}(\omega)}{\sqrt{\sum_j \sum_k |a_{j,k}|^2}}. \tag{3.10}$$

The subset of mutually orthonormal waveforms, (3.10), provides high flexibility for designing a desired pulse shape. Thus, the orthonormal pulses, which satisfy the FCC indoor spectral requirement, can be produced by solving a min-max problem based on (3.4). The pulse shapes at the transmitter also can be generated numerically by the inverse Fourier transform (IFT) of (3.3) with a specific B-spline of order n.

3.3 Examples of Pulses and Discussion

The basic waveform in (3.5) is generated numerically by using the orthogonalized B-spline function of order $(n = 3)$ [80], and the functions used for generation are briefly presented in Appendix A. With the basic waveform, two examples of pulses that satisfy the FCC indoor spectral mask as well as mutual orthonormality at the receiver are produced by (3.10). The frequency-domain representations of each pulse are described in (3.11) and (3.12), respectively,

$$\Gamma_{J_1,K_1}(\omega) = \frac{1}{\sqrt{3}} \sum_{k=-1}^{1} (-1)^k \Psi_{3,k}(\omega) \tag{3.11}$$

$$\Gamma_{J_2,K_2}(\omega) = \frac{1}{\sqrt{7}} \sum_{k=-3}^{3} a_{4,k} \Psi_{4,k}(\omega), \tag{3.12}$$

where $J_1 = \{3\}, K_1 = \{\pm 1, 0\}, J_2 = \{4\}, K_2 = \{\pm 3, \pm 2, \pm 1, 0\}$, and $\{a_{4,k}\} = \{-1, 1.5, -2.2, 2.2, -3, 1.75, -1.5\}$.

Since the antenna pair is assumed to be a second-order differentiator as discussed in Section 2.4, the pulses at the transmitter can be generated with the channel information from (3.3). Fig. 3.1 (a) shows two examples of pulses, $p_{tx1}(t)$ and $p_{tx2}(t)$, at the transmitter over an AWGN channel. Fig. 3.1 (b) shows the PSDs of the radiated signals of the two pulses $p_{tx1}(t)$ and $p_{tx2}(t)$ with pulse position modulation and infinite time hopping (PPM-TH) [42]. The PSDs of the two pulses not only meet the FCC spectral mask for the indoor UWB system, but their energy is mostly concentrated in the 3.1-10.6 GHz frequency band (about 94% of total energy is in the band for both pulses). The two examples of pulses, $p_{tx1}(t)$ and $p_{tx2}(t)$, can be generated by double integration of the received pulses or by (3.3) as follows:

$$p_{tx1}(t) = IFT\left\{\frac{\Gamma_{J_1,K_1}(\omega)}{(j\omega)^2}\right\} \tag{3.13}$$

$$p_{tx2}(t) = IFT\left\{\frac{\Gamma_{J_2,K_2}(\omega)}{(j\omega)^2}\right\}, \tag{3.14}$$

where $g_l = (-1)^l \frac{\sqrt{2}}{2\pi} \int_0^{2\pi} \sqrt{\frac{\cos^8(\omega/2)\{1208+1191\cos(\omega)+120\cos(2\omega)+\cos(3\omega)\}}{1208+1191\cos(2\omega)+120\cos(4\omega)+\cos(6\omega)}} e^{j\omega(1-l)} d\omega$ and $c_m = FT\left\{\frac{1}{\sqrt{\frac{17}{315}+\frac{4}{7}\cos^2(\omega/2)+\frac{38}{105}\cos^4(\omega/2)+\frac{4}{315}\cos^6(\omega/2)}}\right\}$, and the parameter values can be easily computed by using a scientific computing tool like Mathematica.

3.4   Modulation for High Data Rates

Since the proposed waveforms have the orthonormal property at the correlation receiver, additional information can be carried by the pulse shapes
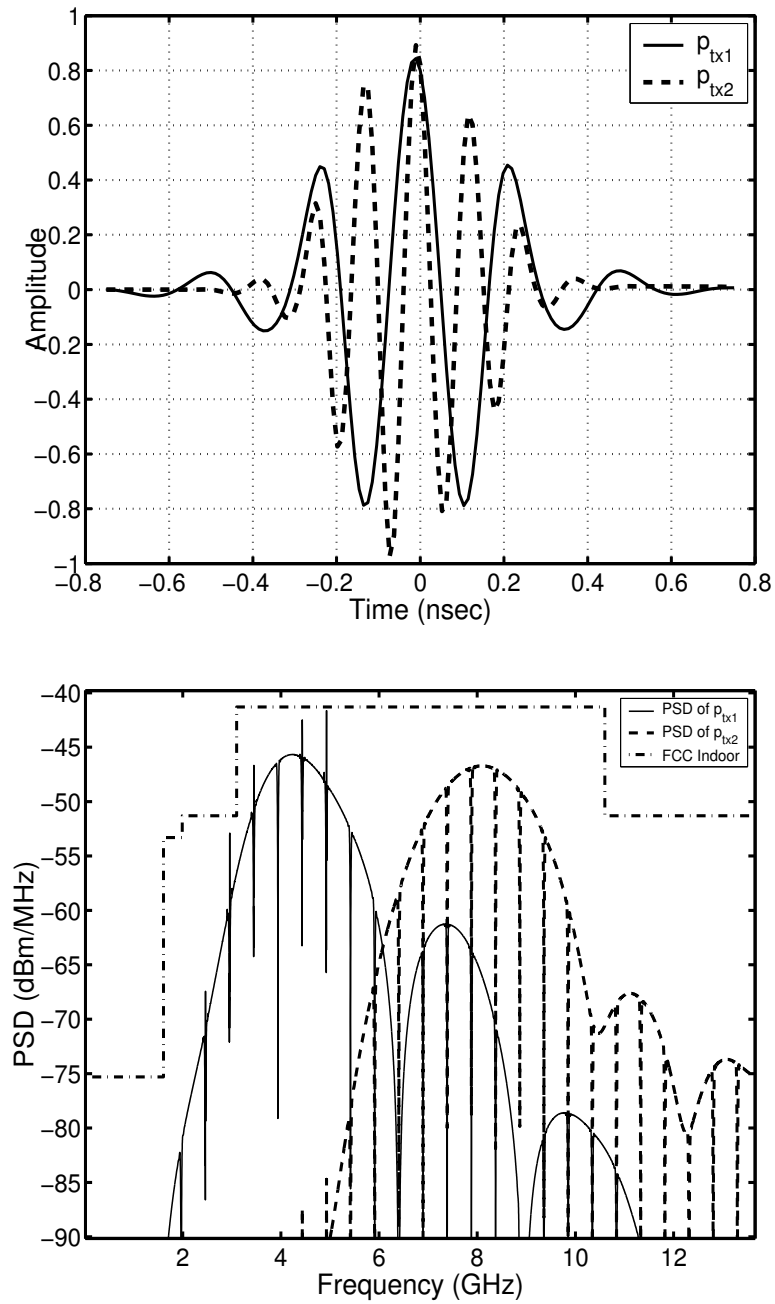
Figure 3.1: Example of pulses at the transmitter and their PSDs with FCC mask for indoor UWB system (a)Pulse shapes of $p_{tx1}(t)$ and $p_{tx2}(t)$ and (b)PSD

54

[37] [38] [81] [82]. For example, by employing PPM and pulse shape modulation (PSM) simultaneously (PPM-PSM), 2 bits of data can be transmitted with the two pulses, $p_{tx1}(t)$ and $p_{tx2}(t)$. Table 3.1 shows the modulation scheme to transmit 2 bits of data. Since only a single pulse is transmitted per pulse repetition time, the energy is kept constant when it is compared with 1-bit transmission [38]. The selection of pulse shape is based on the statistical properties of the source in the modulation scheme. If the probability of selecting the waveform $p_{tx1}(t)$ is q, then the probability of selecting the waveform $p_{tx2}(t)$ is $1 - q$. Thus, the PSD of the radiated pulses with PPM-PSM and infinite time hopping can be derived as

$$S_{txed}(f) = \frac{q|P_{rx1}(f)|^2 + (1-q)|P_{rx2}(f)|^2}{|H_{ch}(f)A_{rx}(f)|^2}S_M(f) \qquad (3.15)$$

where $P_{rx1}(f)$ and $P_{rx2}(f)$ are two examples of pulses from (3.11) and (3.12), respectively. Since (3.15) is the averaged PSD of each pulse, it also satisfies the FCC indoor mask. In the PPM, the optimal position primarily determines the BER performance of the correlation receiver, because the minimum auto-correlation of the received signal is derived directly from the optimal position [83]. The optimal position for a given waveform can be found by using the following function [83]:

$$\delta_{opt} = \arg \min_{\delta}[\int_{-\infty}^{\infty} p_{tx}(t)p_{tx}(t-\delta)dt]. \qquad (3.16)$$

This function will be discussed further in Chapter 4.

For the computer simulations, I used two truncated examples of pulses that contain 99.99% of the total energy because they decay exponentially [80].
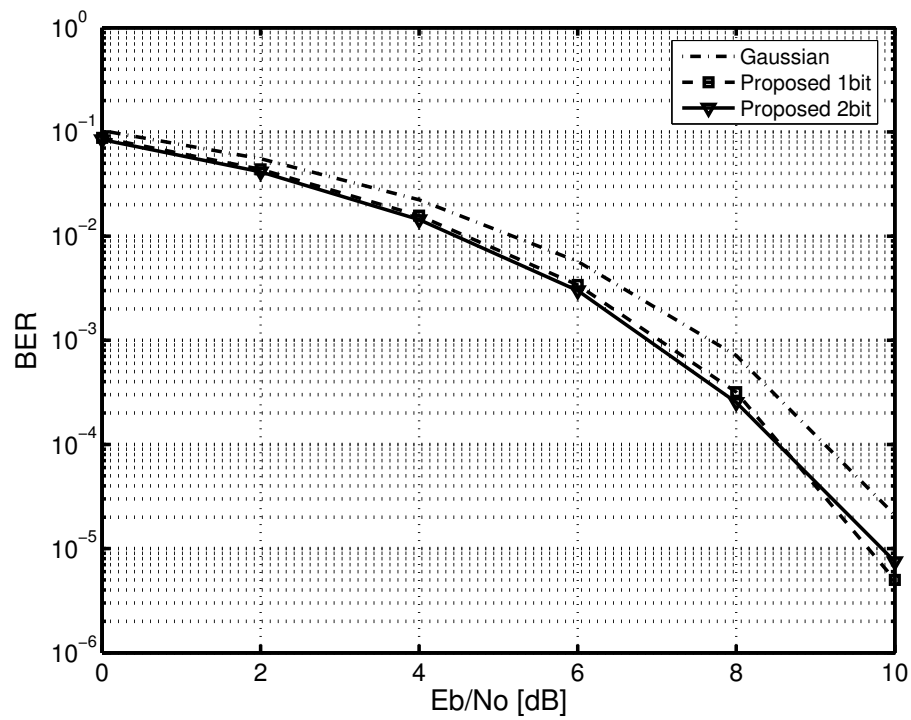
Figure 3.2: The error probability for the system using a Gaussian pulse (solid line) and the proposed systems using two pulses over an additive white Gaussian channel with variance $N_0/2$. Energy per bit is denoted as E_b.

Table 3.1: Modulation scheme for 2 bits

	Position	
Source	T_f	$T_f + \delta_{opt}$
00	p_{tx1}	0
11	0	p_{tx1}
01	p_{tx2}	0
10	0	p_{tx2}

Fig. 3.2 shows the BER performance of the system using a Gaussian pulse (solid line) and using two pulses in an AWGN channel with variance $N_0/2$. Under the assumption of unitary energy of all the waveforms and perfect synchronization between a transmitter and a receiver, the waveforms are detected by the correlation receiver with maximum likelihood detection. The sampling rate used in the simulation was 100 GHz. A conventional PPM with a proposed pulse is used for 1-bit transmission, and the PPM-PSM scheme with two proposed pulses is used for 2-bit transmission. When four different alphabets are used for 2-bit data transmission as shown in the Table 3.1, the detection process are performed with template, $v(t) \triangleq w_{rx}(x) - w_{rx}(x - \delta_{opt})$ where $w_{rx}(x)$ is a received pulse shape. As shown in Fig. 3.2, the BER performance of the systems that use the proposed pulses is better than that of the system using a Gaussian pulse. The reason for the difference is that the minimum autocorrelations of the proposed pulses are smaller than that of the Gaussian pulse [83]. Furthermore, it is shown that the modulation scheme with two proposed pulses achieves almost the same BER performance, while the data

rate is doubled. Thus, high-data-rate communications can be achieved by the proposed orthonormal pulses via PPM-PSM. The modulation schemes for data rate enhancement will be discussed more in Chapter 5.

3.5 Summary

I have proposed novel pulses that not only meet the FCC indoor spectral mask without additional filtering or frequency shifting but also preserve orthonormality at the correlation receiver. Since the proposed pulses have an orthonormal property, multiple access schemes or high data rates for UWB systems can be achieved by using the proposed waveforms. Enhancements to the transmission reliability of the UWB systems will be presented in Chapter 6. Two examples of pulses that satisfy the FCC indoor spectral mask were shown from the proposed orthonormal set, and their PSDs were also presented.

The proposed subset of mutually orthonormal waveforms provides high flexibility in designing a desired pulse shape. Thus, the orthonormal pulses that comply with the FCC indoor spectral mask can be generated for high data communications and/or the enhancement of transmission reliability in UWB systems. Computer simulations showed that high-data-rate communications could be achieved by using the proposed orthonormal pulses via PSM and PPM.

Chapter 4

Performance Evaluation of TH-PPM UWB Systems Exploiting Orthonormal Pulses

The auto- and cross-correlation characteristics of the pulses are important factors in determining the performance of a correlation receiver of a system based on PPM. In this chapter, the impact of the correlation characteristics of the proposed waveforms on the performance of a correlation receiver is analyzed and a performance comparison of different waveforms under various conditions, such as multipath fading, timing mismatch, and multiuser interference, is provided. Through the results of a theoretical analysis and simulation experiments, this chapter shows that the proposed orthonormal pulses provide enhanced BER performance of the correlation receiver compared to the well-known orthonormal MHPs and even a Gaussian monocycle [73]. The applications of the proposed pulses for enhancing data rates and/or transmission reliability, based on the orthogonality between the multiple pulses at the correlation receiver, will be discussed in Chapter 5 and 6 with examples of modulation schemes.

This chapter is organized as follows. In Section 4.1, the system model and the pulse shapes for the indoor UWB system are briefly described. In Section 4.2, the performance analysis of the correlation receiver in single-user

and multiuser environments is discussed. The summary is given in Section 4.3.

4.1 Pulse Shapes for TH-PPM UWB Systems

In this section, a typical model for the TH-PPM UWB systems is presented. In Subsection 4.1.1, the considered system model is described with the transmitted and the received signal models. The decision rule of the correlation receiver for the detection of the transmitted data also is presented. In Subsection 4.1.2, the several pulse shapes for the indoor UWB systems are introduced for performance comparisons.

4.1.1 System Model

In UWB systems adopting binary PPM and TH, the kth transmitter's pulse train, which carries the ith bit, can be represented as [84]

$$p_{tx-bit}^{(k)}(t, i) = \sqrt{\frac{E_b}{N_s}} \sum_{j=iN_s}^{(i+1)N_s-1} p_{tx}(t - jT_f - c_j^{(k)}T_c - \delta d_i^{(k)}), \qquad (4.1)$$

where E_b is the energy per bit, N_s is the number of pulses to transmit a bit, $p_{tx}(t)$ represents the waveform of a single pulse at the transmitter, and the waveform begins at time zero on the transmitter clock. The expression $\{c_j^{(k)} \in [0, N_c)\}$ is an integer TH sequence of the kth user for avoiding catastrophic collisions among users in multiple access systems. T_c is the time period of a TH chip, and T_f is the frame period, which may be ten to a thousand times that of a single waveform width, T_p. δ is the time offset of binary PPM, and $d_i^{(k)} \in \{0, 1\}$ is the ith bit data to be transmitted from the kth transmitter. To

avoid inter-symbol interference (ISI), it is assumed that $N_c T_c + 2\delta < T_f$.

When N_u transmitters are active in a dense multipath fading channel, the received signal $r(t)$ at a certain user's receiver can be represented as

$$r(t) = \sum_{k=1}^{N_u} \sum_{i=0}^{\infty} \sum_{m=1}^{M} A_{km} p_{rx-bit}^{(k)}(t - \tau_k - \mu_m, i) + n(t), \qquad (4.2)$$

where $p_{rx-bit}^{(k)}(t, i)$ is the received pulse train of (4.1). Note that the antenna systems change the waveform from $p_{tx}(t)$ to $p_{rx}(t)$ at the output of the receiver antenna. A_{km} models the attenuation factor of the mth multipath channel between the kth transmitter and the desired receiver. A_{km} follows a log-normal distribution with random polarity [79], but I assume a fixed-channel realization to compare the impact of the different waveform properties on the correlation receiver under various conditions such as multipath fading, timing mismatch, and multiuser interference. τ_k represents the time asynchronism between the clocks of the kth transmitter and receiver, and μ_m is the mth multipath time delay. $n(t)$ is additional interference and/or noise, which may exist at the correlator input and is assumed to be as white Gaussian noise with two-sided PSD $N_0/2$.

When only a single user is active in the system and the data sequence, $\{d_i^{(k)}\}$, is a sampled sequence from a wide-sense stationary process of equally likely binary symbols, it is known that the correlation receiver with maximum likelihood detection is the optimal receiver [85]. Under the assumption of perfect synchronization for the reference signal, the decision rule of the correlation receiver for the detection of the ith bit transmitted from the kth transmitter

61

can be expressed as follows [31]:

$$decide" d_i^{(k)} = 0" \Leftrightarrow$$

$$\underbrace{\sqrt{\frac{N_s}{E_b}} \sum_{j=iN_s}^{(i+1)N_s-1} \int_{\tau_k+jT_f}^{\tau_k+(j+1)T_f} r(t)v(t - \tau_k - jT_f - c_j^{(k)}T_c)dt}_{\alpha} > 0, \qquad (4.3)$$

where $v(t) \triangleq p_{rx}(t) - p_{rx}(t - \delta)$ is the correlation template waveform and α is the decision variable.

In a multiuser environment, the decision rule of (4.3) is no longer optimal because the Gaussian approximation for the multiuser interference (MUI) is not valid [52] [84] [86] [87] [88] [89]. Under the assumption that the receiver knows the structure of the MUI, the optimal receiver can enhance the system performance. However, the optimal receiver requires both high complexity in receiver design and more computational cost in the decision process [90] [91]. Thus, the decision rule of (4.3) is used in the performance comparison for the multiuser system using different waveforms, which will be discussed in the following section, because it is simpler for theoretical analysis and practical implementation [52] [84].

4.1.2 Orthogonal Pulses

The two proposed waveforms that satisfy the FCC indoor spectral mask as well as mutual orthonormality at the receiver are presented in Section 3.3. Although the waveforms can be generated even for a frequency-selective fading channel, the two waveforms are produced as the received waveforms at the correlation receiver under the assumption that the channel is AWGN and the

antennas are differentiators [31] [36] for a fair comparison of the different waveforms. The proposed waveforms are evaluated by comparing the performance for a correlation receiver with MHP orthogonal pulses mentioned in Section 2.3.2 [36] [38] [62]. As discussed in Section 2.3.2, the mutual orthogonality of the received prolate spheroidal pulses is not preserved when the characteristic of antenna is applied. Thus, the PS pulses are eliminated from the comparison. The third-order MHP is used as a radiated pulse, and the fourth-order MHP is used for the received waveform under the assumption that the antennas are differentiators. The Gaussian monocycle is employed as a reference for a single type of waveform [92]. The fourth- and the fifth-order Gaussian monocycles are used as a radiated pulse and a received waveform, respectively. For a fair performance comparison, the same -10 dB bandwidth is considered for all the waveforms.

4.2 Performance of the UWB Correlation Receiver

In this section, a typical model for the received signal is presented, and the performance analysis of the correlation receiver in single-user and multiuser environments is discussed.

4.2.1 Single User System over an AWGN Channel

When only the kth user is active in the system, the received signal for the ith bit of (4.2) can be written as

$$r(t) = \sum_{m=1}^{M} A_{km} p_{rx-bit}^{(k)}(t - \tau_k - \mu_m, i) + n(t). \tag{4.4}$$

By plugging (4.4) into the decision rule of (4.3) under the perfect synchroniza-

tion assumption, the decision variable, α, can be written as

$$\alpha \triangleq \sqrt{\frac{N_s}{E_b}} \sum_{j=iN_s}^{(i+1)N_s-1} \int_{\tau_k+jT_f}^{\tau_k+(j+1)T_f} \left[\sum_{m=1}^{M} A_{km} p_{rx-bit}^{(k)}(t - \tau_k - \mu_m, i) + n(t) \right]$$

$$\cdot v(t - \tau_k - jT_f - c_j^{(k)} T_c) dt$$

$$= \underbrace{\sum_{j=iN_s}^{(i+1)N_s-1} \int_{jT_f}^{(j+1)T_f} \left[\sum_{m=1}^{M} A_{km} \{ \sum_{l=iN_s}^{(i+1)N_s-1} p_{rx}(t - \mu_m - lT_f - c_l^{(k)} T_c - \delta d_i^{(k)}) \} \right] \cdot v(t - jT_f - c_j^{(k)} T_c) dt}_{S_k} \tag{4.5}$$

$$+ \underbrace{\sqrt{\frac{N_s}{E_b}} \sum_{j=iN_s}^{(i+1)N_s-1} \int_{\tau_k+jT_f}^{\tau_k+(j+1)T_f} n(t) \cdot v(t - \tau_k - jT_f - c_j^{(k)} T_c) dt}_{n_k},$$

and the desired signal term, S_k, and the variance of the noise term, $\sigma_n^2 (= \mathbb{E}[n_k^2])$, are summarized as [52] [84]

$$S_k = \sum_{m=1}^{M} A_{km} N_s \{ \tilde{R}(\mu_m + \delta d_i^{(k)}) \} \tag{4.6}$$

$$\sigma_n^2 = N_0 N_s^2 \tilde{R}(0) / E_b, \tag{4.7}$$

where $\tilde{R}(x) = R(x) - R(x - \delta)$, and $R(\cdot)$ represents the auto-correlation of a specific waveform, $p_{rx}(t)$. Thus, the SNR_{out} at the receiver output can be derived as

$$SNR_{out}^{(k)}(\delta) = \frac{E_b}{N_0} \cdot \frac{\{\sum_{m=1}^{M} A_{km} \tilde{R}(\mu_m + \delta d_i^{(k)})\}^2}{\tilde{R}(0)} \tag{4.8}$$

64

which is a function of δ, given that the waveform is determined. For the system using the decision rule of (4.3), the conditional probability of bit error is given by [30]

$$P_e^{(k)}(\delta|\{A_{km}\}_{m=1}^M) = Q\left(\sqrt{SNR_{out}^{(k)}(\delta)}\right), \quad (4.9)$$

where $Q(x) = \frac{1}{\sqrt{2\pi}} \int_x^\infty e^{(-x^2/2)} dx$ is related to the complementary error function as $Q(x) = \frac{1}{2} erfc\left(\frac{x}{\sqrt{2}}\right)$. As shown in (4.9), the conditional probability of the bit error also is a function of δ and the auto-correlation of a specific waveform.

With a given waveform, therefore, the optimal time offset, which maximizes $SNR_{out}^{(k)}$ (or minimizes the probability of bit error), can be found by using the following function:

$$\delta_{opt} = \arg\max_\delta[\text{SNR}_{out}^{(k)}]. \quad (4.10)$$

As shown in (4.8), however, the value of $SNR_{out}^{(k)}$ may be affected by a random factor, multipath delay μ_m, which makes it difficult to find the optimal time offset. Thus, the optimal time offset is defined in an ideal direct path condition, $(M = 1, \mu_1 = 0)$, and then the effects from multipath fading and timing mismatch are investigated.

Under the assumption of a single direct path and no timing mismatch, the optimal time offset is obtained from (4.8) and (4.10) as follows:

$$\delta_{opt} = \arg\min_\delta[\text{R}(\delta)]. \quad (4.11)$$

Therefore, the BER depends on the waveforms and their minimal auto-correlation values of $R(\delta)$, when an equal mean power is assumed for all the different wave-

forms. Fig. 4.1 shows the auto-correlations, which are numerically generated and normalized, in terms of δ for the fifth-order Gaussian monocycle, MHP ($n = 4$), and the two proposed pulses, $p_{rx1}(t)$ and $p_{rx2}(t)$ (the computation of the proposed pulses is described in Appendices A and B). As shown in the figure, the proposed pulses provide smaller minimal $R(\delta_{opt})$ than the MHP ($n = 4$) and even the fifth-order Gaussian monocycle. Therefore, it can be concluded that the proposed pulses provide higher SNR_{out} at an equal mean power than the MHPs and even the fifth-order Gaussian monocycle. In other words, the proposed pulses are more power-efficient waveforms than any other considered waveforms for a given BER. Note that the similar results are observed with the MHPs of different order n.

4.2.2 Single User System over Multipath Fading Channel

Given the optimum time offset δ_{opt}, the impact of the multipath fading on the BER performance was investigated. Since the received waveform consists of a number of multipath components, two types of received signal model can be considered. One type represents the received signal with the overlapped multipath components within one pulse duration, and the other type of received signal model consists of all the resolvable multipath components. To exploit the multipath diversity, the resolvable components of the second signal model can be collected by a RAKE receiver with multiple fingers. However, I will not discuss this issue here because it is beyond the scope of this dissertation. Information on how the system collects more energy with
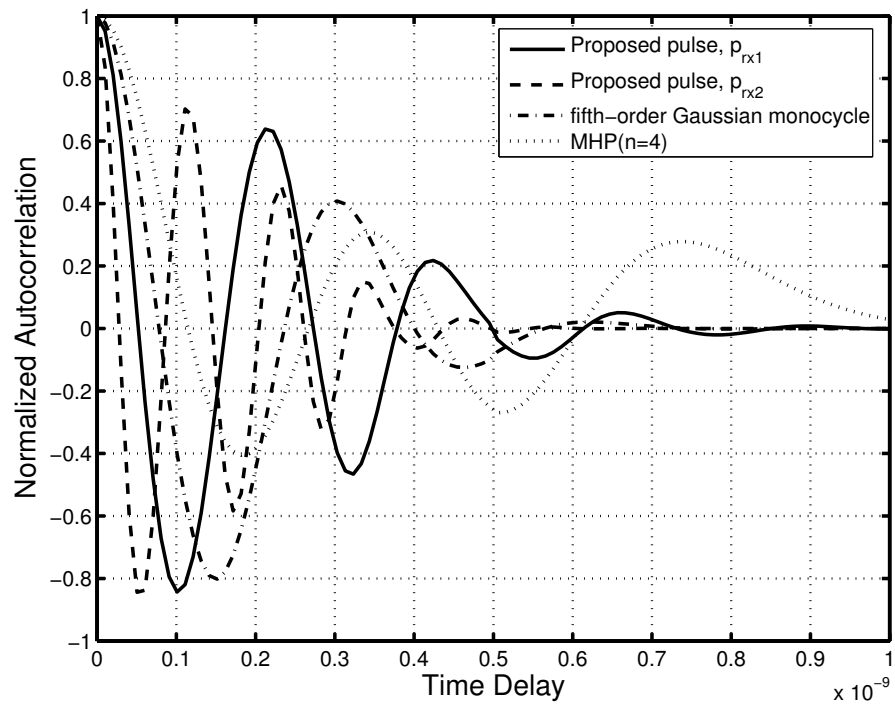
Figure 4.1: Normalized auto-correlations for the fifth-order Gaussian monocycle, MHP ($n = 4$), and the proposed pulses, $p_{rx1}(t)$ and $p_{rx2}(t)$.

67

a RAKE receiver can be found in [93] [94] [95] [96] [97] [98] [99]. For the purpose here, however, since the overlapped multipath components within one pulse duration are not resolvable, the impact of the overlapped multipath components on the employed correlation receiver is investigated with a simplified two-path model. From (4.4), the received signal with one overlapped component can be expressed as follows:

$$r(t) = A_{k1}p^{(k)}_{rx-bit}(t - \tau_k, i) + A_{k2}p^{(k)}_{rx-bit}(t - \tau_k - \mu_2, i) + n(t), \qquad (4.12)$$

where $\mu_2 (\leq T_p)$ is assumed to be a random variable uniformly distributed on $[0, t_m]$ and t_m represents the maximum delay. Since μ_2 is a random variable, the expected desired signal term, after applying to the decision rule of (4.3), can be derived as follows:

$$\mathbb{E}[S_k] = \begin{cases} A_{k1}N_s\tilde{R}(0) + A_{k2}N_s\mathbb{E}[\tilde{R}(\mu_2)], & \text{for } d^{(k)}_i = 0 \\ A_{k1}N_s\tilde{R}(0) + A_{k2}N_s\mathbb{E}[\tilde{R}(\mu_2 + \delta_{opt})], & \text{for } d^{(k)}_i = 1. \end{cases} \qquad (4.13)$$

Therefore, the average BER is given by

$$
\begin{aligned}
P^{(k)}_e(\delta_{opt}|\{A_{km}\}^2_{m=1}) &= \frac{1}{2}Pr(\alpha < 0|d^{(k)}_i = 0, \{A_{km}\}^2_{m=1}) \\
&\quad + \frac{1}{2}Pr(\alpha > 0|d^{(k)}_i = 1, \{A_{km}\}^2_{m=1}) \\
&= \frac{1}{2}Q\left(\sqrt{\frac{E_b}{N_0} \cdot \frac{(A_{k1}\tilde{R}(0) + A_{k2}\mathbb{E}[\tilde{R}(\mu_2)])^2}{\tilde{R}(0)}}\right) \\
&\quad + \frac{1}{2}Q\left(\sqrt{\frac{E_b}{N_0} \cdot \frac{(A_{k1}\tilde{R}(0) + A_{k2}\mathbb{E}[\tilde{R}(\mu_2 + \delta_{opt})])^2}{\tilde{R}(0)}}\right).
\end{aligned}
\qquad (4.14)
$$

Fig. 4.2 shows the comparison of BER performance over the multipath fading channel for the fifth-order Gaussian monocycle, MHP ($n = 4$), and the proposed pulses, $p_{rx1}(t)$ and $p_{rx2}(t)$, when $E_b/N_0 = 10$ dB and $t_m \in [0, 1\text{ns}]$. As
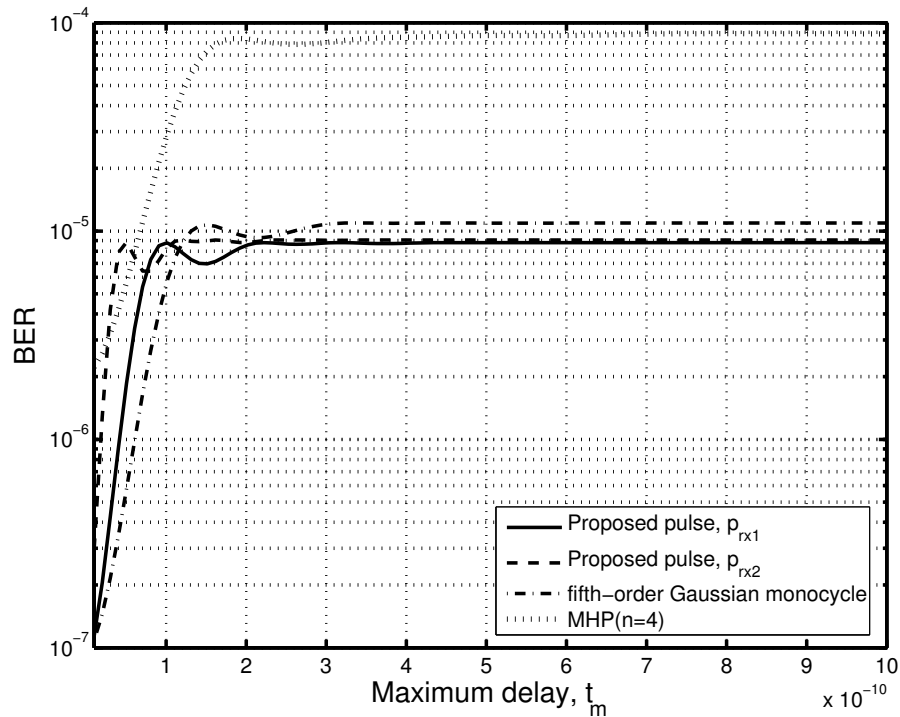
Figure 4.2: Comparison of BER performance over multipath fading channel for the fifth-order Gaussian monocycle, MHP ($n = 4$), and the proposed pulses, $p_{rx1}(t)$ and $p_{rx2}(t)$, when $E_b/N_0 = 10$dB.

shown in the figure, the proposed pulses outperform the MHP pulses and even the fifth-order Gaussian monocycle. It is also shown that the system using the proposed pulses achieves about 10 dB more gain in the BER performance than the system using MHP pulses.

4.2.3 Single User System with Timing Mismatch

In a fielded system, perfect timing is not always achieved at the receiver. Thus, resistance against timing mismatch is investigated for all of

the waveforms considered. When the timing mismatch is considered under a non-inter-symbol-interference assumption, the received signal for the ith bit of (4.4) can be written as

$$r(t) = \sum_{m=1}^{M} A_{km} p_{rx-bit}^{(k)}(t - \tau_k - \mu_m - t_s, i) + n(t), \qquad (4.15)$$

where t_s represents a timing mismatch. The desired signal term of (4.6) at the receiver can be written as

$$S_k = \sum_{m=1}^{M} A_{km} N_s \{\tilde{R}(\mu_m + t_s + \delta_{opt} d_i^{(k)})\}, \qquad (4.16)$$

and the timing mismatch, t_s, may cause an incorrect decision in (4.3) by changing the value of $\tilde{R}(\cdot)$ of a specific waveform. Under a single-path condition, Fig. 4.3 shows $\tilde{R}(t_s)$ as a function of t_s for the fifth-order Gaussian monocycle, MHP ($n = 4$), and the proposed pulses, $p_{rx1}(t)$ and $p_{rx2}(t)$. As shown in the figure, the proposed pulses have narrower main lobes and higher side lobes, which indicate that their sensitivity to the timing mismatch is higher than the other waveforms. Thus, additional performance degradation may be caused compared to the performance of the other waveforms unless a sufficient timing accuracy is provided for the proposed pulses.

Moreover, it is observed that the $\tilde{R}(\cdot)$ of the proposed waveforms decays faster than that of the MHP pulses. It is known that waveforms having fast-decaying auto-correlation functions are desirable to mitigate the MUI even though those waveforms are more sensitive to timing jitter [100] [101]. Thus, the BER performance comparisons of all the waveforms with MUI are presented in the following section.

70
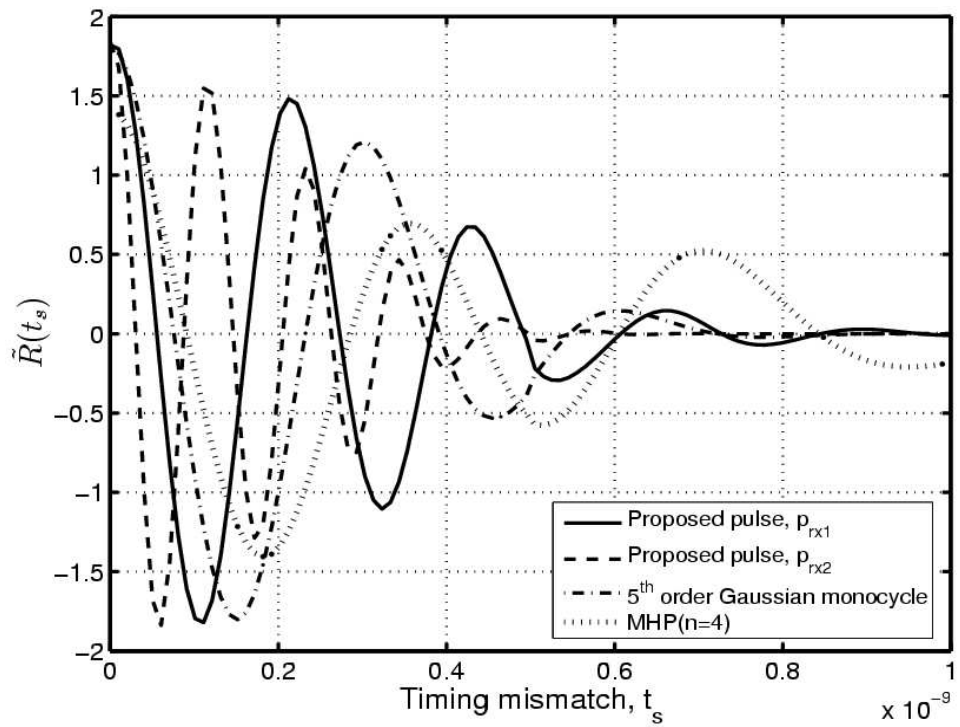
Figure 4.3: $\tilde{R}(t_s)$ versus timing mismatch for the fifth-order Gaussian mono-cycle, MHP ($n = 4$), and the proposed pulses, $p_{rx1}(t)$ and $p_{rx2}(t)$.

4.2.4 Multiuser System Using a Single Waveform

When N_u asynchronous users are active in the system and the signal from the kth transmitter is the desired signal, the received signal model of (4.2) can be rewritten as

$$
\begin{aligned}
r(t) = &\sum_{m=1}^{M} A_{km} p^{(k)}_{rx-bit}(t - \tau_k - \mu_m) + \\
&\sum_{k'=1, k' \neq k}^{N_u} \sum_{m=1}^{M} A_{k'm} p^{(k')}_{rx-bit}(t - \tau_{k'} - \mu_m) + n(t).
\end{aligned}
\tag{4.17}
$$

With the decision rule of (4.3), it is shown that an additional MUI term, $n^{(k)}_{MUI}$, is added to the decision variable of a single user system, α, and $n^{(k)}_{MUI}$ can be derived as [52] [84]

$$
\begin{aligned}
n^{(k)}_{MUI} = &\sqrt{\frac{N_s}{E_b}} \sum_{j=0}^{N_s-1} \int_{\tau_k + jT_f}^{\tau_k + (j+1)T_f} \sum_{k'=1, k' \neq k}^{N_u} \Bigg[\sum_{m=1}^{M} A_{k'm} \cdot \\
&p^{(k')}_{rx-bit}(t - \tau_{k'} - \mu_m) \Bigg] \cdot v(t - \tau_k - jT_f - c^{(k)}_j T_c) dt.
\end{aligned}
\tag{4.18}
$$

When both the waveform used in the pulse train, $p^{(k')}_{rx-bit}(t)$, and the waveform used in the template, $v(t) \triangleq p^{(k)}_{rx}(t) - p^{(k)}_{rx}(t - \delta)$, are the same, the MUI term can be expressed as the linear summation of multipath components, where each component consists of only the auto-correlation function of a specific waveform.

4.2.5 Multiuser System Using Multiple Waveforms

When the received waveforms from different users k' are different from the waveform used in the template, the MUI term of (4.18) can be expressed as

the linear summation of the cross-correlation among the waveforms. Fig. 4.4 shows the cross-correlation properties, which are numerically generated and normalized, of both the MHP pulses between $n = 4$ and $n = 3, 5, 9$ and the proposed pulses between $p_{rx1}(t)$ and $p_{rx2}(t)$. As shown in the figure, the proposed pulses have smaller variance of cross-correlation than that of the MHP pulses, and both waveforms have zero mean. Therefore, it can be concluded that the proposed pulses are more reliable for the orthogonal detection at the correlation receiver than for the MHP pulses as they will enhance BER performance in a multiuser environment.

The exact BER performance analysis of TH-PPM UWB systems in the presence of MUI was recently developed in [84] [88]. The closed form, which is presented in [84], is used for the BER analysis of the system using the proposed pulses, as well as the MHP pulses and fifth-order Gaussian monocycle with the auto- and cross-correlation functions of each waveform. Fig. 4.5 shows the comparison of the BER performance with MUI on the AWGN channel for the fifth-order Gaussian monocycle, MHP pulses ($n = 4$ and $n = 5$), and the proposed pulses, $p_{rx1}(t)$ and $p_{rx2}(t)$. As shown in the figure, the proposed pulses significantly outperform the MHP pulses and even the fifth-order Gaussian monocycle. In the figure, moreover, it is shown that the systems using the multiple waveforms for multiusers outperforms the system using only a single waveform. Note that the probability of users selecting each waveform is assumed to be equal, and certain values for the parameters such as $N_s = 4$, $N_u = 8$, $N_c = 8$, $T_f = 50$ns, $T_c = 2$ns are used for all of the waveforms.

73
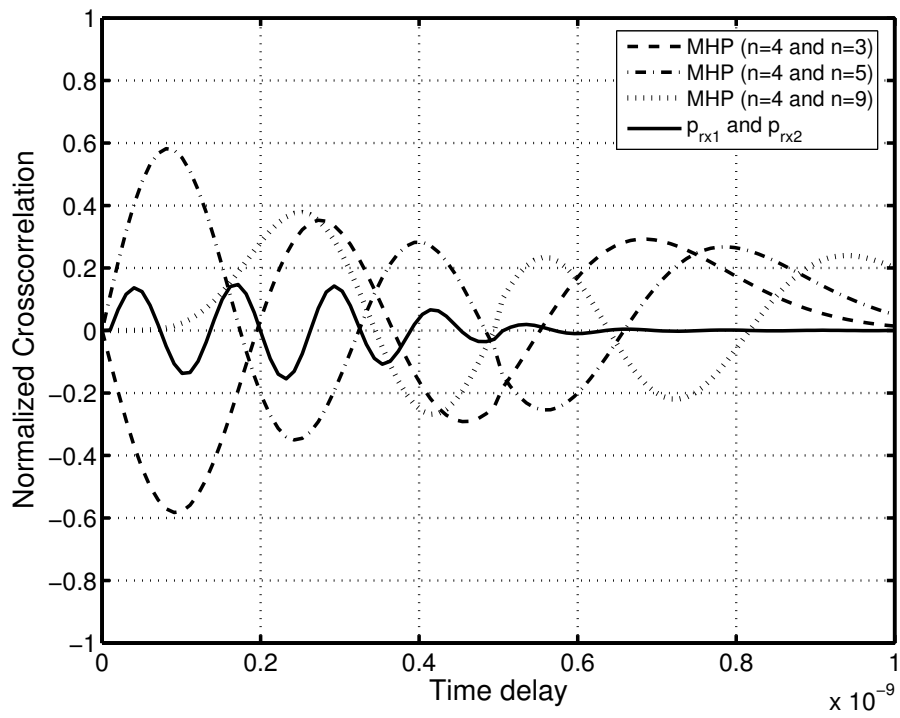
Figure 4.4: Normalized cross-correlations for the MHP pulses between $n = 4$ and $n = 3, 5, 9$ and the proposed pulses between $p_{rx1}(t)$ and $p_{rx2}(t)$.
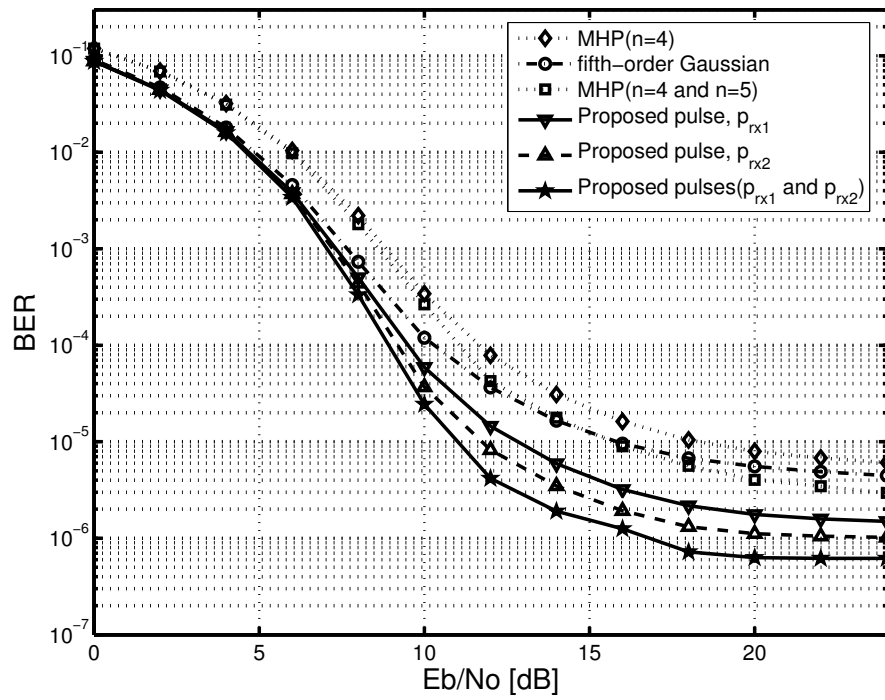
Figure 4.5: Comparison of the BER performance with multiuser interference (MUI) on AWGN channel for the fifth-order Gaussian monocycle, MHP pulses ($n = 4$ and $n = 5$), and the proposed pulses, $p_{rx1}(t)$ and $p_{rx2}(t)$.

4.3 Summary

Using the novel multiple orthonormal pulses proposed in [59], I analyzed the impact of the properties of the proposed pulses, such as auto- and cross-correlations, on the correlation receiver. I also provided a performance comparison of the correlation receiver with different waveforms, such as the fifth-order Gaussian monocycle and MHP pulses under various conditions, such as multipath fading, timing mismatch, and multiuser interference. According to the results of the performance comparison, it is shown that the proposed pulses outperform the multiple orthogonal MHP pulses on the correlation receiver because the proposed pulses provide lower minimum auto-correlation as well as smaller variance of cross-correlation. Therefore, the enhancement of the BER performance can be achieved by using the proposed pulses. Because of the higher sensitivity to the timing mismatch than that of MHP pulses, however, more timing accuracy may be needed for the system using the proposed pulses than for the system using the MHP pulses.

Chapter 5

Data-Rate Enhancement Using Pulse Shape Modulation (PSM)

In Chapter 4, the impact of the correlation characteristics of the proposed waveforms on the performance of a correlation receiver is analyzed and a performance comparison with different waveforms is performed under various conditions, such as multipath fading, timing mismatch, and multiuser interference. In this chapter, based on the orthogonality between the multiple pulses at the correlation receiver, the application of the proposed pulses for enhancing the data rates is discussed for modulation schemes using pulse shape modulation (PSM).

The chapter is organized as follows. In Section 5.1, the PPM-PSM scheme with optimal pulse position is presented, and its effectiveness is demonstrated by computer simulations. In Section 5.2, the PPM-PSM scheme with polarity method is presented for higher data rates. The summary is given in Section 5.3.

5.1 PPM-PSM Scheme with Optimal Pulse Position

In this section, the application of the multiple orthogonal waveforms for enhancing the data rates is discussed, with an example of a modulation scheme. When multiple types of waveforms have the orthonormal property at the correlation receiver, unlike a single type of waveform, additional information can be carried by exploiting the different waveforms [37] [38] [81] [82] [102]. As discussed in Section 3.4, I can transmit 2 bits of data with the two pulses, $w_{tx1}(t)$ and $w_{tx2}(t)$, by employing PPM and PSM simultaneously. Table 5.1 shows an example of a modulation scheme to transmit 2 bits of data. Note that the optimal time offsets for the given waveforms are defined by using (4.11). In Table 5.1, I adopt a Gray coding scheme with consideration of the different distances among the alphabets at the correlation receiver. Moreover, since only a single pulse is transmitted per frame, the PSD of the radiated signal over the PPM-PSM scheme still satisfies the FCC indoor mask, and the energy is kept constant when it is compared with 1-bit transmission [38]. Note that in the modulation scheme the selection of the waveform is based on the statistical properties of the data source.

Under the assumption of unitary energy of all of the waveforms and perfect synchronization between the transmitter and the receiver, the orthonormal waveforms can be detected by the correlation receiver with maximum likelihood detection. When four different alphabets are used for 2-bit data transmission as shown in the Table 5.1, the detection process with two templates, $v_z(t) \triangleq w_{rxz}^{(k)}(t) - w_{rxz}^{(k)}(t - \delta_{w_{rxz}})$ for $z \in \{1, 2\}$, can be expressed as

Table 5.1: Modulation scheme for 2 bits

Data	Position		
Source	T_f	$T_f + \delta_{w_{rx2}}$	$T_f + \delta_{w_{rx1}}$
00	w_{tx1}	0	0
01	w_{tx2}	0	0
10	0	w_{tx2}	0
11	0	0	w_{tx1}

follows:

$$\hat{d}_i^{(k)} = \begin{cases} 00, & \text{if } |\alpha_1| > |\alpha_2| \text{ and } \alpha_1 > 0 \\ 11, & \text{if } |\alpha_1| > |\alpha_2| \text{ and } \alpha_1 < 0 \\ 01, & \text{if } |\alpha_1| < |\alpha_2| \text{ and } \alpha_2 > 0 \\ 10, & \text{if } |\alpha_1| < |\alpha_2| \text{ and } \alpha_2 < 0, \end{cases} \tag{5.1}$$

where $\hat{d}_i^{(k)}$ is the estimate of the transmitted data source, and $\alpha_z(t) = \sqrt{\frac{N_s}{E_b}} \cdot \sum_{j=iN_s}^{(i+1)N_s-1} \int_{\tau_k+jT_f}^{\tau_k+(j+1)T_f} r(t)v_z(t - \tau_k - jT_f - c_j^{(k)}T_c)dt$ for $z \in \{1, 2\}$ is a decision variable.

By inspecting the decision variable, $\alpha_z(t)$, it is observed that the auto-correlation as well as the cross-correlation characteristics of the waveforms have significant impact on the BER performance of the correlation receiver. Under the assumption of an AWGN channel, it is clear that the desirable waveforms need to have both the smaller minimum auto-correlation values of each wave-form and the smaller variance of cross-correlation between the two waveforms for obtaining the longer distance between $|\alpha_1|$ and $|\alpha_2|$. Furthermore, when more asynchronous users are active in the system, the waveforms, which have the smaller variance of cross-correlation, are more desirable for mitigating the

79

Figure 5.1: Comparison of BER performances with and without the MUI between the system using the two proposed pulses and the system using the MHP pulses ($n = 4$ and $n = 5$) over the E_b/N_0 in AWGN channel.

interference from other users.

According to Fig. 4.1 and Fig. 4.4, the proposed waveforms have both the smaller minimum auto-correlation values and the smaller variance of cross-correlation compared to the MHP pulses ($n = 4$ and $n = 5$). Thus, it is expected that the system using the proposed waveforms outperforms the system using the MHP pulses ($n = 4$ and $n = 5$) in the BER performance, and this superiority is confirmed in the computer simulations. Fig. 5.1 shows a comparison of BER performances between the system using the two proposed

pulses and the system using the MHP pulses ($n = 4$ and $n = 5$) over the E_b/N_0 in an AWGN channel. A conventional PPM with a single waveform is used for 1-bit transmission, and the PPM-PSM scheme with the two orthonormal waveforms is used for 2-bit transmission. In addition, a simple system with two asynchronous users is simulated to show the effect of the correlation characteristics of the waveform on the BER performance in the presence of MUI. The asynchronous delay of the received signal from an interfering user is assumed to have a uniform distribution of $[0, T_f = 50\text{ns})$, and the optimal time offsets for the waveforms are defined as follows: δ_{prx1}=0.1146ns, δ_{prx2}=0.0625ns, $\delta_{MHP(n=4)}$=0.182ns, and $\delta_{MHP(n=5)}$=0.162ns. The sampling rate used in the simulation was 100 GHz. As shown in Fig. 5.1, the BER performance of the systems using the proposed pulses is an improvement over that for the system using MHP pulses in all the cases. It also is shown that the BER performance degradation of the system using the two proposed pulses for 2-bit is relatively moderate, while that of the system using MHP pulses becomes severe as the E_b/N_0 increases.

The BER performances of the system using the two proposed pulses and the system using the MHP pulses are also compared on the realistic channel model. The modified Saleh-Valenzuela channel model, which is presented in Section 2.5, is adopted, and the same parameters are chosen for a non-line-of-sight channel model, (τ_m=17ns, τ_{rms}=15ns and NP$_{10\text{dB}}$=35), which are given by Table 11 of [79]. The channel coefficients are normalized to remove the path loss, and the BER is obtained by averaging conditional BERs over 10000 chan-
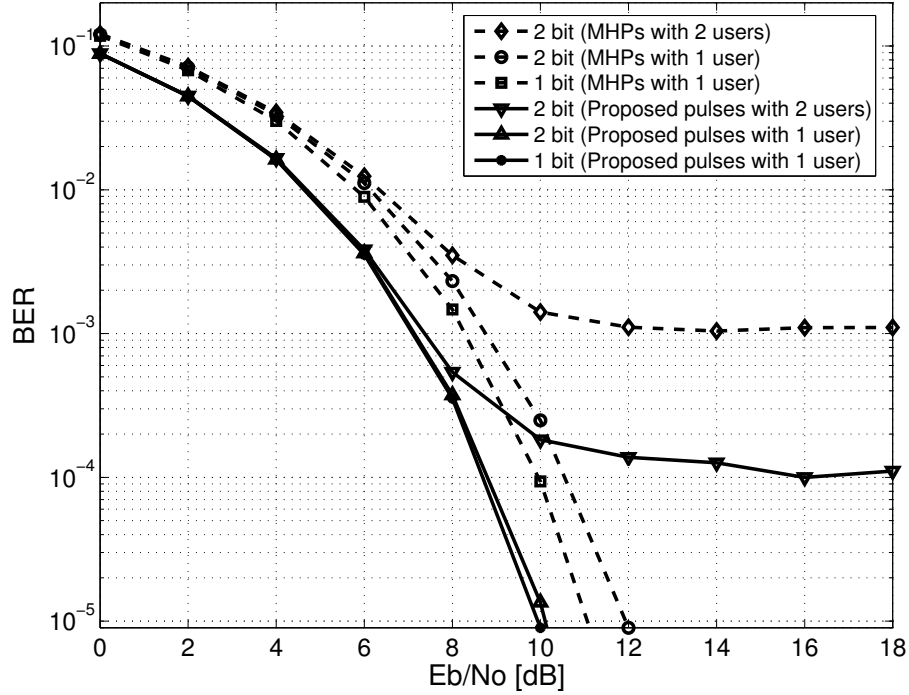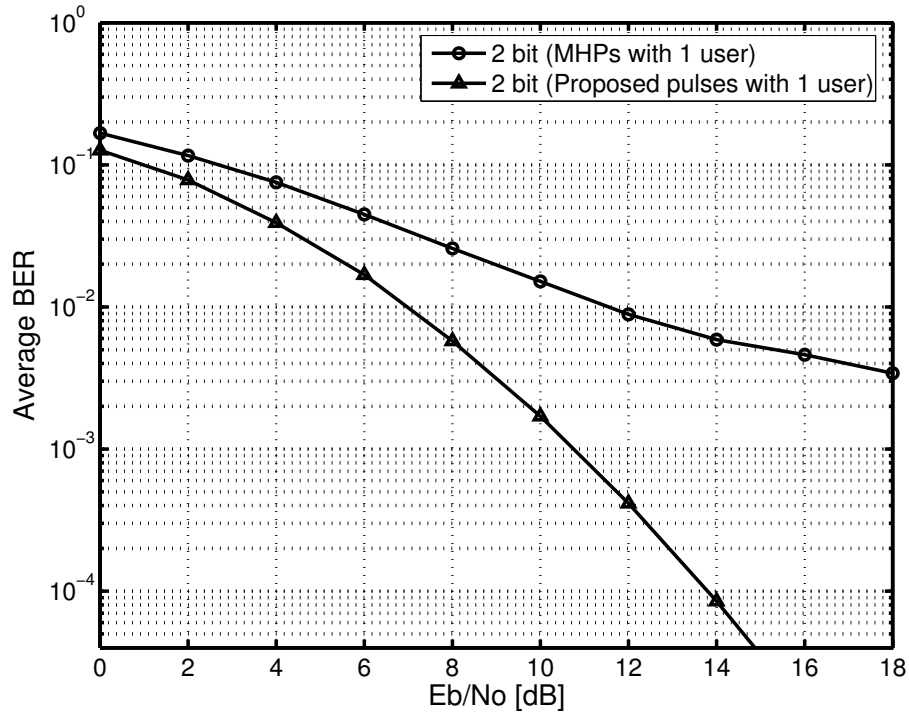
Figure 5.2: Comparison of BER performances between the system using the two proposed pulses and the system using the MHP pulses ($n = 4$ and $n = 5$) over the E_b/N_0 on the modified Saleh-Valenzuela channel model.

nel realizations. Fig. 5.2 shows the comparison between BER performances of the system using the two proposed pulses and of the system using the MHP pulses ($n = 4$ and $n = 5$) over the E_b/N_0 on the modified Saleh-Valenzuela channel model. As shown in the figure, the simulation results confirm that the systems using the proposed pulses remarkably outperform the system using MHP pulses on the realistic channel. Note that a realistic E_b/N_0 setting can be ranged between 7 dB and 20 dB [25].

5.2 PPM-PSM with Polarity Method

When the technology of changing the polarity of the waveform is employed on the PPM-PSM modulation scheme, I can transmit more data by using the multiple orthonormal pulses and PPM-PSM with the polarity scheme. For example, by employing the polarity changes of the pulse shape, the above proposed scheme for 2 bits can be simply extended with the increased number of alphabets. Table 5.2 shows the modulation scheme for transmitting 3 bits of data and the templates for the correlation receiver. Similar to the modulation scheme for 2 bits, each optimal time offset is determined by considering both the auto- and the cross-correlations simultaneously. Since polarity is applied, however, the time offset for the minimum auto-correlation is not the optimal time offset anymore, even in a single-user environment, because it makes the distance between the desired alphabet and the polarized alphabet with time offset closer than that between orthogonal alphabets. Thus, the optimum time offset used for the 2-bit modulation scheme in a single-user system degrades the BER performance if it is used for a 3-bit modulation scheme. For example, when the desired data source is 000 from Table 5.2, the auto-correlation between the waveform for 000 and the template for 100 is closer to 1 than the correlation value between the waveform and any other templates. Thus, the error probability is increased in the correlation receiver because the distance between alphabets becomes closer. Therefore, the time offset of each pulse, which makes the waveform orthogonal with its time-shifted waveform and all other waveforms, can be considered optimum for each pulse in both single-user

83

Table 5.2: Modulation scheme for 3 bits and templates

Data Source	Position			Receiver template
	T_f	$T_f + \delta_{rx2}$	$T_f + \delta_{rx1}$	
000	p_{tx1}	0	0	$v_1(t) = p_{rx1}(t)$
011	0	0	p_{tx1}	$v_2(t) = p_{rx1}(t - \delta_{rx1})$
010	p_{tx2}	0	0	$v_3(t) = p_{rx2}(t)$
001	0	p_{tx2}	0	$v_4(t) = p_{rx2}(t - \delta_{rx2})$
111	$-p_{tx1}$	0	0	$v_5(t) = -p_{rx1}(t)$
100	0	0	$-p_{tx1}$	$v_6(t) = -p_{rx1}(t - \delta_{rx1})$
101	$-p_{tx2}$	0	0	$v_7(t) = -p_{rx2}(t)$
110	0	$-p_{tx2}$	0	$v_8(t) = -p_{rx2}(t - \delta_{rx2})$

and multiuser environments. In addition, by adopting a Gray coding scheme along with consideration of the different distances among the alphabets, the maximum distance between the desired alphabet and the polarized alphabet can be used for the worst case, and it can enhance the BER performance of the system over $\frac{E_b}{N_o}$. With the proposed modulation scheme of Table 5.2, the properties of the templates can be expressed as

$$\int v_z(t)v_{z'}(t)dt = \begin{cases} 1 & \text{if } z = z' \\ 0 & \text{if } z \neq z' \text{and } z \neq z' + 4 \\ -1 & \text{if } z = z' + 4. \end{cases} \quad (5.2)$$

The selection of the pulse shape is also based on the statistical properties of the source in the modulation scheme.

Under the assumption of unitary energy of all pulses and perfect synchronization between a transmitter and a receiver, the orthonormal or the

antipodal waveforms can be transmitted, and they are detected by the correlation receiver with maximum likelihood detection. When eight different alphabets are used for 3-bit data transmission, as shown in the Table 5.2, the detection process with eight templates can be expressed as

$$\hat{z} = \{z | \beta_z(t) \geq \beta_{z'}(t), \forall z' \in \{1, 2, ..., 8\}\} \tag{5.3}$$

where $\beta_z(t) = \sum_{j=iN_s}^{(i+1)N_s-1} \int_{\tau_k+jT_f}^{\tau_k+(j+1)T_f} r(t)v_z(t - \tau_k - jT_f - c_j^{(k)}T_c)dt$ is a decision variable. The data source corresponding to the estimate $\hat{z}$ is the estimate of the transmitted data source. The correlation receiver structure for the proposed modulation scheme is illustrated in Fig. 5.3.

Fig. 5.4 shows the BER performances of systems using the two proposed pulses over the Eb/No in an AWGN channel. A conventional PPM with a proposed pulse is used for 1-bit transmission, and the PPM-PSM scheme with the two proposed pulses is used for 2-bit transmission. The PPM-PSM with polarity scheme and the two proposed pulses are used for 3-bit transmission. As shown in the figure, the proposed modulation scheme with the two proposed pulses achieves the enhancement of BER performance even while the data rate is increased. Thus, high data-rate communication can be achieved by the proposed orthonormal pulses and PPM-PSM with the polarity scheme.

Fig. 5.5 shows the BER performances of the systems using the two proposed pulses over the Eb/No on the modified Saleh-Valenzuela channel model. It also is demonstrated with simulation results that the proposed orthonormal pulses and PPM-PSM with polarity scheme for high data-rate communication are still valid on the realistic channel.
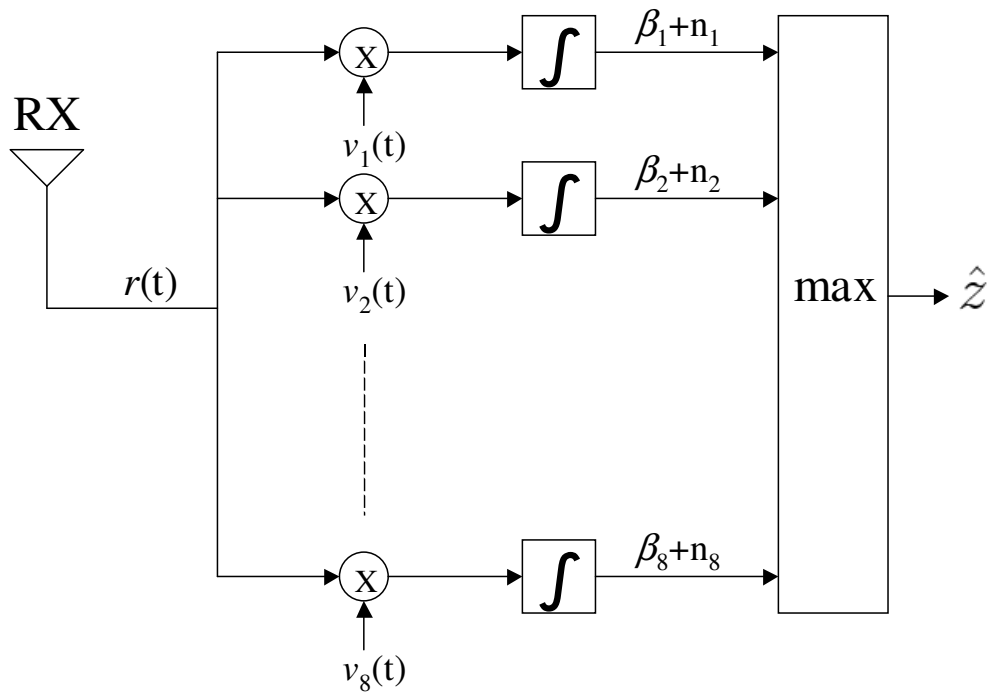
Figure 5.3: Correlation receiver structure for the proposed modulation scheme
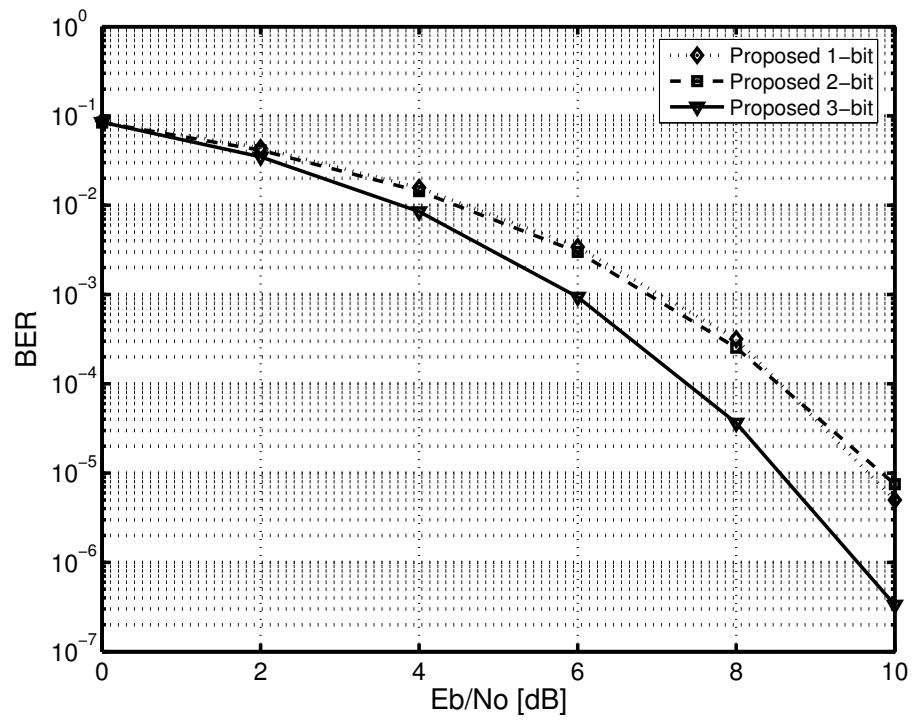
Figure 5.4: BER performance of the systems using the proposed pulses in the AWGN channel model when a binary PPM, PPM-PSM, and PPM-PSM with polarity are adopted for 1 bit, 2 bits, and 3 bits, respectively
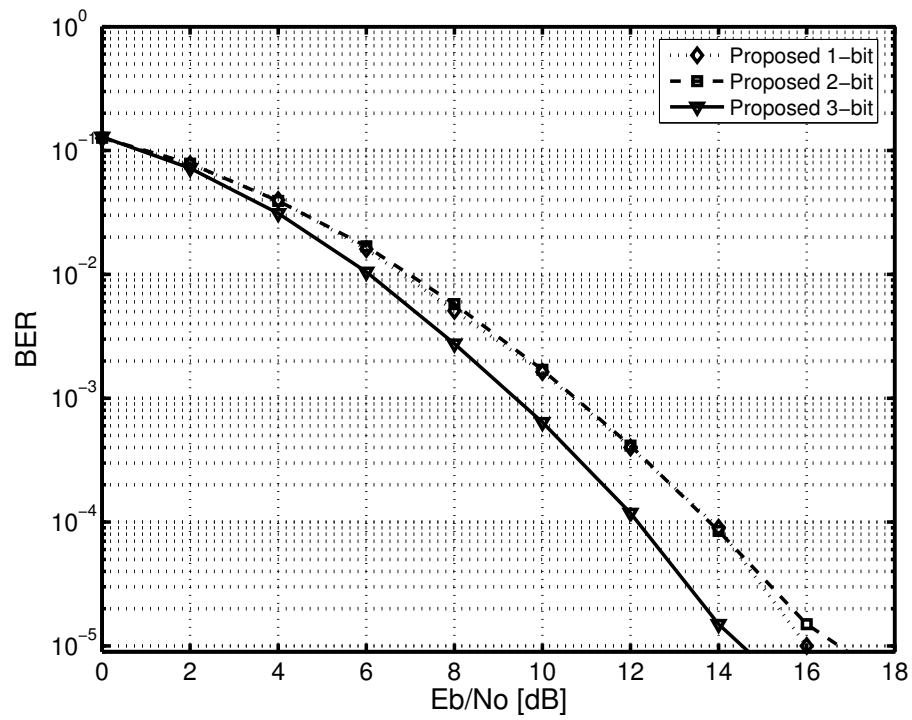
Figure 5.5: BER performance of the systems using the proposed pulses on the modified Saleh-Valenzuela channel model when a binary PPM, PPM-PSM, and PPM-PSM with polarity are adopted for 1 bit, 2 bits, and 3 bits, respectively

5.3   Summary

The application of the multiple orthogonal waveforms for enhancing the data rates is discussed with two examples of modulation schemes, PPM-PSM and PPM-PSM with the polarity scheme. It is shown that a data-rate enhancement can be achieved by the modulation schemes utilizing the orthogonality between the pulses at the correlation receiver.

Given the correlation receiver structure for the proposed modulation schemes, the simulation results demonstrated that the system using the proposed waveforms outperforms the system using the MHP pulses in the BER performance because the proposed waveforms have both smaller minimum auto-correlation values and a smaller variance of cross-correlation compared to those of the MHP pulses.

Chapter 6

Signal Detection Enhancement Using Transmit Diversity

Recently, multiantenna-based coding schemes, such as an analog space-time coding (STC) scheme and an adaptive transmit diversity scheme, have been developed to enhance the transmission reliability of the UWB-IR communication systems [103] [104] [105] [106] [107] [108] [109] [110]. However, all the approaches are restricted in using a single type of waveform, while further enhancement of transmission reliability can be achieved by employing multiple orthogonal waveforms (e.g., [32] [36] [59]) in designing the coding scheme. By applying the multiple orthogonal waveforms to the coding scheme based on spatial diversity, I can obtain an additional dimension for designing the coding scheme and relax the commonly assumed time constraint, where the channel coefficients are invariant over two frames or more. Furthermore, if the multiple waveforms with non-overlapped PSDs are used, the spectrum utilization efficiency (SUE) [57] [111] can be increased while the FCC spectral regulation for indoor UWB systems is satisfied [1].

In this chapter, I propose a novel space-shape (SS) coding scheme with multiple antennas and multiple orthonormal waveforms for the UWB-IR systems [112]. Unlike the schemes in [103] [104] [105] [106] [107] [108] [109] [110],

the proposed SS coding scheme can be applied to a single frame because the proposed scheme is not based on time diversity. Therefore, the commonly assumed time-invariant channel condition for the STC scheme can be relaxed. Furthermore, an additional power gain enhancing the BER performance can be achieved by the proposed scheme when the pulses with non-overlapped PSDs are used.

This chapter is organized as follows. In Section 6.1, the system model for the proposed SS coding scheme is introduced. In Section 6.2, the novel SS coding scheme is proposed with two different power control schemes depending on the PSD characteristic of waveforms. The effectiveness of the proposed scheme is demonstrated by computer simulations in Section 6.3. The summary is given in Section 6.4.

6.1   System Model

In the UWB systems adopting binary PPM and the TH code, the kth transmitter's pulse train, which carries the ith bit, from a single transmit antenna can be represented as [92]

$$p_{tx-bit}^{(k)}(t;i) = \sqrt{P} \sum_{j=iN_s}^{(i+1)N_s-1} p_{tx_a}(t - jT_f - c_j^{(k)}T_c - \epsilon d_i^{(k)}), \qquad (6.1)$$

where P is the transmit power, and $p_{tx_a}(t)$ represents the waveform of a single pulse at the transmitter. The waveform is normalized to have unit energy, and it begins at time zero on the transmitter clock. The expression $\{c_j^{(k)} \in [0, N_c)\}$ is an integer TH sequence of the kth user. T_c is the time period of a TH chip,

91
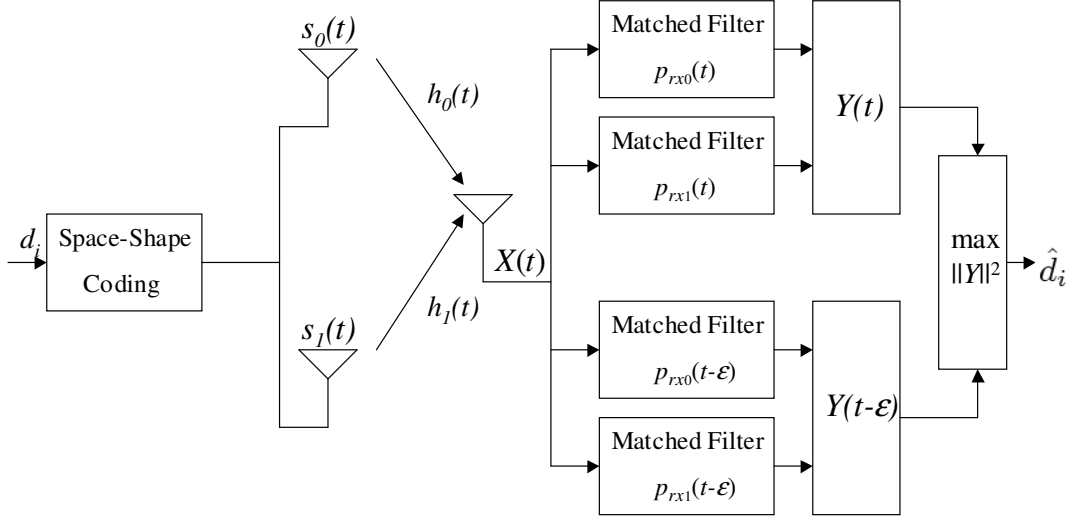
Figure 6.1: UWB-IR system with two-branch transmit diversity and one receiver

and T_f is a frame period. ϵ is the time offset of binary PPM, and $d_i^{(k)} \in \{0, 1\}$ is the ith bit of data to be transmitted from the kth transmitter. N_s is the number of pulses to transmit a bit. When perfect synchronization is assumed, I can rewrite (6.1) for a single user system as follows:

$$p_{tx-bit}(t; i) = \sqrt{P} \sum_{j=iN_s}^{(i+1)N_s-1} p_{tx_a}(t - jT_f - \Delta), \qquad (6.2)$$

where $\Delta \in \{0, \epsilon\}$.

Fig. 6.1 shows the configuration of the proposed system. For the proposed SS coding scheme, a simple system with two transmit and one receive antennas is considered, and two orthonormal pulses are employed. In addition, non-coherent detection is adopted under the assumption that the orthogonal PPM is employed and channel state information is unknown to the receiver.

Based on the measurements, a UWB indoor channel model with multipath fading was developed by Intel Labs [79], and, as presented in Section 2.5, the impulse response of the channel can be expressed as

$$h(t) = \sum_{l=0}^{L-1} \alpha(l)\delta(t - \tau(l)), \qquad (6.3)$$

where L is the number of resolvable multipath components; $\delta(t)$ is the Dirac delta functional; $\alpha(l)$ is the fading coefficient, which is log-normal-distributed with random polarity, of the lth resolvable path; and $\tau(l)$ represents the delay, which is integer multiples of the path resolution of 0.167ns, of the lth path.

Note that a single user system is assumed for simplicity, but the system can be extended to a multiuser system under the consideration of the multiuser interferences [52]. Moreover, I can extend the system with a RAKE receiver to achieve multipath diversity [93] [97] [98] [104].

6.2   Space-Shape Coding Scheme

In this section, I propose the novel SS coding scheme with two different power-control schemes, depending on the PSD characteristic of waveforms.

6.2.1   Orthogonal Pulses with Overlapped PSDs

The two orthonormal waveforms for the proposed SS coding scheme are denoted as $p_{tx_a}(t)$ for $a \in \{0, 1\}$. Without loss of generality, I can consider that the transmitted ith bit data is 0, then Table 6.1 depicts the SS coding scheme for the jth frame of a symbol over two transmit antennas. As shown

Table 6.1: Space-shape coding scheme

	Antenna 0	Antenna 1
Shape 0	$p_{tx_0}(t)$	$-p_{tx_0}(t)$
Shape 1	$p_{tx_1}(t)$	$p_{tx_1}(t)$

in the table, the SS coding scheme can be employed frame by frame, and the coded waveforms that were transmitted from the zeroth and the first antennas can be expressed as

$$s_0(t; i, j) = \sqrt{\frac{P}{4}} \left[p_{tx_0}(t; i, j) + p_{tx_1}(t; i, j) \right] \tag{6.4}$$

and

$$s_1(t; i, j) = \sqrt{\frac{P}{4}} \left[p_{tx_1}(t; i, j) - p_{tx_0}(t; i, j) \right], \tag{6.5}$$

respectively, where $p_{tx_0}(t; i, j)$ and $p_{tx_1}(t; i, j)$ are the two orthonormal pulses of the jth frame for the ith bit. Note that the power of each pulse with overlapped PSD is limited to $\frac{P}{4}$ for ensuring the same total transmit power with a single antenna transmission.

The two multipath channels from the zeroth and the first transmit antennas to the receive antenna are assumed to be mutually independent and denoted with $h_0(t)$ and $h_1(t)$, respectively. Then, the jth received frame is

given by

$$X(t; i, j) = s_0(t; i, j) * h_0(t) + s_1(t; i, j) * h_1(t) + n(t)$$

$$= \sqrt{\frac{P}{4}} \left[\sum_{l_0=0}^{L_0-1} \alpha_0(l_0) p_{rx_0}(t - \tau_0(l_0); i, j) + \sum_{l_0=0}^{L_0-1} \alpha_0(l_0) p_{rx_1}(t - \tau_0(l_0); i, j) \right. \tag{6.6}$$

$$\left. + \sum_{l_1=0}^{L_1-1} \alpha_1(l_1) p_{rx_1}(t - \tau_1(l_1); i, j) - \sum_{l_1=0}^{L_1-1} \alpha_1(l_1) p_{rx_0}(t - \tau_1(l_1); i, j) \right] + n(t),$$

where $*$ stands for convolution, $n(t)$ is an AWGN with PSD $\frac{N_0}{2}$, and $p_{rx_0}(t)$ and $p_{rx_1}(t)$ are the received waveforms, which are changed by the differential characteristic of antennas [52].

Since the received waveforms consist of the two orthonormal waveforms, the matched filters, which use each received waveform and its time-shifted waveform $p_{rx_a}(t - \Delta)$ for $a \in \{0, 1\}$ and $\Delta \in \{0, \epsilon\}$ as reference, are employed to detect the jth transmitted frame in a vector form. Thus, the output of the matched filters for the jth frame of the ith symbol can be derived as follows:

$$Y(t; i, j) = \begin{bmatrix} \int_{jT_f}^{(j+1)T_f} X(t; i, j) p_{rx_0}(t - \Delta) dt \\ \int_{jT_f}^{(j+1)T_f} X(t; i, j) p_{rx_1}(t - \Delta) dt \end{bmatrix}$$

$$= \sqrt{\frac{P}{4}} \begin{bmatrix} \sum_{l_0=0}^{L_0-1} \alpha_0(l_0) R_0(\Delta - \tau_0(l_0)) - \sum_{l_1=0}^{L_1-1} \alpha_1(l_1) R_0(\Delta - \tau_1(l_1)) \\ \sum_{l_0=0}^{L_0-1} \alpha_0(l_0) R_1(\Delta - \tau_0(l_0)) + \sum_{l_1=0}^{L_1-1} \alpha_1(l_1) R_1(\Delta - \tau_1(l_1)) \end{bmatrix} + \begin{bmatrix} \tilde{n}_0(t) \\ \tilde{n}_1(t) \end{bmatrix}, \tag{6.7}$$

where $R_0(\Delta) = \int_{jT_f}^{(j+1)T_f} p_{rx_0}(t; i, j) p_{rx_0}(t - \Delta) dt$ and $R_1(\Delta) = \int_{jT_f}^{(j+1)T_f} p_{rx_1}(t; i, j) \cdot p_{rx_1}(t - \Delta) dt$ are the normalized auto-correlation functions of the two orthonormal pulses, respectively. The expression $\tilde{n}_a(t) = \int_{jT_f}^{(j+1)T_f} n(t) p_{rx_a}(t - \Delta) dt$, where $a \in \{0, 1\}$, is the filtered noise with PSD $\frac{N_0}{2}$.

The decoding scheme using the squared Euclidean norm (SEN) of the received vector is optimal for the noncoherent, orthogonal PPM UWB systems when the multipath-free channel is assumed [103]. Based on the optimal

scheme, a simple decoding scheme using the SEN is considered for the considered multipath channel model. In the absence of noise, the SEN of the ith bit, $\|Y\|^2$, can be derived by using (6.7) as follows:

$$\begin{aligned}
\|Y\|^2 &= Y^T(t;i)Y(t;i) \\
&= \sum_{j=iN_s}^{(i+1)N_s-1} \frac{P}{4}[\beta_0^2 + \beta_1^2 + \gamma_0^2 + \gamma_1^2 + 2(\gamma_0\gamma_1 - \beta_0\beta_1)]
\end{aligned} \tag{6.8}$$

where $(\cdot)^T$ denotes transposition, $Y(t;i) = \sum_{j=iN_s}^{(i+1)N_s-1} Y(t;i,j)$ is the filtered symbol for the ith bit, $\beta_c = \sum_{l_c=0}^{L_c-1} \alpha_c(l_c)R_0(\Delta - \tau_c(l_c))$, and $\gamma_c = \sum_{l_c=0}^{L_c-1} \alpha_c(l_c)R_1(\Delta - \tau_c(l_c))$ for $c \in \{0,1\}$. Given the decision statistic of (6.8), the estimation of the ith transmitted symbol can be obtained as follows

$$\hat{d}_i = (\arg\max_\Delta[\|Y\|^2]), \tag{6.9}$$

where $\Delta \in \{0, \epsilon\}$.

6.2.2 Orthogonal Pulses with Non-Overlapped PSDs

In Section 6.2.1, the proposed SS coding scheme limits the transmit power of each waveform to $\frac{P}{4}$ to comply with the FCC spectral mask. Since the limited transmit power of each waveform resulted from the overlapped PSDs of waveforms, however, the transmit power of each waveform can be increased if the PSDs of orthonormal waveforms are not overlapped. That is, the FCC spectral mask can be met with the proposed scheme even if more transmit power is applied for each pulse. As a result, the BER performance of the system can be enhanced because of the increased total transmit power

or the enhanced SUE.

While the SUE is enhanced, the increased diversity gain can be preserved without loss of the coding gain. For example, if the two orthonormal pulses, $p_{tx_0}(t)$ and $p_{tx_1}(t)$, have the non-overlapped PSDs at the transmitter, the transmit power of each pulse over the SS coding scheme can be doubled. Thus, the coded waveforms (6.4) and (6.5) can be rewritten as

$$s_0(t;i,j) = \sqrt{\frac{P}{2}} \left[p_{tx_0}(t;i,j) + p_{tx_1}(t;i,j) \right] \tag{6.10}$$

and

$$s_1(t;i,j) = \sqrt{\frac{P}{2}} \left[p_{tx_1}(t;i,j) - p_{tx_0}(t;i,j) \right], \tag{6.11}$$

respectively. Note that the power of each pulse with non-overlapped PSD is extended to $\frac{P}{2}$ while complying with the FCC spectral mask. Therefore, the suboptimal decoding scheme for the ith transmitted symbol is the same as (6.9) with the doubled SEN as follows:

$$\|Y\|^2 = \sum_{j=iN_s}^{(i+1)N_s-1} \frac{P}{2} [\beta_0^2 + \beta_1^2 + \gamma_0^2 + \gamma_1^2 + 2(\gamma_0\gamma_1 - \beta_0\beta_1)] \tag{6.12}$$

Compared with (6.8), it is clearly shown that there is a 3 dB gain resulted from the increased total transmit power. Thus, the SS coded UWB-IR system using the orthonormal pulses with non-overlapping PSDs enhances the BER performance even more than that of the system using the pulses with overlapped PSDs.

6.3 Simulation Results

In this section, the proposed scheme is compared with the single antenna system and the analog ST-coded system with two transmit antenna of [103]. Since the two different power control schemes depending on the PSD characteristic of waveforms are proposed, the two pairs of orthonormal waveforms with overlapped and non-overlapped PSDs, which were developed in [59], are employed for the proposed scheme. The same parameters are chosen for a non-line-of-sight channel model (τ_m=17ns, τ_{rms}=15ns and NP$_{10\text{dB}}$=35), which are given by Table 11 of [79]. The channel coefficients are normalized to remove the path loss, and the BER is obtained by averaging conditional BERs over 10000 channel realizations for each path.

Fig. 6.2 shows the BER performances of the proposed systems with two transmit antennas and the SS coding schemes over Eb/No, which are compared to the system using a single antenna and the analog ST-coded system with two transmit antenna [103]. As shown in the figure, the proposed systems outperform the conventional system using a single antenna. Moreover, as I already mentioned in Section 6.2.2, it is shown that the proposed system using pulses with non-overlapped PSDs achieves about 3 dB more gain due to the doubled total transmit power than the system using pulses with overlapped PSDs. Note that the BER performance of the proposed system using pulses with overlapped PSDs is almost same as that of the analog ST-coded system because both systems achieve the same diversity at the same transmit power.

Fig. 6.3 shows the PSDs of the proposed SS-coded waveforms with

98
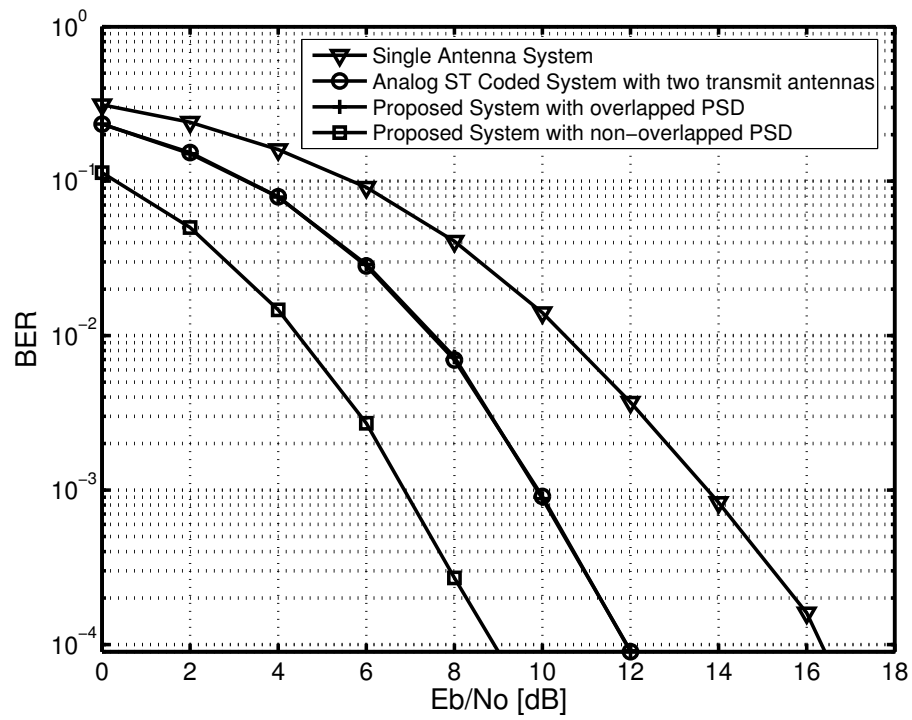
Figure 6.2: Comparison of the BER performance for a conventional single antenna system, the analog space-time-coded system, and the proposed space-shape-coded systems

99
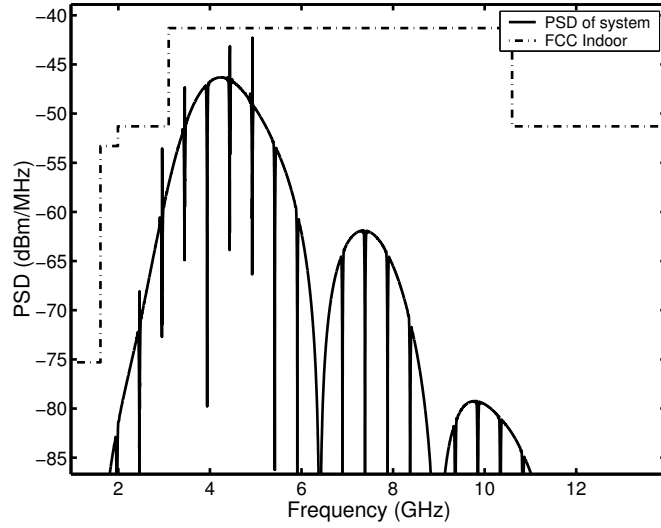
(a)
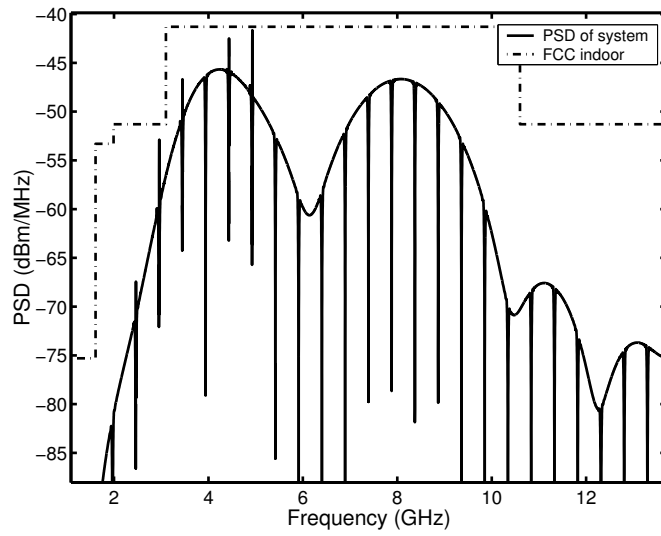
(b)

Figure 6.3: PSDs of the proposed SS-coded waveforms at the transmitter (a) Orthogonal pulses with overlapped PSDs and (b) Orthogonal pulses with non-overlapped PSDs

100

PPM and infinite time hopping (PPM-TH) at the transmitter. As shown in the figure, both proposed schemes using pulses with overlapped and non-overlapped PSDs satisfy the FCC spectral mask. Moreover, it is shown that the enhanced SUE is achieved by using pulses with non-overlapped PSDs when it is compared with the system using pulses with overlapped PSDs.

6.4 Summary

I proposed a novel SS-coding scheme with two transmit antennas and two orthonormal waveforms for the UWB-IR systems. Without the invariant channel condition over frames, the spatial diversity can be achieved by the proposed schemes. Furthermore, it was shown that an additional power gain can be achieved by the proposed scheme by using pulses with non-overlapped PSDs while the FCC spectral regulation is satisfied. Simulation results demonstrated that the proposed schemes can enhance BER performance.

Chapter 7

Conclusions and Future Work

7.1 Summary of Contributions

In this dissertation, I proposed the principle of generating orthonormal pulse shapes that comply with the FCC mask without additional frequency shifting or bandpass filters. Under various conditions, the performance of the systems using the proposed waveforms was analyzed and compared with the systems using different waveforms. I also proposed several schemes that use the multiple orthogonal pulses to achieve high data rates or enhanced transmission reliability in UWB systems.

Chapter 2 showed the effects of the modulation scheme and the pulse shape on the PSD of the radiated signal, and then reviewed the previous pulse shapes, including recently developed multiple orthogonal pulses. The channel models for indoor UWB systems were also presented.

Chapter 3 presented the limitations of the two previous multiple orthogonal pulse shapes and described the needs that motivated the search for new pulse shapes for UWB-IR systems. Then I proposed the novel concept of orthonormal pulses, which not only meet the power spectral mask of the FCC for indoor UWB systems but also preserve orthogonality at the corre-

lation receiver. The basic waveform for the proposed waveforms is obtained from the Battle-Lemarie wavelet, and a set of orthogonal basis waveforms is obtained from the dilation and translation of the basic waveform. When the basis waveforms were linearly combined, two examples of pulses were provided that comply with the FCC spectral mask without additional frequency shifting or bandpass filters, and their PSDs were presented. Note that the computation of the proposed pulses is described in Appendices A and B.

Chapter 4 analyzed the impact of the correlation characteristics of the proposed waveforms on the performance of a correlation receiver and provided performance comparisons with different waveforms under various conditions, such as multipath fading, timing mismatch, and multiuser interference. A theoretical analysis and simulation experiments showed that an enhanced BER performance of the correlation receiver could be achieved by using the proposed orthonormal pulses, when compared to the well-known orthonormal MHP pulses and even a Gaussian monocycle.

Chapter 5 discussed the application of the multiple orthonormal waveforms for enhancing the data rates. Two examples of modulation schemes, the PPM-PSM and PPM-PSM with the polarity schemes, were presented, and it was shown that the data-rate enhancement could be achieved by the presented modulation schemes utilizing the orthonormality between the pulses at the correlation receiver. Simulation results demonstrated that the system using the proposed waveforms outperforms the system using the MHP pulses in the BER performance because the proposed waveforms have both the smaller

103

minimum auto-correlation values and the smaller variance of cross-correlation.

Chapter 6 proposed a novel Space-Shape coding scheme with multiple antennas and multiple orthonormal waveforms for the UWB-IR systems. Since the proposed coding scheme can be applied for every frame, the spatial diversity can be achieved even without the invariant channel condition over frames. Furthermore, the proposed scheme can provide additional power gain to enhance the BER performance while the FCC spectral regulation is satisfied. The validation of the proposed scheme was demonstrated with computer simulations.

The computation of the basic waveform is described in Appendix A, and the Matlab source code to generate the proposed pulses is presented in Appendix B.

7.2   Future Work

In the future, I can extend the proposed schemes to further enhance the data rate and/or transmission reliability.

In Chapter 2, I assumed an ideal antenna model, which has unity gain over the entire occupied bandwidth, and I maintained that assumption throughout the dissertation. However, when the impulse response of a fielded antenna is measured and adopted for the considered systems, the transmitted and the received pulse shapes will be distorted by the antenna characteristics, and the estimated performance of the systems using the previously developed

waveforms will be degraded. As shown in Chapter 3, however, the impulse response of the antenna is considered a parameter in the proposed algorithm for the waveform design. Thus, new pulse shapes that preserve the orthogonality at the receiver may be designed even with a non-ideal antenna model. With the characteristics of the fielded antennas, therefore, the optimum system design can be developed by simultaneously considering pulse shape design and modulation schemes.

In Chapter 3, the examples of the proposed pulse design algorithm are produced by using the third-order B-spline function. However, different sets of orthonormal waveforms can also be designed by changing the order of the B-spline function. Since the orthogonality among the waveforms is preserved if the order of the B-spline function is the same, various multiple orthonormal waveforms that have different auto- and cross-correlation properties can be designed. Moreover, in future work the design of optimal orthonormal waveforms that fill up as much area under the FCC power spectral mask as possible will be investigated.

In Chapter 4, a simplified two-path model was adopted for a received signal with overlapped multipath components within one-pulse duration, and the model was used to investigate the impact of the signal on the correlation receiver. Since the resolvable multipath components of the signal can be collected by a RAKE receiver with multiple fingers, I can extend the systems, which were proposed for high data rates in Chapter 5, to exploit the multipath diversity while increasing the data rates. Therefore, I will be able to increase

the data rate and enhance the transmission reliability simultaneously. However, the number of resolvable multipath components in the received signal is generally too large to collect all the components. Thus, a subset of multipath components needs to be selected and combined by a RAKE receiver. If the Rake has only a few fingers, the energy captured by the receiver would be low, and the complexity of the receiver would not be an issue. On the other hand, the more energy that a RAKE receiver can capture, the greater, the cost in increased complexity. Thus, a tradeoff exists between the performance and complexity for a RAKE receiver, and the optimal or suboptimal solutions for the proposed systems in Chapter 5 can be examined in the future studies. Furthermore, when the number of fingers is determined, an optimal combining technique (for example, maximal ration combining (MRC)) can be adopted for the PPM-PSM scheme to achieve the maximum output signal-to-noise ratio. In addition, the square-law combining (SLC) technique can be adopted for the PPM-PSM with a polarity scheme. The SLC technique, which is commonly employed with orthogonal modulation, does not require the optimal weights for all the fingers [99]. Thus, enhanced performance may be achieved by adopting the SLC technique for the PPM-PSM with polarity scheme with a reduced cost in complexity.

When the optimal time offset is defined for PPM in Chapter 4, I assumed a single direct-path and no timing mismatch. In addition, the multipath effects were investigated with a simplified two-path model. However, there is a large number of multipath components in the received signal. Therefore, the

106

optimal time offset for PPM can be defined with consideration of the effects of the multipath, which is more than two path. With information for the resolvable multipath components, the optimal time offset can be redefined, and the system performance can be evaluated again in various conditions, including a timing mismatch and/or multiuser interference.

In Chapter 6, for simplicity, the proposed SS-coding scheme is applied to a single-user system, but the system can be extended to a multiuser system with consideration of multiuser interference. Moreover, the proposed system can be extended with a RAKE receiver to achieve multipath diversity.

Recently, another approach, one that designs new UWB pulses by using B-splines, was introduced, and an analog circuit and digital filter for the generation of B-splines were developed [113] [114] [115]. Therefore, additional research on the implementation of systems using the proposed pulses could be performed to realize the proposed systems.

Moreover, there are other design challenges in UWB-IR systems. One challenge is to design a UWB antenna. Unlike a narrowband antenna, the electrical properties of UWB antennas depend on frequency over extremely broad bandwidths. In addition, antenna size is also an important constraint because a potential application is portable wireless communication devices [77]. Another challenge is synchronization. Since the TH-PPM UWB-IR systems use a low-duty cycle pseudo randomly time-hopped pulse train, the receivers need to be synchronized for the correct detection of the received pulse train. As investigated in Chapter 4, moreover, the BER performance of UWB-IR

systems can be significantly degraded with timing mismatches.

On the other hand, in the presence of channel uncertainties, the synchronization of the PPM UWB-IR system becomes problematic, because synchronization can be significantly impaired in a dense multipath fading channel [116]. As the number of multiple paths increases with transmission bandwidth, even an optimal maximum likelihood detector cannot achieve synchronization for practical growth rates on the multipath [116]. Therefore, further research is needed to develop alternative modulation methods for UWB-IR systems. One example of an alternative modulation method is the Multi-Tone Frequency Shift Keying (MFSK) scheme described in [117]. In the PPM UWB-IR system, the lack of channel state information (CSI) can adversely affect the performance, whereas the MFSK scheme does not require CSI. Moreover, in [117] the authors insist that, as bandwidth increases, the capacity can approach the capacity of the AWGN channel. Another version of the MFSK scheme, one using feedback, has also been introduced to enhance error performance in a frequency-selective time-varing channel [118]. Those methods, however, are based on a scheme that tunes waveforms to specific frequencies. By using multiple waveforms that reside in different frequency bands, future studies will be able to investigate new modulation methods based on the MFSK scheme.

Appendices

Appendix A

Basic Waveform Generation

The basic waveform with the orthogonalized B-spline function of order $(n = 3)$ is expressed as follows:

$$\psi(t) = \sqrt{2} \sum_l \sum_m g_l c_m \beta_3(2t - l - m), \tag{A.1}$$

where

$$\beta_3(t) = \frac{1}{8}\left\{ \tilde{\beta}_3(2t+2) + 4\tilde{\beta}_3(2t+1) + 6\tilde{\beta}_3(2t) + 4\tilde{\beta}_3(2t-1) + \tilde{\beta}_3(2t-2) \right\}, \tag{A.2}$$

$$\tilde{\beta}_3(t) = \frac{1}{6}\left\{ [t+2]_+^3 - 4[t+1]_+^3 + 6[t]_+^3 - 4[t-1]_+^3 + [t-2]_+^3 \right\}, \tag{A.3}$$

$$[t]_+^3 = \left(\max(0,t)\right)^3. \tag{A.4}$$

The coefficient g_l can be expressed as $g_l = (-1)^l h_{1-l}$, where $\{h_k\}$ are the coefficients appearing in the dilation equation of a scaling function [80]. As shown in [80], the coefficients $\{h_k\}$ can be computed as the kth Fourier coefficient of $H(\omega)$, where $H(\omega)$ for $(n = 3)$ is expressed as

$$H(\omega) = \frac{1}{2^4}\sqrt{\frac{\sum_8(\omega)}{\sum_8(2\omega)}}, \tag{A.5}$$

where

$$\sum_8(\omega) = \frac{\cos^6(\omega/2)\csc^2(\omega/2)}{20160} + \frac{19\cot^4(\omega/2)\csc^4(\omega/2)}{13440} + \frac{\cot^2(\omega/2)\csc^6(\omega/2)}{448} + \frac{17\csc^8(\omega/2)}{80640}. \tag{A.6}$$

110

Therefore, the coefficient g_l can be computed by the following function:

$$g_l = (-1)^l \frac{\sqrt{2}}{2\pi} \int_0^{2\pi} \sqrt{\frac{\cos^8(\omega/2)\{1208 + 1191\cos(\omega) + 120\cos(2\omega) + \cos(3\omega)\}}{1208 + 1191\cos(2\omega) + 120\cos(4\omega) + \cos(6\omega)}} e^{j\omega(1-l)} d\omega. \tag{A.7}$$

In the basic waveform of (A.1), the scaling function $\phi(t)$ is defined as [119]

$$\phi(t) = \sum_m c_m \beta_3(t - m), \tag{A.8}$$

and $\{c_m\}$ are coefficients that orthogonalize the scaling functions. The coefficient values can be obtained by the following function:

$$c_m = FT\left\{\frac{1}{\sqrt{b(\omega)}}\right\}, \tag{A.9}$$

where $b(\omega) = \frac{17}{315} + \frac{4}{7}\cos^2(\omega/2) + \frac{38}{105}\cos^4(\omega/2) + \frac{4}{315}\cos^6(\omega/2)$ is defined for the desired scaling function [120]. With the basic waveform, the Matlab source code to generate the proposed waveforms is presented in Appendix B. For the B-spline function of a different order, moreover, different coefficients can be computed by using the general expressions for $\beta_n(t)$, $b(\omega)$, and $H(\omega)$ that are found in [80] [119] [120].

111

Appendix B

Matlab Source Code for Waveform Generation

```
      clear all;
c1 = [-0.0000300159 0.0000580049 -0.00011237 0.00021831
-0.000425552 0.000832836 -0.00163778 0.00323986 -0.00645749
0.0129982 -0.0265203 0.0551915 -0.11852 0.268704 -0.67243
1.96976 -0.67243 0.268704 -0.11852 0.0551915 -0.0265203 0.0129982
-0.00645749 0.00323986 -0.00163778 0.000832836 -0.000425552
0.00021831, -0.00011237, 0.0000580049, -0.0000300159];


c = [-2.1938817973176134*10.^-6 4.209098213906452*10.^-6
-8.087535917747982*10.^-6 0.00001556584632845917 c1
0.00001556584632845917 -8.087535917747982*10.^-6
4.209098213906452*10.^-6 -2.1938817973176134*10.^-6];


g = [0.0115986 -0.0122829 -0.0254308 0.024291 0.0594936
-0.0453692 -0.155616 0.070996 0.613659 -1.08347 0.613659 0.070996
-0.155616 -0.0453692 0.0594936 0.024291 -0.0254308 -0.0122829
0.0115986];
```

```
          %Initialization

d4_1 = zeros(19,39);

d4_2 = zeros(19,39);

d4_3 = zeros(19,39);

d4_4 = zeros(19,39);

d4_5 = zeros(19,39);

d4_6 = zeros(19,39);

d4_7 = zeros(19,39);

d5_1 = zeros(19,39);

d5_2 = zeros(19,39);

d5_3 = zeros(19,39);

d5_4 = zeros(19,39);

d5_5 = zeros(19,39);

d5_6 = zeros(19,39);

d5_7 = zeros(19,39);

d5_8 = zeros(19,39);

e4_1 = zeros(1,19);

e4_2 = zeros(1,19);

e4_3 = zeros(1,19);

e4_4 = zeros(1,19);

e4_5 = zeros(1,19);

e4_6 = zeros(1,19);

e4_7 = zeros(1,19);
```

```
e5_1 = zeros(1,19);

e5_2 = zeros(1,19);

e5_3 = zeros(1,19);

e5_4 = zeros(1,19);

e5_5 = zeros(1,19);

e5_6 = zeros(1,19);

e5_7 = zeros(1,19);

e5_8 = zeros(1,19);

    t = [-0.49:0.01:1.5]; for i =1:length(t)

for l = 1:19

for k = 1:39

d4_1(l,k) = c(k)*beta(2.0*(8*t(i)-3)-l-k+29);

d4_2(l,k) = c(k)*beta(2.0*(8*t(i)-4)-l-k+29);

d4_3(l,k) = c(k)*beta(2.0*(8*t(i)-2)-l-k+29);

d4_4(l,k) = c(k)*beta(2.0*(8*t(i)-1)-l-k+29);

d4_5(l,k) = c(k)*beta(2.0*(8*t(i)-5)-l-k+29);

d4_6(l,k) = c(k)*beta(2.0*(8*t(i)-0)-l-k+29);

d4_7(l,k) = c(k)*beta(2.0*(8*t(i)-6)-l-k+29);

d5_1(l,k) = c(k)*beta(2.0*(16*t(i)-5)-l-k+29);

d5_2(l,k) = c(k)*beta(2.0*(16*t(i)-6)-l-k+29);

d5_3(l,k) = c(k)*beta(2.0*(16*t(i)-7)-l-k+29);

d5_4(l,k) = c(k)*beta(2.0*(16*t(i)-8)-l-k+29);

d5_5(l,k) = c(k)*beta(2.0*(16*t(i)-4)-l-k+29);
```

114

```
d5_6(l,k) = c(k)*beta(2.0*(16*t(i)-3)-l-k+29);

d5_7(l,k) = c(k)*beta(2.0*(16*t(i)-2)-l-k+29);

d5_8(l,k) = c(k)*beta(2.0*(16*t(i)-1)-l-k+29);

end


    e4_1(l) = g(l)*sum(d4_1(l,:));

e4_2(l) = g(l)*sum(d4_2(l,:));

e4_3(l) = g(l)*sum(d4_3(l,:));

e4_4(l) = g(l)*sum(d4_4(l,:));

e4_5(l) = g(l)*sum(d4_5(l,:));

e4_6(l) = g(l)*sum(d4_6(l,:));

e4_7(l) = g(l)*sum(d4_7(l,:));

e5_1(l) = g(l)*sum(d5_1(l,:));

e5_2(l) = g(l)*sum(d5_2(l,:));

e5_3(l) = g(l)*sum(d5_3(l,:));

e5_4(l) = g(l)*sum(d5_4(l,:));

e5_5(l) = g(l)*sum(d5_5(l,:));

e5_6(l) = g(l)*sum(d5_6(l,:));

e5_7(l) = g(l)*sum(d5_7(l,:));

e5_8(l) = g(l)*sum(d5_8(l,:));

end

    %Scaled or Dilated wavelet

wav4_1(i) = sqrt(2).^3*sum(e4_1);
```

```
wav4_2(i) = sqrt(2).^3*sum(e4_2);

wav4_3(i) = sqrt(2).^3*sum(e4_3);

wav4_4(i) = sqrt(2).^3*sum(e4_4);

wav4_5(i) = sqrt(2).^3*sum(e4_5);

wav4_6(i) = sqrt(2).^3*sum(e4_6);

wav4_7(i) = sqrt(2).^3*sum(e4_7);

wav5_1(i) = sqrt(2).^4*sum(e5_1);

wav5_2(i) = sqrt(2).^4*sum(e5_2);

wav5_3(i) = sqrt(2).^4*sum(e5_3);

wav5_4(i) = sqrt(2).^4*sum(e5_4);

wav5_5(i) = sqrt(2).^4*sum(e5_5);

wav5_6(i) = sqrt(2).^4*sum(e5_6);

wav5_7(i) = sqrt(2).^4*sum(e5_7);

wav5_8(i) = sqrt(2).^4*sum(e5_8);

end

      rx1 = 1.0*wav4_1 - 1.0*wav4_2 - 1.0*wav4_3;

      EP_RX1 = sum(rx1.^2);

p_rx1 = 1/sqrt(3)*[rx1]./sqrt(EP_RX1);

      %In the channel for pulse1

for i =1:length(p_rx1)

p_ch1(i) = sum(p_rx1(1:i));

end
```

%In the Tx for pulse1

```
for i =1:length(p_ch1)
p_tx1(i) = sum(p_ch1(1:i));
end
```

```
    rx2 = 2.2*wav5_1 - 2.2*wav5_2 - 3.0*wav5_5 + 1.5*wav5_3 +
1.75*wav5_6 - 1.0*wav5_4 - 1.5*wav5_7;
```

```
    EP_RX2 = sum(rx2.^2);
p_rx2 = 1/sqrt(7)*[rx2]./sqrt(EP_RX2);
```

%In the channel for pulse2

```
for i =1:length(p_rx2)
p_ch2(i) = sum(p_rx2(1:i));
end
```

%In the Tx for pulse2

```
for i =1:length(p_ch2)
p_tx2(i) = sum(p_ch2(1:i));
end
```

%beta.m

```
function[b] = beta(t)
b = 1/8*( beta2(2*t+2) + 4*beta2(2*t+1) + 6*beta2(2*t) +
4*beta2(2*t-1) + beta2(2*t-2) );
```

%beta2.m

```
function[c] = beta2(t)
c = 1/6*( (max(0,t+2)).^3 - 4*(max(0,t+1)).^3 + 6*(max(0,t)).^3
- 4*(max(0,t-1)).^3 + (max(0,t-2)).^3);
```

Bibliography

[1] FCC, "Revision of Part 15 the Commission's rules regarding ultra-wideband transmission systems," ET Docket 98-153, 2002.

[2] S. Verdu, "Wireless bandwidth in the making," *IEEE Communications Magazine*, vol. 38, pp. 53–58, 2000.

[3] L. Yang and G. B. Giannakis, "Ultra-wideband communications: An idea whose time has come," *IEEE Signal Processing Magazine*, vol. 21, pp. 26–54, Nov. 2004.

[4] C. Lanzl, "Categorization of call for applications response, IEEE P802.15-03/442r1-SG4a," *IEEE P802.15 Working Group for WPANs*, Nov. 2003.

[5] G. Brown, "Ultrawideband: Spectrum for free," *Unstrung Insider Report*, vol. 4, April 2004.

[6] B. Allen, T. Brown, K. Schwieger, E. Zimmermann, W. Malik, D. Edwards, L. Ouvry, and I. Oppermann, "Ultra wideband: Applications, technology and future perspectives," *International Workshop on Convergence Technologies*, pp. 1–6, Jun. 2005.

[7] J. Walko, "Ultra Wide Band," *The IEE Communications Engineer*, Dec/Jan 2003/4B.

[8] T. W. Barrett, "History of ultra wideband (UWB) radar and communications: Pioneers and innovators," *Proc. Progress in Electromagnetics Symposium*, 2000.

[9] G.F. Ross, *The transient analysis of multiple beam feed networks for array systems,* P*h*.D. *dissertation,* Polytechnic Institute of Brooklyn, 1963.

[10] G.F. Ross and K.W. Robbins, "Base-band radiation and reception system," *U.S. Patent 3,739,392*, Jun. 1973.

[11] "Assessment of ultra-wideband (UWB) technology," *OSD/DARPA, Ultra-Wideband Radar Review Panel, R-6280*, July 1990.

[12] R. J. Fontana, "Recent applications of ultra wideband radar and communications systems," *presented at EuroEM, Edinburgh*, 2000, [Online]. Available: http://www.multispectral.com/pdf/AppsVGs.pdf.

[13] D. Porcino and W. Hirt, "Ultra-wideband radio technology: potential and challenges ahead," *IEEE Communications Magazine*, vol. 41, pp. 66–74, July 2003.

[14] M. Hamalainen, J. Saloranta, J-P. Makela, I. Oppermann, and T. Patana, "Ultra-wideband signal impact on the performances of IEEE 802.11b and Bluetooth networks," *International Journal of Wireless Information Networks*, vol. 10, pp. 201–210, Oct. 2003.

[15] R. Giuliano, G. Guidoni, J. Habib, and F. Mazzenga, "Coexistence of an ultra wideband spread spectrum system with fixed wireless access systems," *Computer Networks*, vol. 44, pp. 583–598, Apr. 2004.

[16] D. K. Borah, R. Jana, and A. Stamoulis, "Performance evaluation of IEEE 802.11a Wireless LANs in the presence of ultra- wideband interference," *Proc. IEEE Wireless Communications Networking Conference*, pp. 83–87, Mar. 2003.

[17] I. Bellorado, S.S. Ghassemzadeh, L. J. Greenstein, T. Sveinsson, and V. Tarokh, "Coexistence of.ultra-wideband systems with IEEE 802.11a Wireless LANs," *Proc. IEEE Globecom 2003*, pp. 410–414, Dec. 2003.

[18] M. Hamalainen, V. Hovinen, R. Tesi, J. Iinatti, and M. Latva-aho, "On the UWB system co-existence with GSM900, UMTS/WCDMA and GPS," *IEEE Journal on Selected Areas in Communications, special issue on UWB*, vol. 20, pp. 1712–1721, Dec. 2002.

[19] G. Yue, L. Ge, and S. Li, "Ultra wideband impulse radio signal interference to code division multiple access system," *IEEE International Symposium on Personal, Indoor and Mobile Radio Communications (PIMRC)*, pp. 2437–2441, Sep. 2003.

[20] IEEE 802.15 WPAN High Rate Alternative PHY Task Group 3a (TG3a), [Online]. Available: http://www.ieee802.org/15/pub/TG3a.html.

[21] IEEE 802.15 WPAN Low Rate Alternative PHY Task Group 4a (TG4a), [Online]. Available: http://www.ieee802.org/15/pub/TG4a.html.

[22] S. Stroh, "Ultra-wideband: Multimedia unplugged," *IEEE Spectrum*, pp. 23–27, Sep. 2003.

[23] S. Roy, J. R. Foerster, V. S. Somayazulu, and D. G. Leeper, "Ultrawideband radio design: The promise of high-speed, short-range wireless connectivity," *Proc. of the IEEE*, vol. 92, pp. 295–311, Feb. 2004.

[24] A. Batra, J. Balakrishnan, G. R. Aiello, J. R. Foerster, and A. Dabak, "Design of a multiband OFDM system for realistic UWB channel environments," *IEEE Transactions on Microwave Theory and Techniques*, vol. 52, pp. 2123–2138, Sep. 2004.

[25] J. R. Foerster, E. Green, V. S. Somayazulu, and D. Leeper, "Ultrawideband technology for short- or medium-range wireless communications," *Intel Technology Journal Q2*, 2001.

[26] I. Oppermann, L. Stoica, A. Rabbachin, Z. Shelby, and J. Haapola, "UWB wireless sensor networks: UWEN - a practical example," *IEEE Communications Magazine*, vol. 42, pp. S27–S32, Dec. 2004.

[27] S. Tilak, N. B. Abu-Ghazaleh, and W. Heinzelman, "A taxonomy of wireless micro-sensor network models," *Mobile Computing Communications*, vol. 6, pp. 28–36, 2002.

[28] I. F. Akyildiz, W. Su, Y. Sankarasubramaniam, and E. Cayirci, "A survey on sensor networks," *IEEE Communications Magazine*, vol. 40, pp. 102–114, 2002.

[29] J. Ryckaert, B. V. Poucke, B. Gyselinckx, and S. Donnay, "Wireless body area networks," *IEEE 802.15-03/484r0*, Nov. 2003 [Online]. Available: http://grouper.ieee.org/groups/802/15/pub/03/15-03-0484-00-004a-sg4a-cfa-response-wireless-body-area-networks.ppt.

[30] R. A. Scholtz, "Multiple access with time-hopping impulse modulation," *Proc. Military Communications Conf.*, vol. 2, pp. 447–450, Oct. 1993.

[31] M. Z. Win and R. A. Scholtz, "Impulse Radio: How it works," *IEEE Communications Letters*, vol. 2, pp. 36–38, Feb. 1998.

[32] B. Parr, B. Cho, K. Wallace, and Z. Ding, "A novel ultra-wideband pulse design algorithm," *IEEE Communications Letters*, vol. 7, pp. 219–221, May 2003.

[33] B. Parr, B. Cho, and Z. Ding, "A new UWB pulse generator for FCC spectral masks," *The 57th IEEE Vehicular Technology Conference*, vol. 3, pp. 1664–1666, April 2003.

[34] Z. Luo, H. Gao, Y. Liu, and J. Gao, "A new UWB pulse design method for narrowband interference suppression," *Global Telecommunications Conference, 2004. GLOBECOM '04. IEEE*, vol. 6, pp. 3488–3492, Nov.-Dec. 2004.

[35] Y. Wu, F. S. Molischm, S.Y. Kung, and J. Zhang, "Impulse radio pulse shaping for ultra-wide bandwidth (UWB) systems," *IEEE International Symposium on Personal, Indoor and Mobile Radio Communications (PIMRC)*, vol. 1, pp. 877–881, 2003.

[36] L. B. Michael, M. Ghavami, and R. Kohno, "Multiple pulse generator for ultra-wideband communication using Hermite polynomial based orthogonal pulses," *Proc. 2002 IEEE Conf. on Ultra Wideband Systems and Tech.*, pp. 47–51, May 2002.

[37] M. Ghavami, L. B. Michael, S. Haruyama, and R. Kohno, "A novel UWB pulse shape modulation system," *Kluwer International Journal on Wireless Personal Communications*, vol. 23, pp. 105–120, 2002.

[38] C. Mitchell and R. Kohno, "High data rate transmissions using orthogonal modified Hermite pulses in UWB communications," *Telecommunications, 2003 10th International Conf. on - ICT*, vol. 2, pp. 1278–1283, Feb. 2003.

[39] M. G. Di Benedetto and B. Vojcic, "Ultra-wideband (UWB) wireless communications: A tutorial," *Journal of Communications and Networks*, vol. 5, pp. 290–302, Dec. 2003.

[40] J. Romme and L. Piazzo, "On the power spectral density of time-hopping impulse radio," *Proc. Ultra-Wideband Systems and Technologies*, pp. 241–244, 2002.

[41] M. Z. Win, "On the power spectral density of digital pulse streams generated by M-ary cyclostationary sequences in the presence of stationary timing jitter," *IEEE Transactions on Communications.*, vol. 46, pp. 1135–1145, 1998.

[42] N. H. Lehmann and A. M. Haimovich, "The power spectral density of a time hopping UWB signal: a survey," *IEEE Conf. on Ultra Wideband Systems and Tech.*, pp. 234–239, Nov. 2003.

[43] H. Sheng, P. Orlik, A. M. Haimovich, L. J. Cimini, and J. Zhang, "On the spectral and power requirements for ultra-wideband transmission," *IEEE International Conf. on Communications*, vol. 1, pp. 738–742, May 2003.

[44] M. Z. Win, "A unified spectral analysis of generalized time- hopping spread-spectrum signals in the presence of timing jitter," *IEEE Journal On Selected Areas In Communications*, vol. 20, pp. 1664–1676, Dec. 2002.

[45] A. Taha and K. M. Chugg, "On the power spectral density of wireless multiple-access UWB impulse radio under realistic propagation conditions," *Proc. IEEE Vehicular Technology Conference*, pp. 1298–1302, Oct. 2003.

[46] G. Yue, H. Chen, and S. Li, "Ultra wideband time hopping impulse radio signal impact on performance of TD-SCDMA," *IEICE Transactions on*

Fundamentals of Electronics, Communications and Computer Sciences, vol. E88-A, pp. 2373–2380, Sep. 2005.

[47] M. Z. Win and R. A. Scholtz, "On the robustness of ultra-wide bandwidth signals in dense multipath environments," *IEEE Communications Letters.*, vol. 2, pp. 51–53, Feb. 1998.

[48] I. Guvenc and H. Arslan, "Design and performance analysis of TH sequences for UWB-IR systems," *Proc. IEEE Wireless Communications and Networking Conf. (WCNC 2004)*, vol. 2, pp. 914–919, Mar. 2004.

[49] K. S. Shanmugan and A. M. Breipohl, *Random Signals and Noise,* John Wiley, 1988.

[50] J. Brauer, "A rectangular beam waveguide resonator and antenna," *IEEE Transactions on Antennas and Propagation*, vol. 20, pp. 595–601, Sep. 1972.

[51] H. F. Harmuth, *Radiation of Nonsinusoidal Electromagnetic Waves,* Academic Press, 1990.

[52] M. Z. Win and R. A. Scholtz, "Ultra-wide bandwidth time-hopping spread-spectrum impulse radio for wireless multiple-access communications," *IEEE Transactions on Communications*, vol. 48, pp. 679–689, April 2000.

[53] J. T. Conroy, J. L. LoCicero, and D. R. Ucci, "Communication techniques using monopulse waveforms," *Proc. of IEEE Military Communications Conference (MILCOM 1999)*, vol. 2, pp. 1181–1185, 1999.

[54] X. Chen and S. Kiaei, "Monocycle shapes for ultra wideband system," *IEEE International Symposium on Circuits and Systems (ISCAS 2002)*, vol. 1, pp. 597–600, May 2002.

[55] X. Luo, L. Yang, and G. B. Giannaskis, "Designing optimal pulse-shapers for ultrawideband radios," *IEEE Conf. on Ultra Wideband Systems and Tech.*, pp. 349–353, Nov. 2003.

[56] X. Luo, L. Yang, and G. B. Giannaskis, "Designing optimal pulse-shapers for ultrawideband radios," *Journal of Communications and Networks*, vol. 5, pp. 344–353, Dec. 2003.

[57] X. Wu, Z. Tian, T. N. Davidson, and G. B. Giannakis, "Optimal waveform design for UWB radios," *Proc. IEEE International Conf. on Acoustics, Speech, and Signal Processing (ICASSP 04)*, pp. 521–524, May 2004.

[58] N. C. Beaulieu and B. Hu, "A novel pulse design algorithm for ultra-wideband communications," *IEEE Global Telecommunications Conf.*, vol. 5, pp. 3220–3224, Nov. 2004.

[59] Y. Kim, B. Jang, C. Shin, and B. F. Womack, "Orthonormal pulses for high data rate communications in indoor UWB systems," *IEEE*

Communications Letters, vol. 9, pp. 405–407, May 2005.

[60] H. F. Engler, "Advanced technologies for ultrawideband system design," *Proc. of the IEEE International Symposium on Electromagnetic Compatibility*, vol. 2, pp. 250–253, Aug. 1993.

[61] J. D. Taylor, *Introduction to Ultra-Wideband Radar Systems*, CRC Press, 1995.

[62] M. Ghavami, L. B. Michael, and R. Kohno, "Hermite function based orthogonal pulses for ultra wideband communication," *Proc. International Symposium on Wireless Personal Multimedia Communications (WPMC)*, pp. 437–440, Sep. 2001.

[63] K. Wallace, B. Parr, B. Cho, and Z. Ding, "Performance analysis of a spectrally compliant ultra-wideband pulse design," *IEEE Transactions on Wireless Communications*, vol. 4, pp. 2172–2181, Sep. 2005.

[64] L. Bin, E. Gunawan, and L. C. Look, "On the BER performance of TH-PPM UWB using Parr's monocycle in the AWGN channel," *IEEE Conference on Ultra Wideband Systems and Technologies*, pp. 403–407, Nov. 2003.

[65] E. Kreyszic, *Advanced Engineering Mathematics*, John Wiley and Sons, 1988.

[66] J. B. Martens, "The Hermite transform - Theory," *IEEE Transaction on Acoustics, Speech and Signal Processing*, vol. 38, pp. 1595–1606, Sep. 1990.

[67] M. R. Walton and H. E. Hanrahan, "Hermite wavelets for multicarrier data transmission," *Proc. of the IEEE South African Symposium on Communications and Signal Processing ComSIG 93*, pp. 40–45, Aug. 1993.

[68] W. Hu and G. Zheng, "Orthogonal Hermite pulses used for UWB M-ary communication," *Proc. Intenational Conf. on Information Technology: Coding and Computing*, vol. 1, pp. 97–101, Apr. 2005.

[69] R. Cramer, *An Evaluation of Ultra-Wideband Propagation Channels, Ph.D. dissertation*, Dept. of Electrical Engineering, University of Southern California, Los Angeles, CA USA, Dec. 2000.

[70] D. Slepian and H. O. Pollak, "Prolate spheroidal wave functions, Fourier analysis, and uncertainty-I," *Bell System Technical Journal*, vol. 40, pp. 43–46, Jan. 1961.

[71] D. Slepian, "Prolate spheroidal wave functions, fourier analysis, and uncertainty- V: The discrete case," *Bell System Technical Journal*, vol. 57, pp. 1371–1430, May 1978.

[72] B. Hu and N. C. Beaulieu, "Pulse shapes for ultrawideband communication systems," *IEEE Transactions on Wireless Communications*, vol.

4, pp. 1789–1797, July 2005.

[73] Y. Kim and B. F. Womack, "Performance evaluation of UWB systems exploiting orthonormal pulses," *IEEE Transactions on Communications*, Aug. 2005 (submitted).

[74] F. Ramirez-Mireles, "On the performance of ultra-wide-band signals in Gaussian noise and dense multipath," *IEEE Transactions on Vehicular Technology*, vol. 50, pp. 244–249, Jan. 2001.

[75] X. Chu and R. D. Murch, "Multidimensional modulation for Ultra-wideband multiple-access impulse radio in wireless multipath channels," *IEEE Transactions on Wireless Communications*, vol. 4, pp. 2373–2386, Sep. 2005.

[76] S. Licul and W. A. Davis, "Unified frequency and time-domain antenna modeling and characterization," *IEEE Transactions on Antennas and Propagation*, vol. 53, pp. 2882–2888, Sep. 2005.

[77] W. Sorgel, C. Waldschmidt, and W. Wiesbeck, "Transient responses of a Vivaldi antenna and a logarithmic periodic dipole array for ultra wideband communication," *IEEE Antennas and Propagation Society International Symposium*, vol. 3, pp. 592–595, June 2003.

[78] A. A. M. Saleh and R. A. Valenzuela, "A statistical model for indoor multipath propagation," *IEEE Journal On Selected Areas In Communications*, vol. 5, pp. 128–137, 1987.

[79] J. Foerster and Q. Li, "UWB channel modeling contribution from intel," *IEEE P802.15-02/279r0-SG3a*, Sep. 2002 [Online]. Available: http://grouper.ieee.org/groups/802/15/pub/2002/Jul02.

[80] S. G. Mallat, "A theory for multiresolution signal decomposition: the wavelet representation," *Pattern Analysis and Machine Intelligence*, vol. 7, pp. 674–693, July 1989.

[81] C. Mitchell, G. T. F. Abreu, and R. Kohno, "Combined pulse shape and pulse position modulation for high data rate transmissions in ultra-wideband communications," *International Journal of Wireless Information Networks*, vol. 10, pp. 167–178, Oct. 2003.

[82] K. Usuda, H. Zhang, and M. Nakagawa, "M-ary pulse shape modulation for PSWF-based UWB systems in multipath fading environment," *IEEE Global Telecommunications Conf. 2004*, vol. 6, pp. 3498–3504, Nov. 2004.

[83] X. Huang and Y. Li, "Performances of impulse train modulated ultra-wideband systems," *Proc. 2002 International Conf. on Communications*, vol. 2, pp. 758–762, April 2002.

[84] B. Hu and N. C. Beaulieu, "Accurate evaluation of multiple access performance in TH-PPM and TH-BPSK UWB systems," *IEEE Transactions on Communications*, vol. 52, pp. 1758–1766, Oct. 2004.

[85] J. G. Proakis, *Digital Communications*, McGraw- Hill, 1995.

[86] G. Durisi and G. Romano, "On the validity of Gaussian approximation to characterize the multiuser capacity of UWB TH-PPM," *Proc. IEEE Conf. on Ultra Wideband Systems and Technologies*, pp. 157–161, May 2002.

[87] G. Durisi and S. Benedetto, "Performance evaluation of TH-PPM UWB systems in the presence of multiuser interference," *IEEE Communications Letters*, vol. 7, pp. 224–226, May 2003.

[88] B. Hu and N. C. Beaulieu, "Exact bit error rate analysis of TH-PPM UWB systems in the presence of multiple-access interference," *IEEE Communications Letters*, vol. 7, pp. 572–574, Dec. 2003.

[89] B. Hu and N. C. Beaulieu, "Accurate performance evaluation of time-hopping and direct-sequence UWB systems in multi-user interference," *IEEE Transactions on Communications*, vol. 53, pp. 1053–1062, June 2005.

[90] H. V. Poor, "Signal processing for wideband communications," *IEEE Information Theory Society Newsletter*, June 1992.

[91] S. Verdu, "Recent progress in multiuser detection," *Multiple Access Communications: Foundations for Emerging Technologies*, pp. 164–175, 1993.

[92] J. Zhang, T. D. Abhayapala, and R. A. Kennedy, "Performance of ultra-wideband correlator receiver using Gaussian monocycles," *IEEE*

International Conf. on Commun., vol. 3, pp. 2192–2196, May 2003.

[93] J. D. Choi and W. E. Stark, "Performance analysis of RAKE receivers for ultra-wideband communications with PPM and OOK in multipath channels," *IEEE International Conference on Communications, ICC 2002.*, vol. 3, pp. 1969–1973, May 2002.

[94] J. Zhang, R. A. Kennedy, and T. D. Abhayapala, "Performance and parameter optimization of UWB RAKE reception with interchip interference," *Proc. IEEE International Conference on Communications, ICC 2005*, pp. 2830–2834, May 2005.

[95] H. Sheng, A. M. Haimovich, A. F. Molisch, and J. Zhang, "Optimum combining for time hopping impulse radio UWB RAKE receivers," *IEEE Conference on Ultra Wideband Systems and Technologies*, pp. 224–228, Nov. 2003.

[96] N. Guney, H. Delic, and M. Koca, "Robust rake receiver for TH-PPM impulse radio," *IEEE International Conference on Ultra-Wideband*, pp. 373–378, Sep. 2005.

[97] Z. Tian and G. B. Giannakis, "BER sensitivity to mistiming in ultra-wideband impulse radios-Part I: Modeling," *IEEE Transactions on Signal Process*, vol. 53, pp. 1550–1560, April 2005.

[98] Z. Tian and G. B. Giannakis, "BER sensitivity to mistiming in ultra-wideband impulse radios-Part II: Fading channels," *IEEE Transactions*

on Signal Process, vol. 53, pp. 1897–1907, May 2005.

[99] J. D. Choi and W. E. Stark, "Performance of ultra-wideband communications with suboptimal receivers in multipath channels," *IEEE Journal On Selected Areas In Communications*, vol. 20, pp. 1754–1766, Dec. 2002.

[100] S. Gezici, H. Kobayashi, H. V. Poor, and A. F. Molisch, "Performance evaluation of impulse radio UWB systems with pulse-based polarity randomization in asynchronous multiuser environments," *Proc. IEEE Wireless Communications and Networking Conf. (WCNC 2004)*, vol. 2, pp. 908–913, Mar. 2004.

[101] S. Gezici, H. Kobayashi, H. V. Poor, and A. F. Molisch, "The trade-off between processing gains of an impulse radio system in the presence of timing jitter," *Proc. IEEE International Conf. on Commun. (ICC 2004)*, vol. 6, pp. 3596–3600, June 2004.

[102] C. J. Mitchell and R. Kohno, "Orthogonalized and coded modulation for combined pulse position and pulse shape modulation," *International Workshop on Ultra Wideband Systems, 2004. Joint with Conference on Ultrawideband Systems and Tech.*, pp. 177–181, May 2004.

[103] L. Yang and G. B. Giannakis, "Space-time coding for impulse radio," *Proc. IEEE Conf. UltraWideband Systems and Technologies*, pp. 235–240, May 2002.

[104] L. Yang and G. B. Giannakis, "Analog space-time coding for multi-antenna ultra-wideband transmissions," *IEEE Transactions on Communications*, vol. 52, pp. 507–517, Mar. 2004.

[105] S. Niranjayan, A. Nallanathan, and B. Kannan, "An adaptive transmit diversity scheme based on spatial signal combining for TH-PPM UWB," *IEEE International Symposium on Spread Spectrum Techniques and Applications*, pp. 150–154, Aug. 2004.

[106] T. Ezaki and T. Ohtsuki, "Diversity gain in ultra wideband impulse radio (UWB-IR)," *IEEE Conference on Ultra Wideband Systems and Technologies*, pp. 56–60, Nov. 2003.

[107] S. S. Tan, B. Kannan, and A. Nallanathan, "Ultra-wideband impulse radio systems with temporal and spatial diversities," *IEEE 58th Vehicular Technology Conference*, vol. 1, pp. 607–611, Oct. 2003.

[108] S. S. Tan, B. Kannan, and A. Nallanathan, "Multiple access performance of UWB M-ary impulse radio systems with diversity reception," *International Workshop on Ultra Wideband Systems, 2004. Joint with Conference on Ultrawideband Systems and Tech.*, pp. 346–350, May 2004.

[109] E. Baccarelli, M. Biagi, C. Pelizzoni, and P. Bellotti, "A novel multi-antenna impulse radio UWB transceiver for broadband high-throughput 4G WLANs," *IEEE Communications Letters*, vol. 8, pp. 419–421, July 2004.

[110] E. Baccarelli, M. Biagi, C. Pelizzoni, N. Cordeschi, and F. Garzia, "Space-Time orthogonal M-ary PPM (STOMP) coding for coverage extension of MIMO UWB-IR systems," *International Symposium on Wireless Communication Systems*, pp. 263–267, Sep. 2005.

[111] X. Wu, Z. Tian, T. N. Davidson, and G. B. Giannakis, "Optimum waveform design for UWB radios," *IEEE Transactions on Signal Processing*, vol. 54, 2006.

[112] Y. Kim and B. F. Womack, "Space-shape codes for UWB systems," *IEICE Transactions on Communications*, Feb. 2006 (submitted).

[113] M. Matsuo, M. Kamada, and H. Habuchi, "Design of UWB pulses in terms of B-splines," *IEICE Transactions on Fundamentals*, vol. E88-A, pp. 2287–2298, Sep. 2005.

[114] M. Kamada, K. Toraichi, and R. E. Kalman, "A smooth signal generator based on quadratic B-spline functions," *IEEE Transactions on Signal Processing*, vol. 43, pp. 1252–1255, 1995.

[115] K. Ichige, M. Kamada, and R. Ishii, "A simple scheme of decomposing and reconstructing continuous-time signals by B-splines," *IEICE Transactions on Fundamentals*, vol. E81-A, pp. 2391–2399, 1998.

[116] D. Porrat and U. Mitra, "On synchronization of wideband impulsive systems in multipath," *Proc. International Symposium on Information Technology*, pp. 107–111, Sep. 2005.

136

[117] C. Luo, M. Médard, and L. Zheng, "Error exponents for Multitone Frequency Shift Keying on wideband Rayleigh fading channels," *Global Telecommunications Conference, 2003. GLOBECOM '03. IEEE*, vol. 2, pp. 779–783, Dec. 2003.

[118] C. Luo, M. Médard, L. Zheng, and D. S. Lun, "Multi-tone FSK with feedback," *Proc. International Symposium on Information Technology*, pp. 112–116, Sep. 2005.

[119] I. Daubechies, *Ten Lectures on Wavelets*, Society for Industrial and Applied Mathematics, Philadelphia, 1992.

[120] C. K. Chui, *An Introduction to Wavelets*, Academic Press, San Diego, 1992.

Vita

Youngok Kim was born in Seoul, Korea on July 2, 1971, the son of Pansul Kim, and Soonhee Park. After completing his work at Munil High School, Seoul, Korea in 1991, he entered Yonsei University, Seoul, Korea in 1993. He received the degree of Bachelor of Science from the Yonsei University in February 1999. In August 2000, he started his Master's program in the University of Texas at Austin. After completing his Master's degree, he continued the Ph.D. program at the Department of Electrical and Computer Engineering, The University of Texas at Austin. He focuses his research on ultra-wideband systems exploiting orthogonal waveforms to enhance data rates and transmission reliability.

Permanent address: 378-267 Doksandong Gumchun-Gu, Seoul, South
                               Korea.

This dissertation was typeset with LaTeX[†] by the author.

[†]LaTeX is a document preparation system developed by Leslie Lamport as a special version of Donald Knuth's TeX Program.